

**"Fluid evolution, vein formation and alteration associated
with a low angle shear zone at the northern Variscan fold-
and-thrust belt in the vicinity of the Aachen Geothermic-
drilling, western Germany"**

Von der Fakultät für Georessourcen und Materialtechnik der
Rheinisch-Westfälischen Technischen Hochschule Aachen

zur Erlangung des akademischen Grades eines

Doktors der Naturwissenschaften

vorgelegte Dissertation

von **Dipl. Geol.**

Markus Josef Lögering

aus Emsbüren

Berichter: Univ.-Prof. Dr.rer.nat. Franz Michael Meyer
Univ.-Prof. Ph.D Peter Kukla

Tag der mündlichen Prüfung: 19. Juni 2008

Diese Dissertation ist auf den Internetseiten der Hochschulbibliothek online verfügbar

Foreword

This project was carried out at the Institute of Mineralogy and Economic Geology, Rheinisch-Westfälischen Technischen Hochschule (RWTH) Aachen University and made possible through the support of the Deutsche Forschungsgemeinschaft Project (Grant Me 1425-9).

I like to thank Pd. Dr. Jochen Kolb, who has supervised my doctoral thesis at the Institut of Mineralogy and Economic Geology, Aachen University. He has been a great asset and was always helpful, thank you for everything. Thanks to Prof. Dr. F.M. Meyer, head of the Institut of Mineralogy and Economic Geology, for his supervision and understanding in the years of my study. This thesis has also greatly benefited by the suggestions and discussions of Ph.D Annika Dziggel, Dr. Sven Sindern and Prof. Dr. Helge Stanjek. I thank Pd. Dr. Jan Schwarzbauer and Dr. Alexander Kronimus for their supervision at the Institute of Geology and Geochemistry of Petroleum and Coal, Aachen University. I would also like to thank the team of the RWTH-1 project, especially Prof. Ph.D Peter Kukla and Dr. Ute Trautwein-Bruns. Many thanks to Prof. Dr. Torsten Vennemann for his supervision and discussions on stable isotopes at the University of Lausanne, Switzerland.

Thanks to the technical support at the Institute of Mineralogy and Economic Geology: Martin Brand (Electronic/Computer Technican); Thomas Derichs (Thin and Polished Section Laboratory); Monika Wiechert (Photography Laboratory); Dr. Annemarie Wiechowski and Roman Klinghardt (Electron Micro Probe Analysis); Dr. Jens Warnsloh (X-Ray Diffraction Laboratory); as well as Hildegard Breuers and Gudrun Günther from the Secretarial Office.

I also would like to thank Prof. Ph. Muchez, University of Leuven, Belgium for helpful discussions. The allocation of cores at the Geological Survey Brussels, Belgium, by Dr. M. Ducar is much appreciated. Thanks to Prof. Dr. U. Reimold from the Humboldt University Berlin, Germany. I want to thank S. Becker for core work. J. Koester critically improved the final manuscript, thank you a lot.

Furthermore, I would like to thank all the people who support me during my time in Aachen, especially, Katharina Wulf and Alexander Otto. And last but not least, my family and my friends, thank you all a lot.

List of publications

Abstracts:

- Lögering, M.J.; Kolb, J.; Meyer, F.M. (2005): Fluid Systeme der hydrothermalen Mineralisationen in der Aachener Geothermie-Bohrung. Abstract, Berichte der Deutschen Mineralogischen Gesellschaft, Beih. Z. Eur. J. Mineral. Vol. 17, No. 1, 84.
- Lögering, M.J.; Kolb, J.; Meyer, F.M.; Schwarzbauer, J. (2006a): Paläofluide in störungskontrollierten Bruchsystemen der Aachener Geothermie-Bohrung. Extended Abstract, 11. Symposium "Tektonik, Struktur- und Kristallingeologie, 137 – 140.
- Lögering, M.J.; Kolb, J.; Meyer, F.M.; Schwarzbauer, J. (2006b): Geochemie der Paläofluide in der Aachen Überschiebung. Abstract, Berichte der Deutschen Mineralogischen Gesellschaft, Beih. Z. Eur. J. Mineral. Vol. 18, No. 1, 87.
- Lögering, M.J.; Kolb, J.; Meyer, F.M.; Trautwein-Bruns, U. (2006c): Bruchbildung und Fluidtransport in der variszischen Falten- und Überschiebungsfront des linksrheinischen Rhenoharzynikums. Abstract, Schriftenreihe der Deutschen Gesellschaft für Geowissenschaften, Heft 50, 92.

Publications in process:

- Lögering, M. J., Kolb, J., Schwarzbauer, J., Meyer, F.M. (2007): Fluid evolution at the Variscan fold-and-thrust belt in the vicinity of the Aachen eothermic-drilling. Geothermics (submitted).

Contents

Figures	VI
Tables	IX
Zusammenfassung	XI
Abstract	XIII
1 Introduction	1
1.1 Variscan Orogeny	1
1.2 Palaeofluid Flow	2
1.3 Objectives	4
1.4 Methods of Investigation	4
2 Geological Setting	7
2.1 Regional Geology	7
2.2 Stratigraphy and Lithology	8
2.3 Structural Setting	11
2.4 Regional Hydrothermal Evolution	11
2.5 RWTH-1 drill versus Bolland drill (eastern Belgium)	13
2.5.1 Depositional facies	13
2.5.2 Diagenesis and stratigraphy	14
3 Tectonic Evolution	17
4 Petrology of Host Rock, Vein and Alteration Mineralogy	19
4.1 Host Rock	19
4.2 Vein Formation Mineralogy	22
4.2.1 Quartz-carbonate \pm chlorite veins (D_1)	23
4.2.2 Carbonate veins \pm chlorite (D_1)	23
4.2.3 Quartz veins \pm chlorite (D_1)	24
4.2.4 Chlorite paragenesis and alteration	24
4.2.5 Chlorite-sericite-K-feldspar paragenesis	26

4.3 Deformation Patterns	26
4.3.1 Pseudotachylite	28
4.4 Variscan (D ₁) Deformation and Post Variscan (D ₂) Deformation	30
4.5 Geothermometry	31
4.5.1 Calcite-dolomite and chlorite	31
4.6 Summary	32
5 Fluid Inclusions	35
5.1 Fluid Inclusion Petrography	35
5.1.1 Quartz-carbonate veins	36
5.1.2 Carbonate veins	36
5.1.3 Quartz veins	37
5.2 Fluid Inclusion Microthermometry	39
5.2.1 Quartz-carbonate veins	39
5.2.2 Carbonate veins	40
5.2.3 Quartz veins	41
5.3 Fluid Inclusion Pyrolysis-Gas Chromatography-Mass Spectrometry	42
5.4 Interpretation	43
5.4.1 Fluid inclusion trapping processes	43
5.4.2 Fluid inclusion isochores and P-T-path	44
5.4.3 Fluid evolution	47
5.4.4 Palaeotemperature and fluid composition within the regional scale	49
5.5 Summary	51
6 Stable Isotopes	55
6.1 Oxygen (VSMOW) and Hydrogen (VSMOW) Isotopy of Chlorites	55
6.2 Oxygen Isotopy (VSMOW) of Vein Minerals and Whole Rock	56
6.2.1 $\delta^{18}\text{O}$ of quartz-carbonate veins	56
6.2.2 $\delta^{18}\text{O}$ of single quartz and single carbonate veins	57
6.2.3 $\delta^{18}\text{O}$ of siliciclastic rocks, dolostone and limestone	57
6.3 Oxygen (PDB) and Carbon (PDB) Isotopy of Carbonates	58
6.4 Interpretation	59
6.4.1 Fluid composition and source	59

6.4.2 Stable isotope composition of quartz/carbonate veins	60
6.4.3 Carbonate composition and source	62
6.5 δ D and $\delta^{13}\text{C}$ Values of Water from Fluid Inclusions	64
6.5.1 H- and C-isotope composition of water in fluid inclusions and C-isotope composition of methane from fluid inclusions	64
6.5.2 Evolution of isotopic composition of the fluid and fluid source	64
6.5.3 Relations between methane and carbon dioxide	65
6.6 Fluid-Rock Interaction	67
6.7 Summary	70
7 Discussion	73
7.1 Tectono-Sedimentary Evolution	73
7.1.2 Pre-tectonic / burial-diagenetic evolution	74
7.1.3 Tectonic evolution	75
7.2 Palaeotemperature and Fluid Composition	78
7.3 Fluid Origin	80
7.4 Fluid-Rock Interaction	81
7.5 Transport and Precipitation	83
7.6 Genetic Model for the Vein Formation	86
7.7 Geothermal Anomalies and Fluid Flow at the Variscan Thrust Front	88
8 References	91
9 Appendices	105
9.1 Sample and Sections	105
9.2 Electron Micro Probe Analyser	112
9.3 Fluid Inclusion Analyses	114
9.4 Stable Isotopes Analyses	122
9.4.1 Oxygen isotope analysis	125
9.4.2 Hydrogen isotope analysis	127
9.4.3 Carbon isotope analysis	129
9.5 δ D and $\delta^{13}\text{C}$ Values of Fluids	131

Figures

Figure 1.1: Map of the early Palaeozoic tectonostratigraphic terrains in Central European segments of the Variscan fold belt (modified from W. Franke 1989).

Figure 2.1: Geological map of the NW European Variscan orogen (after Hollmann, 2001). Note the NE-SW trend of thrusts of the Variscan (D_1) orogeny. Pb-Zn deposits in the Aachen region are associated with post Variscan (D_2) NW-SE trending fault systems. The dots mark the wells along the MAT.

Figure 2.2: Lithologies of the RWTH-1, (A) massive dolomite with stylocumulates crosscut by fractures, (B) dolomitised limestone with large dissolution seams and a quartz-carbonate vein forming a dilational jog, (C) red, clay-silty sized pelites with a conjugated vein system of carbonate \pm chlorite, (D) brecciated siltstone with quartz \pm chlorite veins, (E) clay sized pelite with chlorite veinlets and a quartz-carbonate \pm chlorite dilational jog, and (F) fine-grained sandstone/siltstone with a quartz-carbonate \pm chlorite vein and the development of pseudotachylites.

Figure 2.3: Sketch of the stratigraphy and the structural situation in the vicinity of the RWTH-1 geothermic drill.

Figure 2.4: Photographs of the Lower Devonian siliciclastic rocks from the RWTH-1 core on the right hand side, and the Bolland drill core on the left hand side. The lithologies comprise the conglomerate, which correspond to the lower Devonian base.

Figure 2.5: Photographs of the Lower Devonian siliciclastic rocks from the RWTH-1 drill core on the right hand side, and the Bolland drill core on the left hand side. The lithologies comprise the red to grey pelites. Notice the syn-Variscan (D_1) veining.

Figure 2.6: Photographs of the Upper Devonian carbonates within the Frasnian stage from the RWTH-1 drill core on the right hand side and the Bolland drill core on the left hand side. The lithologies comprise the nodular limestone. Notice the syn-Variscan (D_1) veining.

Figure 2.7: RWTH-1 stratigraphy versus Bolland stratigraphy.

Figure 2.8: Photomicrograph of a carbonate \pm chlorite vein. Note the rock fragments and the conodont (co.) in the dolomite-marl ground mass.

Figure 3.1: Balanced geological cross section of the stratigraphy and the structural situation in the Stavelot-Venn foreland (after Hollmann, 1997).

Figure 4.1: Photomicrographs of different structures within the lithologies: (A) idiomorphic matrix dolomite and saddle dolomite crystals at the vein margin embedded in smaller grains of dolomite and chalcopyrite, (B) dolomite zonations, note iron rich center (0.7 mole % Fe), (C) fossiliferous limestone nodule (D) dolomitised limestone with stylocumulates, (E) framboidal pyrite in limestone matrix, (F) euhedral pyrite in dolomitised limestone (G) S_1/S_2 foliation in pelites, (H) brecciation of siliciclastic rocks.

Figure 4.2: Distribution of the main hydrothermal minerals in the RWTH-1 drill core. Relative abundance of minerals is indicated by solid and dashed lines.

Figure 4.3: Photomicrographs of different vein types: (A) and (B) quartz-carbonate \pm chlorite veins, (C), (D) and (E) carbonate \pm chlorite veins, (F) and (G) quartz \pm chlorite veins, and (H) K-feldspar vein under cathodoluminescent light.

Figure 4.4: Deformation pattern within different lithologies: (A) shear veins consisting of quartz/K-feldspar/chlorite and brecciation crosscutting foliation, (B) tension gashes

consisting of quartz/chlorite crosscutting foliation, (C) tension gashes consisting of quartz showing zonation under cathodoluminescent light, note also K-feldspar and calcite cements, (D) dilational jog consisting of stretched quartz grains, (E) and (F) pseudotachylites consists of a dark matrix which encloses angular to rounded fragments of the wall rock, and (G) and (H) shear veins of chlorite-sericite-K-feldspar-plagioclase paragenesis.

Figure 4.5: Photograph of clay-silt sized, grey pelites of the RWTH-1 drill core. Note the deformed quartz-carbonate \pm chlorite veins developed during Variscan (D_1) deformation.

Figure 4.6: Photograph of siltstone matrix of the Bolland drill core. Note the undeformed fibrous mineral growth of the quartz vein developed during post Variscan (D_2) deformation.

Figure 4.7: Diagram A, a plot of $X_{Fe,Dol}$ versus $X_{Mg,Cc}$ show the predicted curves for 300°C, 350°C, and 400°C, for equilibrium between calcite and dolomite (Powell et al., 1984). The shaded field depicts the estimated calcite-dolomite thermometer in the system $CaCO_3$, $MgCO_3$ and $FeCO_3$. Diagram B, results of chlorite geothermometry with different calibrations.

Figure 5.1: Photomicrograph (A+B) and cathodoluminescent-photomicrograph (C+D) of vein forming calcite and dolomite. Photomicrograph of primary fluid inclusions (E+F) distributed along zonation.

Figure 5.2: Photomicrographs of fluid inclusions from different vein types: (A) and (B) show quartz-carbonate veins with abundant primary FIA (dark specs) in calcite/dolomite grains and primary FIA along grain boundaries in quartz grains; (C) primary (growth zones) and pseudo-secondary (cluster) FIA in dolomite and quartz grains of a quartz-carbonate vein; (D) and (E) carbonate grains of carbonate veins with growth zones, visible due to the abundance of trapped primary fluid inclusions; (F) intra-granular trails of pseudo-secondary FIA perpendicular to a quartz grain surrounded by chlorite; (G) primary FIA along grain boundaries in quartz grains of a quartz vein; and (H) same vein type with secondary FIA along trans-granular trails in quartz grains.

Figure 5.3: Diagram of salinity (eq.wt.% NaCl) versus homogenisation temperature (Th) of fluid inclusions in quartz and carbonate grains of the quartz-carbonate veins. Classified according to their position within the different minerals.

Figure 5.4: Diagram of salinity (eq.wt.% NaCl) versus homogenisation temperature (Th) of fluid inclusions in dolomite and calcite grains of the carbonate veins, classified according to their position within the different minerals. The picture in the upper left corresponds to Figure 5.2 D.

Figure 5.5: Diagram of salinity (eq.wt.% NaCl) versus homogenisation temperature (Th) of fluid inclusions in quartz grains of the quartz veins. Classified according to their position within the different minerals.

Figure 5.6: (A) Gas-chromatogram with retention time versus relative abundance of gases included in fluid inclusions of a quartz-carbonate vein, and (B) mass-spectrogram of the same sample.

Figure 5.7: P-T diagrams show isochores with the minimum and maximum P-T conditions, calculated from fluid inclusion groups of (A) quartz-carbonate veins, (B) of carbonate veins, and (C) quartz veins. Note isochores of secondary inclusion have generally lower salinities/higher densities and lower temperatures leading to a higher gradient, whereas the primary FI's have higher temperatures and salinities/lower densities leading to flat gradients of the corresponding isochores. Diagram (D) shows the isochore of the high temperature primary fluid inclusions of all the vein types.

Fig. 5.8: P-T diagram show the isochore calculated from the high temperature primary fluid inclusions of different vein types. Note the intersection of the isochores with the chlorite and calcite-dolomite geothermometers at 350°C and 450°C of stable isotope geothermometers. Dashed lines represent lithostatic gradients of 30, 70, 80, 90 and 100°C/km, respectively.

Figure 5.9: Diagram showing the evolution of P-T path inferred for early to late stage fluid inclusion trapping conditions within the RWTH-1 shear zone.

Figure 5.10: Diagram of salinity (eq.wt.% NaCl) versus homogenisation temperature (T_h) of investigated fluid inclusions of the RWTH-1 well. Additionally, regional scale fluid inclusion studies classified in the order of different authors within the Ardennes of Western Germany (east and west of the river Rhine and the Ardennes of Eastern Belgium).

Figure 6.1: $\delta^{18}\text{O}$ (VSMOW) values of different vein types and chlorite assemblages, chlorite alteration and whole rock samples.

Figure 6.2: Oxygen and carbon isotopic composition of the mineralised veins ($n=15$), limestone nodules ($n=2$) and the dolomite host rock ($n=2$). Note, the limestone nodules have a similar isotopy compared to the surrounding mixed calcite/dolomite vein cements of the quartz-carbonate veins.

Figure 6.3: Mineral/water fractionation calculated after Graham et al. (1984b) of $\delta^{18}\text{O}$ values versus δD values of chlorite in veins and alteration zones. The field of metamorphic water combines the values of Taylor (1974) and Sheppard (1986), the field of magmatic water is from Taylor (1974), and the meteoric water line (MWL) from Epstein (1970).

Figure 6.4: Oxygen isotope fractionation of coexisting quartz-calcite, quartz-dolomite, and quartz-calcite-dolomite pairs within the quartz-carbonate veins. Factors of fractionation after Zheng (1993a & 1999). Temperatures calibrations after Sharp & Kirschner (1994).

Figure 6.5: $\delta^{18}\text{O}$ (PDB) versus $\delta^{13}\text{C}$ (PDB) plot showing the composition of a variety of carbonate environments. Note the calculated $\delta^{18}\text{O}$ values and $\delta^{13}\text{C}$ values of limestone, dolostone and carbonate veins, plot close to the field of hydrothermal carbonates.

Figure 6.6: Isotopic compositions ($\delta^{18}\text{O}/\delta\text{D}$) of vein chlorite and chlorite alteration compared to the isotopic composition of fluid inclusion waters that formed vein quartz and carbonates. The δD values of waters were measured from fluid inclusions and $\delta^{18}\text{O}$ were measured from the minerals hosted the fluid inclusions (FI's).

Figure 6.7: Fractionation of carbon species relative to CO_2 (redrawn from Ohmoto and Rye, 1979). Note the field of isotopic composition of water from fluid inclusions in quartz and carbonates related to the fractionation of CH_4 versus CO_2 .

Figure 7.1: Schematic 3D block of the different lithologies during the D_1 stage, illustrating the structural fabrics, hydrothermal veining as well as the infiltrating fluid and its physicochemical conditions during convective fluid flow.

Figure 7.2: Stability relationships for Na-K aluminosilicates as a function of fluid composition at 350°C and 2 kbar. The pH conditions are for 6 eq.wt.% NaCl. Data from Bowers et al. (1984), Eugster and Baumgartner (1987), and Shock and Helgeson (1988).

Figure 7.3: Retrograde P-T path from fluid inclusion temperatures and salinities in conjunction with higher temperatures of isotope geothermometry.

Figure 7.4: Schematic tectonic scetch along the seismic profile in the Aachen Region, (pers. com. S. Back).

Tables

Table 2.1: Stratigraphic column of the RWTH-1 drill.

Table 2.2: Conodont thermal alteration patterns and fluid inclusion homogenisation temperatures in Palaeozoic rocks from eastern Belgium, western Germany, and Rechtsrheinisches Schiefergebirge.

Table 2.3: Conodont thermal alteration patterns in Palaeozoic rocks from the Bolland and the RWTH-1 core in eastern Belgium and western Germany.

Table 6.1: Results of stable isotope analyses of chlorite (δD) and ($\delta^{18}O$) in ¹⁾ quartz-chlorite veins, ²⁾ carbonate-chlorite veins, and ³⁾ chlorite alteration.

Table 6.2: Oxygen isotopy (VSMOW) of quartz-carbonate pairs.

Table 6.3: Results of calculated mineral-water fractionation of chlorite (δD) and ($\delta^{18}O$) in ¹⁾ quartz-chlorite veins, ²⁾ carbonate-chlorite veins, and ³⁾ chlorite alteration. Factors of fractionation after Graham et al. (1984b).

Table 6.4: Results of calculated mineral-water fractionation of oxygen isotopy (VSMOW) of quartz-carbonate pairs (Zheng, 1993a/Zheng, 1999). Results of oxygen isotope thermometry in shaded fields (Sharp & Kirschner, 1994).

Table 6.5: Carbon isotopy (VSMOW) of water extracted from quartz-carbonate pairs.

Table 7.1: Conodont thermal alteration patterns and homogenization temperatures [Th] in Palaeozoic rocks from the Bolland and the RWTH-1 drill in eastern Belgium and western Germany.

Table 9.1: Sample list indicating the type and number of sections made.

Table 9.2: Representative geochemical analyses and precipitation temperatures of chlorite examples in I) alteration, II) slickensides and III) in different vein types.

Table 9.3: Representative geochemical analyses of calcite-dolomite assemblages.

Table 9.4: Microthermometric analyses of the two phase liquid-vapour fluid inclusions, from the quartz-carbonate veins (D₁), recalculated using the H₂O-NaCl-[KCl] equation of Bowers & Helgeson (1994).

Table 9.5: Microthermometric analyses of the two phase liquid-vapour fluid inclusions, from the carbonate veins (D₁), recalculated using the H₂O-NaCl-[KCl] equation of Bowers & Helgeson (1994).

Table 9.6: Microthermometric analyses of the two phase liquid-vapour fluid inclusions, from the quartz veins (D₁), recalculated using the H₂O-NaCl-[KCl] equation of Bowers & Helgeson (1994).

Table 9.7: Sample list indicating the isotope analyses completed on the different host rocks and vein systems.

Table 9.8: Oxygen isotopes from the selected samples.

Table 9.9: Hydrogen isotopes from the selected samples.

Table 9.10: Carbon isotopes from the selected samples.

Table 9.11: Mineral-water hydrogen/oxygen fractionation calculations of chlorites in paragenesis with quartz and/or dolomite as well as chlorite alteration.

Table 9.12: Mineral-water oxygen fractionation calculations of quartz/carbonate pairs.

Table 9.13: Hydrogen /(oxygen) isotopy of fluid inclusion water.

Table 9.14: Carbon isotopy (VSMOW) of quartz-carbonate pairs.

Zusammenfassung

In der vorliegenden Arbeit über das linksrheinische Rhenoharzynikum werden geologische Prozesse im Untergrund und deren Verhältnis zum regional-tektonischen Rahmen anhand der Proben aus der Aachener Geothermie-Bohrung (RWTH-1) mit dem Schwerpunkt auf Fluid- und Stofftransport untersucht. Die methodische Vorgehensweise basiert auf einer systematischen und detaillierten Bestandsaufnahme der Paläofluide in Form von Fluideinschlüssen an Kernmaterial der Bohrung.

Die RWTH-1 Bohrung wurde in den Überschiebungsgürtel der variszischen Aachen-Überschiebung abgeteuft und erreicht eine Tiefe von 2544m. Durch die siliziklastischen und karbonatischen Gesteine des Karbon und Devon verlaufen Störungen, die sich bevorzugt an lithologischen Kontakten ausgebildet haben. Bei der Scherung kommt es zur Bildung von befreienden Krümmungen (dilatational jog), Fiederspalten, Pseudotachyliten und einer Foliation.

Die lithologischen Einheiten werden von unterschiedlich orientierten, teilweise konjugierten Gängen und Gangsystemen durchschlagen. Dabei bildeten sich kataklastische und mylonitische Gefüge. Die Gänge variieren in der Breite von <1mm bis 3 cm. Drei Gangtypen werden unterschieden: Quarz-Karbonat Gänge \pm Chlorit, Karbonat Gänge \pm Chlorit und Quarz Gänge \pm Chlorit. Die Gänge sind durch bruchhafte Deformation entstanden und wurden mehrfach reaktiviert. Duktile Deformation wird durch die Rekristallisation und Kornverfeinerung von Quarz, Kalzit und Dolomit angezeigt. Die Rekristallisation findet hauptsächlich an den Gangrändern, aber auch innerhalb der Gänge statt. Durch das hochtemperierte Fluid kam es zu hydrothermalen Alteration. Die damit assoziierte Chlorit Alteration ist wenige mm mächtig.

Flüssigkeitseinschlüsse in den Gangmineralen der unterschiedlichen Gänge haben einheitlich maximale Homogenisierungstemperaturen < 390°C und wurden bei einem Druck von ca. 1.5 bis 2 kbar gebildet. Die eutektischen Temperaturen von ca. -21,7 °C weisen auf ein H₂O-Na-(K)-Cl dominiertes Fluid hin. Das Fluid hat eine Salinität von <2 – 9 Gew. % NaCl-Äquivalent. An den wässrigen Fluiden sind CO₂, CH₄ und N₂ beteiligt. Diese Fluidzusammensetzung ist typisch für die variszischen Fluide in Zentraleuropa. Die hohen Temperaturen sind bisher im linksrheinischen Schiefergebirge nicht beschrieben worden. Die Temperaturen und die Zusammensetzung der Fluide können aufgrund der gleichen

Fluideigenschaften mit den „Tectonic Brines“ im variszischen Grundgebirge von Mitteleuropa (Behr et al., 1993) korreliert werden. Des Weiteren zeigen Ergebnisse der Untersuchungen von Schroyen et al. (2000) und Muchez et. al. (2000) im Falten- und Überschiebungsgürtel von Ostbelgien sowie in den Varisziden von Belgien und Nordfrankreich ähnlich hohe Homogenisierungstemperaturen und Zusammensetzungen der Fluide. Die hohen Fluidtemperaturen im Zusammenhang mit der nicht weit in das Nebengestein reichenden Alteration lassen auf ein geringes Fluid/Gesteins-Verhältnis schließen und implizieren damit einen kurzzeitigen, episodischen Fluidfluss durch tektonische Öffnungsbewegungen entlang von Scherzonen.

Aus den Untersuchungen stabiler Isotope der Gangminerale können Gleichgewichtsbedingungen abgeleitet werden. Die stabilen Isotope von Sauerstoff und Wasserstoff der Chlorite, sowie die Messung der Isotope der Flüssigkeitseinschlüsse selbst, charakterisieren eine metamorphe Herkunft der Fluide.

Die Untersuchungen am Bohrkernmaterial der RWTH-1 Bohrung zeigen eine enge Verknüpfung von seismischer Deformation, Bruchbildung und fokussiertem Fluidfluss entlang der variszischen Strukturen. Wiederholte Bruchbildung entlang des SW-NE streichenden Aachen-Überschiebungssystems schaffte lokale Permeabilitäten für die variszischen Fluide bei typischen P-T-Bedingungen des bruchhaft-duktilen Übergangsbereiches. Dabei wurden durch die bruchhafte Deformation (D_1) in den Scherzonen Permeabilitäten geschaffen, Permeabilitätsbarrieren geschnitten und neue Permeabilitätsbarrieren durch die Fällung hydrothermalen Phasen entwickelt. Der kogenetische Pseudotachylit deutet darauf hin, dass seismische Ereignisse für die Bildung der Bruchpermeabilitäten in der Überschiebungsfront verantwortlich sind und die Fluidmigration durch seismisches Pumpen erfolgte.

Der Fluidtransport erfolgte entlang des o.g. Überschiebungssystems während der variszischen Gebirgsbildung. Demgegenüber stehen die Fluideinschlüsse von postvariszischen Pb-Zn-Gangvorkommen, wobei der Fluidtransport entlang der NW-SE gerichteten postvariszischen Störungssysteme verläuft.

Die Aachener Geothermie-Bohrung stellt das fehlende Glied zwischen den Untersuchungen an Falten- und Überschiebungsfronten der Eifel-Überschiebung und der Faille du Midi-Überschiebung nach Westen und dem Rheinischen Schiefergebirge nach Osten dar.

Abstract

Analyses of fluid inclusions in hydrothermal veins and the alteration mineralogy were performed on samples from the RWTH-1 geothermic well. A detailed textural, structural and fluid inclusion study of distinct vein generations has been performed to correlate the temperature-pressure conditions of vein formation with specific deformation episodes.

The drill site is located in the town of Aachen, Germany and reached a final depth of 2544 m. The Lower and Upper Devonian rocks of the RWTH-1 drill are located within the Aachen fold and thrust belt system. The carbonates and siliciclastic rocks are crosscut by hydrothermal veining and cataclastic to mylonitic deformation processes. Vein formation is related to a low angle shear zone. Veins in some places form a regular and dense network, often displaying a conjugate system.

Three vein types formed synchronous with the progressive deformation (D_1) such as, the quartz-carbonate \pm chlorite veins, the carbonate \pm chlorite veins, and the quartz \pm chlorite veins. These hydrothermal veins are a few millimetres to centimetres thick. Vein structures are formed in the transition from brittle to ductile deformation. Brittle deformation is indicated by dilational jogs, tension gashes and pseudotachylites. Ductile deformation is indicated by the undulous extinction of the quartz and carbonate grains, deformation twinning of carbonates and an initial stage of subgrain development in some of the quartz crystals at the vein margin. High temperature fluid activity led to a hydrothermal alteration by chlorite, extending laterally a few millimetres into the host rock.

Fluid inclusion in quartz and carbonate veins from core samples were studied to characterise the temperature and composition of these fluids, as well as the isotopic composition of vein minerals and the fluid inclusion trapped therein. The maximum homogenisation temperatures of <390 °C of primary fluid inclusions and the calculated pressures of 1.5 to 2 kbar derived from fluid inclusions formed during the progressive deformation; reflect the maximum P-T conditions during the hydrothermal overprint. The eutectic temperature from various fluid inclusion groups is around -21.7°C , indicating that these fluids have a $\text{H}_2\text{O-Na-(K)-Cl}$ composition. The hydrothermal fluids are water-dominant solutions of salinities between <2 and 9 wt% NaCl-eq and contain the gases CO_2 , CH_4 and N_2 . This fluid composition is typical for the Variscan fluids in middle Europe. Such high

temperatures from primary fluid inclusions have not been reported for the German Variscides west of the river Rhine before. The temperature [Th] and fluid composition of these fluids is equivalent to those of the "Tectonic Brines" in the Variscan basement of the Rhenohercynian terrain east of the river Rhine (Behr et al., 1993). These fluid parameters are also in agreement with fluid inclusion studies on Variscan fault and thrust belts in eastern Belgium and northern France (Muecher et al., 2000; Schroyen et al., 2000). The recorded high temperatures in conjunction with the mm-scale hydrothermal alteration adjacent to the host rock indicate small scale fluid/rock interaction within the system and point to a focused fluid flow. These fluid rock interactions imply a short-term, episodic fluid transport due to tectonic opening movements along the shear zones.

Stable isotopes of oxygen and hydrogen were used to constrain the origin of the fluids. The calculated $\delta^{18}\text{O}$ and δD isotopic composition from chlorite separates of vein assemblages as well as the alteration zone and additionally the $\delta^{18}\text{O}$ values of quartz, calcite and dolomite in conjunction with the δD isotopic composition of fluid inclusions therein characterised a metamorphic origin of the fluid source.

This study demonstrates the importance of fluid inclusion research for the reconstruction of the palaeofluid flow and the recognition of multiple fluid flow stages during the evolution of the Devonian strata in the Variscan fold-and-thrust belt. The abundance of extensional fractures (e.g. dilatancy structures) and the cogenetic pseudotachylite can be related to seismic activity during the time of hydrothermal veining. Seismic energy and the resulting brittle deformation are responsible for the development of permeabilities along the shear zones leading to hydrothermal fluid flow controlled by seismic pumping.

The migration of fluids along faults towards the SW-NE trending Midi-Aachen thrust system represents a simple explanation for the hydrothermal veining. In contrast, investigations of fluid inclusion on post Variscan Pb-Zn deposits crosscut the Variscan structures and these fluids migrated along the post Variscan NW - SE trending faults. The Aachen Geothermic-drilling is the missing link between studies on thrust and fault zones in the Eifel thrust belt and the Faille du Midi thrust belt to the west (eastern Belgium) and thrust belts in the Rheinisches-Schiefergebirge to the east of the Variscan front.

Figure 1.1: Map of the early Palaeozoic tectonostratigraphic terrains in Central European segments of the Variscan fold belt (modified from W. Franke 1989).

1.2 Palaeofluid Flow

Fluids play an important role in the evolution of the earth's crust as they transport heat and material, trigger mineral reactions, control diagenesis, metamorphism and hydrothermal veining. Numerous detailed studies are available focussing on the characterisation of fluid flow during metamorphism (e.g. Smith and Yardley 1999; Vry et al., 2001) or tectonometamorphic deformation (e.g. Mullis et al., 1994; Murphy and Roberts 1997; McCuaig and Kerrich 1998). Fluid flow in the deeper subsurface is often focussed into faults and shear zones, which act as highly permeable pathways (e.g. McCaig, 1997). Moreover, there is ample evidence that circulating fluids are physically involved in the rupture mechanics of faults (e.g. Sibson, 2001). Fluids also influence the effective strain of rocks and their brittle-ductile transition (Nesbitt, 1990). In tectonically active settings, hydrothermal fluids migrating along shear and fault zones increase the heat flow by convective heat transport from deeper crustal levels. Whereas the heat flow in impermeable sections of the upper crust is restricted to more conductive heat transport, which results in diagenesis and/or metamorphism of the rocks at low to normal geothermal gradients.

Large-scale migration of fluids may be very important during orogenic deformation. Fluid flow invariably occurs down hydraulic gradients, which can be produced by a variety of processes including thermal expansion, topography changes, overpressuring due to compaction of pore space or liberation of metamorphic fluids, and seismic or dilatancy pumping (Fyfe et al., 1978; Etheridge et al., 1983, 1984; Oliver 1986; Garven et al., 1993; Ferry, 1994; Oliver, 1996). Metamorphic fluids play an important role in processes occurring at different levels in the crust (Fyfe et al., 1978; Shmulovich et al., 1995). The relative age of the veins can be determined by using crosscutting and structural relationships between the veins and cleavage, bedding, folds and faults.

Fluid inclusion studies have been widely used for determining the thermal evolution of geothermal fluids and subsurface temperatures (e.g. Browne et al., 1974; Roedder, 1984). The principal aim of fluid inclusion studies is to determine the physicochemical parameters and geochemical composition of palaeofluid systems. This data permits the identification and the characterization of distinct

fluid compositions and may provide implications for the fluid origin and the reconstruction of the thermal evolution. Fluid data and isotope geochemistry in conjunction with hydrothermal vein, hydrothermal alteration and host rock data provide additional constraints to the origin and composition of the vein forming fluids, and on fluid rock interaction and accompanying P-T conditions (Parry et al., 1991).

Syntectonic veins can form from fluids in a closed or open geothermal system. Rock-buffered veins (Gray, et al., 1991) precipitate under the dominant influence of the host rock, and the isotopic composition of the veins is similar to that of the host rock and results from isotopic equilibrium between the fluid and the rock mass. If the fluids were, however, unable to completely isotopically equilibrate with the host rocks, due to relatively rapid flow and being confined to fractures, they carry the signature of the original fluid source (Cartwright and Buick, 2000).

The aim of this study is the investigation of the fluid flow system that was present during the deformation of Upper and Lower Devonian strata at the northern Variscan thrust front. The RWTH-1 drill site is located in the town of Aachen, Germany and reached a final depth of 2544 m. Fluid inclusion in quartz and carbonates from core samples were studied to characterise the temperature and composition of these fluids. The isotopic composition of vein minerals and trapped fluid inclusion within the minerals were also studied. Since the veins represent the hydrothermal activity, they yield important information on the behaviour and evolution of fluid flow. This study reveals possible effects of fluids on the diagenesis, metamorphism, and palaeo-temperature fields at the Variscan thrust front. From the results obtained, the evolution of fluid flow, fluid chemistry, and temperature conditions of the palaeo-geothermal system can be characterised.

The Aachen geothermal-drilling is similar to studies on thrust and fault zones in the Eifel thrust belt and the Faille du Midi thrust belt to the west (eastern Belgium) and thrust belts in the Rheinisches-Schiefergebirge to the east of the Variscan front. Therefore the drill is located in an ideal area to investigate fluid flow systems at the Variscan thrust front in western Germany.

1.3 Objectives

The study had the following objectives:

- Development of a P-T-t path for the hydrothermal fluid using petrology, fluid inclusion thermometry, and detailed structural analysis of the vein systems and the tectonic setting.
- Characterisation of the geodynamic setting using whole rock geochemistry from the different lithologies adjacent to the vein formation.
- Quantification of the alteration and vein forming processes, as well as whole rock geochemistry, Rietveld phase analysis and isotope geochemistry.
- Qualification of the fluid source by using mineral stability, fluid inclusion composition, and isotope geochemistry.
- Description of fluid transport and precipitation mechanisms.
- Qualitative and quantitative description of the fluid migration and development of pathways in the various host lithologies.

The combination of these points allows the construction of a genetic model for the hydrothermal fluid. The characterisation of the tectono-metamorphic evolution, the geodynamic setting, and regional-scale fluid systems allows the development of vein forming models and the timing of veining within the northern Variscan fold-and-thrust belt. The involvement of orogenic processes suggests that a more dynamic model is required to adequately describe the hydrothermal vein forming process.

1.4 Methods of Investigation

This study is based on samples collected from the core of the RWTH-1 drill. During the first phase detailed core logging and vein description were completed, which included stratigraphy, mineralogy, temporal order of fracture filling and structures. A total of 89 core samples collected from regular depth intervals were used in this study. Hydrothermal vein and alteration minerals and the relative modal proportion of minerals of these samples were studied, using X-ray diffraction (XRD), Electron Microprobe Analyses (EMPA), microthermometry, cathodoluminescence microscopy and gaschromatography, at the RWTH-Aachen University, Germany. The isotope study was carried out on vein forming

minerals, alteration halos around the veins and the unaltered rock. The stable isotopes of oxygen, hydrogen and carbon were investigated, as well as the hydrogen and carbon isotopy of the fluid inclusions at the University of Lausanne, Switzerland. The core sections that were logged and the samples taken are listed in Appendices, Table 9.1. Samples taken for isotopes are listed in Table 9.7.

To achieve the above objectives the following investigations were completed:

- **Petrology:** 69 thin and polished sections were used for rock and vein forming minerals using both transmitted and reflected light microscopy (Institute of Mineralogy and Economic Geology, RWTH Aachen University), enabling the identification of micro-textures, micro-structures and mineral paragenesis. Representative polished sections were chosen for cathodoluminescence microscopy (CL, Department of Geology, RWTH Aachen University). This assisted the identification of carbonate zonations, carbonate cements, K-feldspar and other accessory minerals.
- **Electron Microprobe Analysis (EPMA):** the mineral composition of each of the identified mineral assemblages was determined at the Institute of Mineralogy and Economic Geology, RWTH Aachen University. This was essential for geothermobarometric calculations (i.e. chlorite vein and alteration minerals, and calcite dolomite vein minerals) as well as for the identification of systematic chemical variations (i.e. opaque minerals, K-feldspar and pseudotachylite).
- **X-Ray Diffraction (XRD):** selected samples were analysed to identify host rock composition, vein composition, and alteration minerals. XRD and the applied Rietveld method were used to qualify and quantify the mineral phases present (Institute of Mineralogy and Economic Geology, RWTH Aachen University).
- **Microthermometry:** measurements of fluid inclusions were performed on 45 doubly polished thick sections on a modified USGS cooling-heating stage at the Institute of Mineralogy and Economic Geology, RWTH Aachen University. Fluid inclusions were analysed for fluid compositions and the

calculation of temperature/pressure parameters. A selection of these sections was examined for further analyses by pyrolysis – gas-chromatography / mass-spectrometry (Py-GC/MS). The gas composition of fluid inclusions were then determined qualitatively and semi-quantitatively at the Institute of Geology and Geochemistry of Petroleum and Coal, RWTH Aachen University, Germany.

- **Stable isotopes:** a total of 42 mineral-separates and 17 whole rock samples were analysed for stable isotopes of oxygen, hydrogen and carbon to constrain the origin of fluids as well as to evaluate the extent of fluid-rock interaction and the hydrothermal vein forming mechanisms. All analyses were carried out at the University of Lausanne, Switzerland in collaboration with Prof. Torsten Vennemann.
- **Fluid isotope composition:** Fluid inclusions were extracted by mechanical/crushing decrepitation in a vacuum extraction line. The stable isotopes of hydrogen and carbon were measured to constrain the fluid source and the fluid conditions at the time of hydrothermal veining. This method was carried out at the University of Lausanne, Switzerland.
- **Geochronology:** the pseudotachylite from the pelitic host rocks currently dated by Dr. J. Tieloff, University of Heidelberg, Germany. The Potassium/argon dating of the pseudotachylite provides the important information of the maximum age of the hydrothermal activity. The potassium content of minerals in the pseudotachylite was analysed using the EMPA, including mineral mapping at the Institute of Mineralogy and Economic Geology, RWTH Aachen University.

2. Geological Setting

2.1 Regional Geology

The Northwest European Variscan Orogen within the Rhenoharzynian terrain comprises the Ardennes of western Germany and eastern Belgium and the Rheinisches-Schiefergebirge (Walter, 1995). In the study area, regional-scale synclines, anticlines and locally developed thrusts trend in NE – SW direction, related to the Variscian deformation (D_1). The Wurm Synclinorium and the Aachen Anticlinorium are one of these structures. In Aachen, the Variscan thrust front is represented by the Aachen Thrust, which continues to the west in the Midi Thrust in eastern Belgium (Figure 2.1). In the following they are named together the Midi-Aachen Thrust-System (MAT). Further eastwards from the MAT, in the Rheinisches-Schiefergebirge, the main Variscan faults and thrusts are towards NNE - SSW trending structure. NW - SE trending faults crosscut the Variscan structures and host the Pb-Zn deposits of the Aachen region, in eastern Belgium, and in the Rheinisches-Schiefergebirge (Franke, 1989). They formed during post-Variscan (D_2) deformation.

This study was carried out in Lower and Upper Devonian rocks of the RWTH-1 drill core, located at the northern margin of the MAT, within the Wurm Synclinorium (Figure 2.1). The Wurm Synclinorium is bound at its southern flank by the Aachen Anticlinorium. To the west it grades into the Namur/Verviers Synclinorium in eastern Belgium. The basement is represented by rocks of the Brabant-Massif in the north and rocks of the Stavelot-Venn-Massif in the south. Along the south dipping D_1 shear zones Devonian and Carboniferous rocks were thrust over the Brabant-Massif.

The Lower Devonian siliciclastic sediments in the RWTH-1 drill are overlain by a thin bedded alternation of Upper Devonian siliciclastic rocks and carbonates of the Frasnian to the Famennian stage. The Upper Devonian is followed by Carboniferous rocks of the Namurian and the Westphalian stage (Östereich et al., 2005).

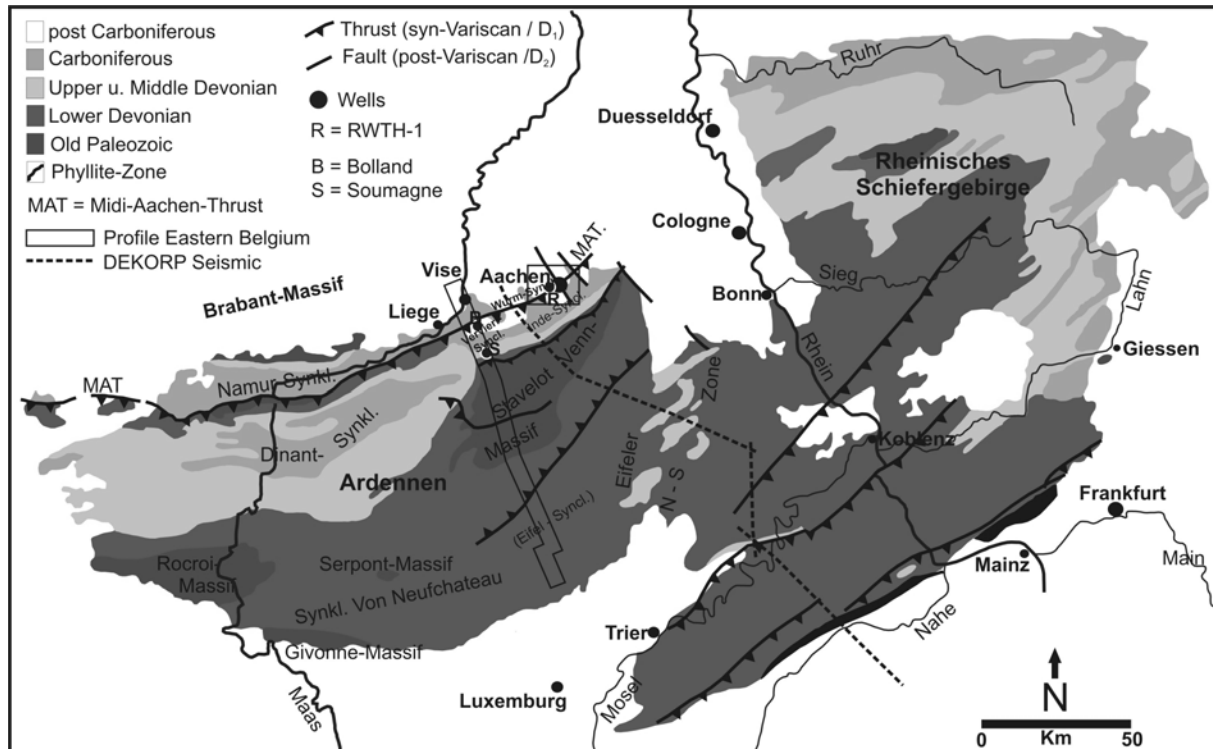


Figure 2.1: Geological map of the NW European Variscan orogen (after Hollmann, 1997). Note the NE-SW trend of thrusts of the Variscan (D_1) orogeny. Pb-Zn deposits in the Aachen region are associated with post Variscan (D_2) NW-SE trending fault systems. The dots mark the wells along the MAT.

2.2 Stratigraphy and Lithology

The Brabant-Massif basement (Old Palaeozoic) is composed of Lower Palaeozoic shale, siltstone, and quartzite (Geomare et al., 1997). Lower Devonian siliciclastic rocks rest unconformably upon the Brabant-Massif basement (Geomare et al., 1997, Stroink, 1993). The lowermost part of the RWTH-1 core consists of dark, silicified shale followed upwards by a conglomerate. The shale possibly correlates with the Old Palaeozoic basement shales and the conglomerate with the bottom of the Lower Devonian rocks.

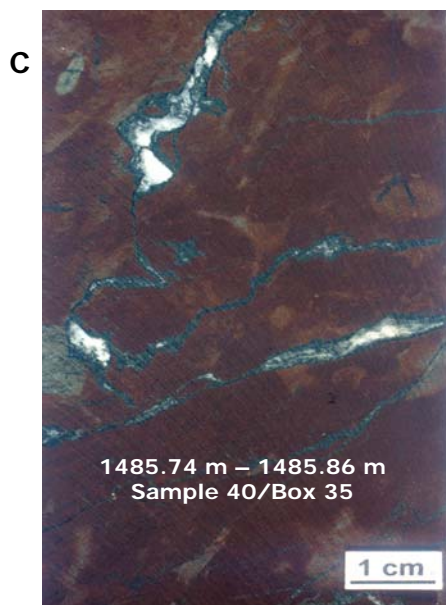
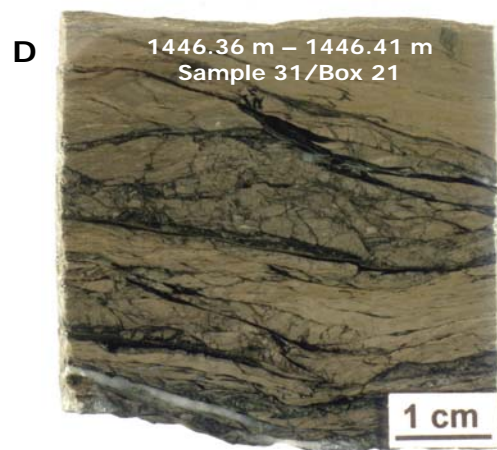
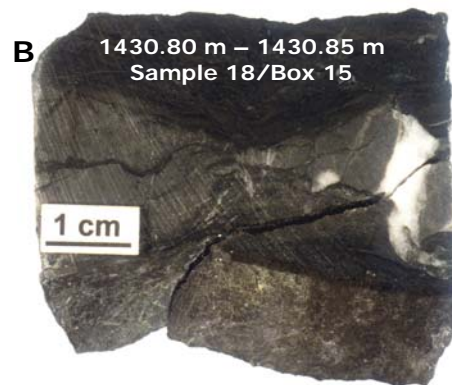
The Lower Devonian sediments in the core from 2542 m to 1438 m consist of siliciclastic sediments with abundant fossils, root fragments, ooides and nodular calcrete horizons. The thinly bedded, clay-silt sized pelites are red to grey and interbedded with fine- to coarse-grained, grey sandstones (Figure 2.2) that contain detritus in an argillaceous ground mass. These rocks developed micrite to microsparite cements. They are overlain by an alternation of Upper Devonian siliciclastic rocks and shallow water carbonates from 1438 m to 1012 m of the

Frasnian to the Famennian stage. They consist of thinly bedded siliciclastic rocks and are intercalated with a dolomite bank, dolomite- and calcite-marl, and a nodular limestone with a biorelic fabric (Figure 2.2). Partial dolomitisation of the rocks is ubiquitous. The Upper Devonian is overlain by Carboniferous rocks of the Namurian and the Westphalian stage from 1012 m to the surface (Östereich et al., 2005).

Table 2.1: Stratigraphic column and thickness of the RWTH-1 drill.

Cretaceous (70 m)	siliciclastic rocks	aeolian sands
Carboniferous (942 m)	siliciclastic rocks	black to dark grey shales
Upper Devonian (426 m)	siliciclastic rocks	clay-silt sized pelites and fine- to coarse-grained, grey sandstones
	shallow water	dolomite bank, dolomite- and calcite-marl and nodular limestone
Stratigraphic Gap /Unconformity		
Lower Devonian (1102.5 m)	siliciclastic rocks	red to grey, clay-silt sized pelites fine- to coarse-grained, grey sandstones
	base	conglomerate
Silurian to Ordovician (0.5 m) [?]	siliciclastic rocks	dark, silicified shale

Figure 2.2: Lithologies of the RWTH-1, (A) massive dolomite with stylolites crosscut by fractures, (B) dolomitised limestone with large dissolution seams and a quartz-carbonate vein forming a dilational jog, (C) red, clay-silty sized pelites with a conjugated vein system of carbonate \pm chlorite, (D) brecciated siltstone with quartz \pm chlorite veins, (E) clay sized pelite with chlorite veinlets and a quartz-carbonate \pm chlorite dilational jog, and (F) fine-grained sandstone/siltstone with a quartz-carbonate \pm chlorite vein and the development of pseudotachylites.



2.3 Structural Setting

The rocks of the RWTH-1 drill in the interval from 1515 m to 1391 m are crosscut by hydrothermal veining and cataclastic to mylonitic deformation processes. One main shear zone was identified within this interval. This low angle shear zone is related to a D_1 fault zone. We propose that the MAT separates the Lower Devonian from the Upper Devonian rocks at this depth. This explains the stratigraphic gap and the lack of the Middle Devonian rocks (Figure 2.3). Due to the abundance of vein material in cutting samples at 1900 m depth, we suggest that another D_1 fault is developed in the Lower Devonian rocks. This fault zone is also indicated on a 2D regional seismic line. Two more fault zones probably occur at 800 m and 2300 m, respectively (pers. com. S. Back).

The Lower Devonian rocks within the core intervals from 2143 m to 2131 m and from 2542 m to 2537 m are weakly crosscut by the Variscan D_1 deformation and veining.

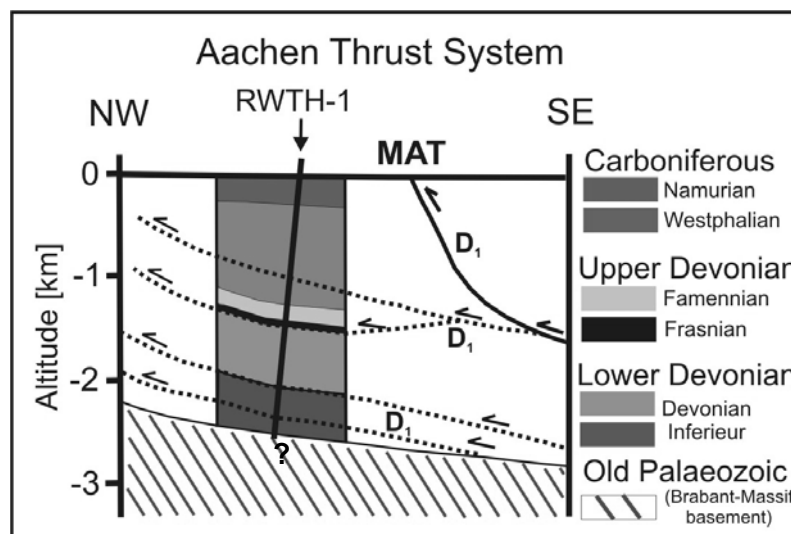


Figure 2.3: Sketch of the stratigraphy and the structural situation in the vicinity of the RWTH-1 geothermic drill.

2.4 Regional Hydrothermal Evolution

The Palaeozoic rocks in the study area were affected by the Variscan orogeny. The degree of diagenesis and metamorphism of the Devonian strata at the subsurface in the Verviers synclinorium of eastern Belgium, the southern and eastern part of the Stavelot-Venn-Massif and in the Rechtsrheinisches Schiefergebirge was estimated using the Colour Alteration Index (CAI) of conodonts (Helsen and Königshof 1994, Schreyer 1975; Kramm 1982; Fransolet

and Kramm 1983). The CAI of the Upper Devonian conodonts in these areas point to a variable thermal overprint with temperatures ranging between 100°C - 420°C (Table 2.2).

During the Variscan orogeny in the Rhenoharzynian terrane, synkinematic fluid flow generated the fluid-system of the so-called "Tectonic Brines" (Behr et al., 1993) with homogenisation temperature of $\leq 350^\circ\text{C}$ (Table 1). Fluid inclusion studies in the Variscan fold and thrust belt in eastern Belgium show a syn-Variscan high temperature fluid with a homogenisation temperature of $\leq 380^\circ\text{C}$ (Table 2.2; Schroyen et al., 2000). The post-Variscan hydrothermal ore deposits of the Rheinisches-Schiefergebirge are derived from so-called "Basement Brines" (Behr et al., 1993). These fluids have a homogenisation temperature of $\leq 200^\circ\text{C}$ (Table 2.2).

The recently measured temperature at the bottom of the RWTH-1 drill hole is at 86°C (pers. com. Lundershausen).

The regional palaeo-geothermal evolution, therefore, is characterised by cooling from temperatures as high as 420°C to about 90°C – 70°C in the drill hole and the geothermal springs in Aachen over the last 360 Ma.

Table 2.2: Conodont thermal alteration patterns and fluid inclusion homogenisation temperatures in Palaeozoic rocks from eastern Belgium, western Germany, and Rechtsrheinisches Schiefergebirge.

	Dinant Synclinorium in the Ardennes of eastern Belgium	Stavelot Venn Massif in the Ardennes of western Germany	Rhenoharzynian and Rechtsrheinisches Schiefergebirge
Conodont Alteration Index (CAI) values from Upper Devonian	¹⁾ 3.5 to 4 CAI (150 – 190 °C)	³⁾ 5.5 to 6 CAI (360 – 420 °C)	¹⁾ 2.5 to 3 CAI (<90 – 120 °C)
Fluid inclusion homogenisation temperatures [Th]	²⁾ Variscan fluids [Th] $\leq 350^\circ\text{C}$ ²⁾ Post Variscan fluids [Th] 70 to <180 °C	⁴⁾ Post Variscan fluids in the Aachen region [Th] 70 to <180 °C	⁵⁾ Tectonic Brines [Th] $\leq 350^\circ\text{C}$ ⁵⁾ Basement Brines [Th] $\leq 200^\circ\text{C}$

¹⁾ Helsen and Königshof, 1994; ²⁾ Muchez et al., Schroyen et al., 2000; ³⁾ Schreyer, 1975; ⁴⁾ Redecke, 1992; Stroink, 1993; Glasmacher, 1995; ⁵⁾ Behr et al., 1993

2.5 RWTH-1 drill versus Bolland drill (eastern Belgium)

2.5.1 Depositional facies

The Lower Devonian siliciclastic rocks that are thrust over the Silurian basement shale and the Lower Devonian conglomerate were deposited in a braided-river system and on a coastal alluvial plain with tidal influences. These depositional features are widespread in the Lower Devonian of eastern Belgium (Geomare et al., 1997) and Western Germany (Stroink, 1993). The conglomerate in the RWTH-1 core (2543.21 m) is similar to the lower Devonian conglomerate in the Bolland core (2420 m) and is interpreted as the base of the Devonian strata (Figure 2.4). The subjacent shale in the RWTH-1 core is most likely the Silurian basement shale, compared to the basement shale of the Bolland core. The dolomite bank, dolomite- and calcite-marl, and nodular limestone are correlated with the Upper Devonian strata southward of the MAT within the Bolland drill core (Figure 2.5 and 2.6). This lithology is typical for the near shore, lagoonal facies of the Frasnian stage and corresponds to the Condroz Group (Thorez and Dreesen, 1986, Geomare et al., 1997). Therefore, the lithologies of the RWTH-1 drill core are believed to represent the Devonian facies which developed at the southern margin of the Brabant-Massif. This is supported by the lack of the characteristic basinal facies of the Variscan front in western Germany which is related to the lithologies of the so-called Lower Carboniferous “Kohlenkalk” and Middle Devonian “Massenkalk”.

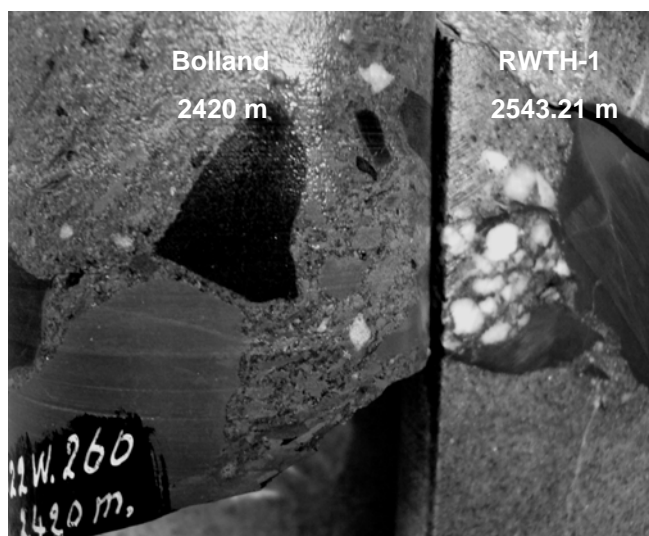


Figure 2.4: Photographs of the Lower Devonian siliciclastic rocks from the RWTH-1 core on the right hand side, and the Bolland drill core on the left hand side. The lithologies comprise the conglomerate, which correspond to the lower Devonian base.

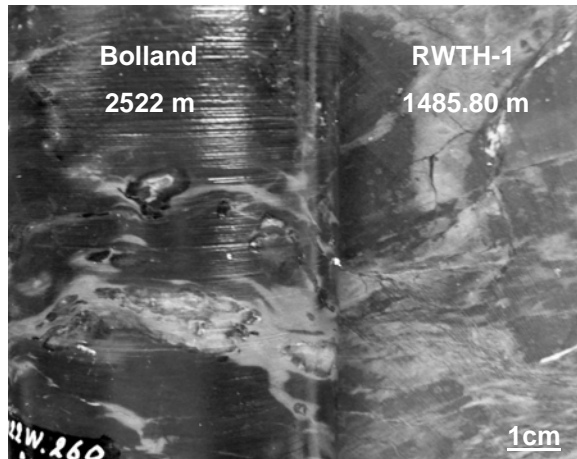


Figure 2.5: Photographs of the Lower Devonian siliciclastic rocks from the RWTH-1 core on the right hand side, and the Bolland core on the left hand side. The lithologies comprise the red to grey pelites. Notice the syn-Variscian (D₁) veining.

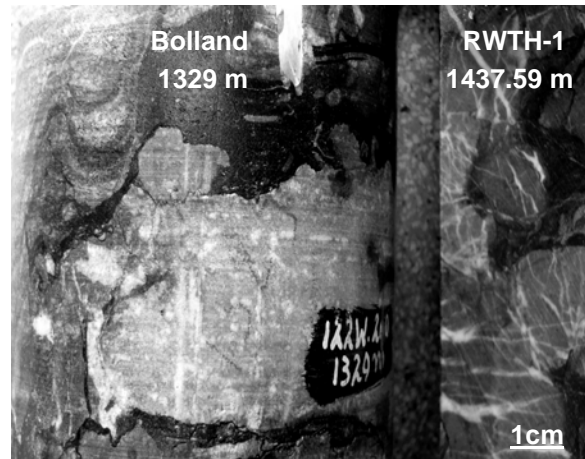


Figure 2.6: Photographs of the Upper Devonian carbonates within the Frasnian stage from the RWTH-1 core on the right hand side and the Bolland core on the left hand side. The lithologies comprise the nodular limestone. Notice the syn-Variscian (D₁) veining.

2.5.2 Diagenesis and stratigraphy

The petrological study of the core revealed no visible porosity in the Carboniferous to Devonian (410 – 290 Ma) lithologies. Due to the cementation by micrite and microsparite the primary depositional porosity was progressively lost during burial diagenesis. Late diagenetic features are overprinted by burial and deformation processes forming a S₁ foliation in the argillaceous and silty rocks. The voids and joints are sealed by quartz, carbonates and chlorite due to the precipitation from a hydrothermal fluid. A comparison of the stratigraphic profiles of the Bolland versus the RWTH-1 drill shows the similarity of the lithologies and the structural situation (Figure 2.6). The case of stratigraphic doubling, which is found in the Bolland drill from 1400 – 500 m, could not be proven for the same depth interval of the RWTH-1 drill, because of the size of selected cutting samples from this interval. However, a stratigraphic doubling is possible due to the fault zone at 800 m within the RTWH-1 obtained from the interpretation of the seismic profile.

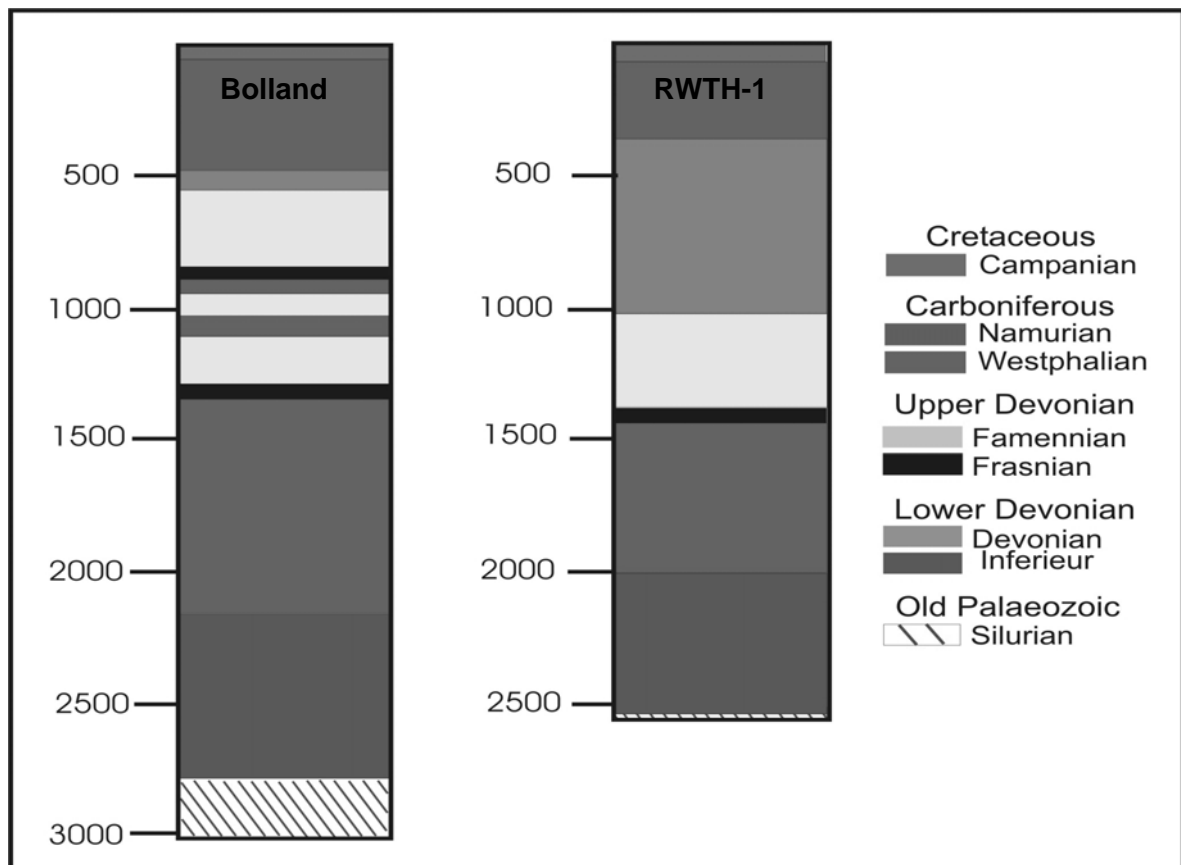


Figure 2.7: RWTH-1 stratigraphy versus Bolland stratigraphy.

The degree of diagenesis and metamorphism was estimated from the Colour Alteration Index (CAI) on conodonts (Figure 2.7) from core samples of the Upper Devonian. The alteration of aminoacids in conodonts is mainly related to temperature and the corresponding time of exposure, which can be used to estimate the degree of thermal overprint of the studied rocks (Pietzner et al., 1968; Savage et al., 1990). CAI with temperatures between 245°C and 320°C has been found in rocks of the Bolland (Muechez et al., 2000) and of the RWTH-1 drill (Table 2.3). The high CAI temperatures could be explained by the fact that conodonts are very sensitive to temperature anomalies and these temperatures are not corresponding to the adjacent host rock temperatures.

Table 2.3: Conodont thermal alteration patterns in Palaeozoic rocks from the Bolland and the RWTH-1 core in eastern Belgium and western Germany.

	Bolland drill in the Vervier Synclinorium within the Ardennes of eastern Belgium	RWTH-1 drill in the Wurm Synclinorium within the Ardennes of western Germany
Conodont Alteration Index (CAI) values from Upper Devonian rocks	¹⁾ 4.5 to 5 CAI (245 - 320°C)	4.5 to 5 CAI (245 - 320°C)

¹⁾ Muchez et al., 2000; ²⁾ Zhang et al., 1997

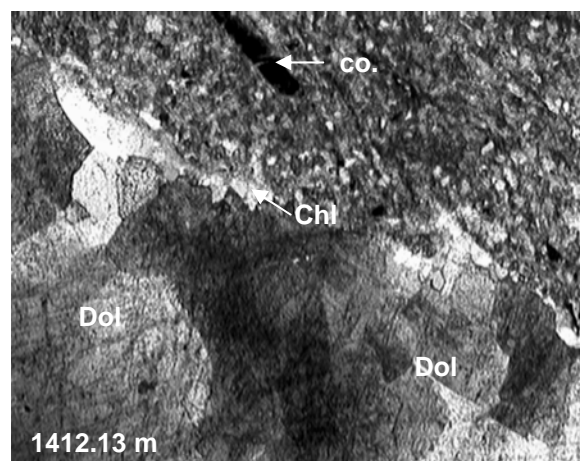


Figure 2.8: Photomicrograph of a carbonate ± chlorite vein. Note the rock fragments and the conodont (co.) in the dolomite-marl ground mass.

3. Tectonic Evolution

The Ardennes of Western Germany (North Eifel) with the Wurm Synclinorium and the Ardennes of East Belgium with the Namur and Vervier Synclinorium comprise the marginal facies of the Rhenish-Ardennen (north-western margin of the Variscan Orogen) and are associated with the MAT. The MAT is the northernmost large-scale thrust fault of the Variscan Orogen (Oncken et al., 1999). The Variscan front is bordered against the Brabant Massiv and the northern basin structures of Belgium-Netherlands-Germany (Hollmann and Walter, 1995). Structural field data, drillings (e.g. Graulich, 1984) and several seismic profiles (e.g. Dejonghe et al., 1989; DEKORP Research Group, 1991) characterised the nappe system of this part of the Variscan Orogen.

The Variscan foreland consists mainly of Palaeozoic sedimentary rocks. The Devonian and Carboniferous rocks of the Rhenohercynian Ocean rest unconformable on the Old Palaeozoic basement units. These basin sediments were deformed during the Variscan orogeny and the resulting structures and deformation features are prevalent until today. The nappe setting and the related stacking patterns of the lithostratigraphic units were confirmed by the drills of the Bolland and Soumage wells (Graulich, 1984). Recently the RWTH-1 core supported the nappe tectonic setting. The extension of these nappe structures of the outer Variscan front were interpreted by seismic processing (e.g. Behrmann et al., 1991; Betz et al., 1988; Dejonghe et al., 1989; DEKORP Research Group, 1991, see figure 2.1). These authors described a slightly south dipping reflector which is interpreted as the basal detachment fault separating the Devonian rocks from the Old Palaeozoic basement. This corresponds to the Midi-Aachen-Thrust system.

The balanced structural model for the Vervier synclinorium (Figure 3.1, see figure 2.1) interpreted the outer Variscan front, as a fold-and-thrust-belt characterised by an intensive ramp-flat-thrust tectonics (Hollmann, 1997). This resulted in a series of detachment controlled faults. The nappe system of the MAT within the North-Eifel and east Ardennes foreland is characterised by the fractured Aachen-Imbrication-Zone which grades to the west into the Herve-Imbrication-Zone (Hollmann and Walter, 1995). These anticlines are followed to the north by the Wurm Synclinorium and the Namur Synclinorium. These units were transported along the Old Palaeozoic detachment. The shearing of the

sediment (detachment faults) is controlled by calcareous and argillaceous horizons (Frasne Carbonates and lower Devonian shales; Hollmann, 1997).

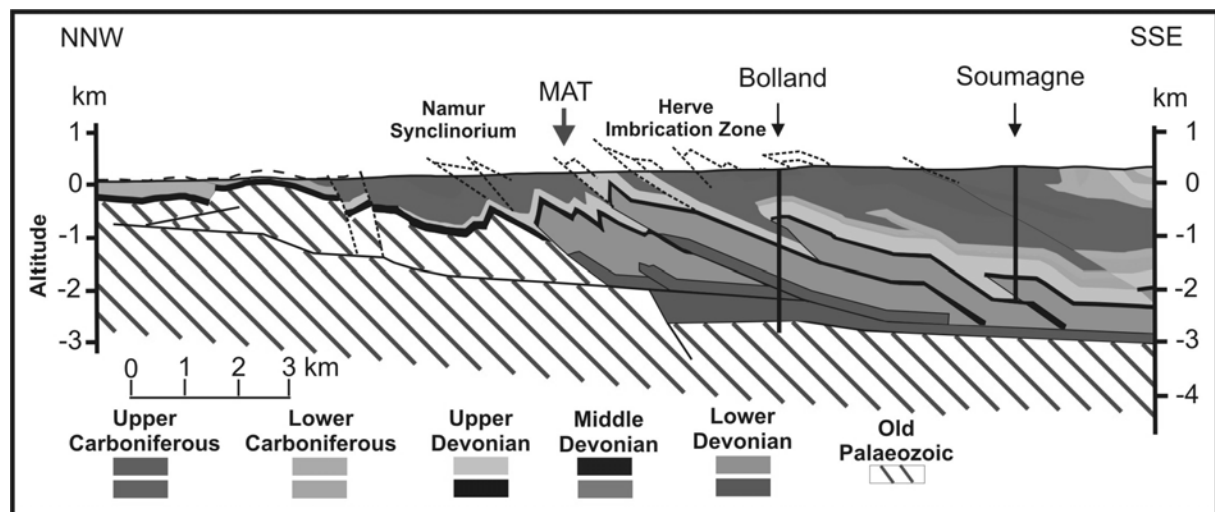


Figure 3.1: Balanced geological cross section of the stratigraphy and the structural situation in the Stavelot-Venn foreland (after Hollmann, 1997).

Palaeoenvironmentally, the lithologies of the Wurm Synclinorium identified in the RWTH-1 core were located on the continental shelf which formed the passive north-western margin of the Rheohercynian Ocean (Oncken et al., 1999; Franke, 2000). The rifting of the continental shelf took place during Early to Middle Devonian time (410 - 380 Ma). The Variscan convergence is linked with closure of the Rheohercynian Ocean during Late Devonian to Early Carboniferous times (360 – 290). Shortening of the sedimentary sequence predates faulting and is regionally more intense (Franke, 2000; Oncken et al., 2000).

The present study proposes the Devonian tectonic evolution of the eastern segment of the Wurm Synclinorium that is associated with the south-eastern marginal facies of the Brabant Massiv and their adjacent tectono-sedimentary units. This interpretation can be considered analogous to the facies distribution found in the Bolland core.

4 Petrology of Host Rock, Vein and Alteration Mineralogy

4.1 Host Rock

The Silurian siliciclastic rocks consist of dark, silicified shale (Lower Palaeozoic basement shales). The shale matrix is composed in increasing abundance of chlorite, illite, k-feldspar, quartz, and clay minerals. These shales form a sharp contact to the overlying conglomerate consisting of angular to rounded clasts varying in size from <1 to 5 cm.

The Lower Devonian sediments consist of siliciclastic rocks. The thinly bedded, clay-silt sized pelites are red to grey and interbedded with fine- to coarse-grained, grey sandstones (Figure 4.1 G) that contain detritus in an argillaceous ground mass with illite/chlorite and muscovite (compare Figure 4.3 B). Clay-silt sized pelites consist mainly of a fossiliferous (root fragments), argillaceous groundmass and calcareous cements, as well as more silty parts partially with oolites and sandy parts with nodular calcrete horizons.

The Upper Devonian sediments consist of alternating siliciclastic rocks and carbonates. They are thinly bedded clay-silt sized pelites and are intersected by a dolomite bank, dolomite- and calcite-marl, and a nodular limestone with a biorelic fabric (Fig. 4.1 C). The carbonate marls contain sparse brachiopods and crinoid ossicles, whereby the limestone nodules are enriched in brachiopods, foraminifers, crinoid ossicles and conodonts. Limestones always show some siliciclastic contamination. The dolomite bank consists of 90 % matrix dolomite crystals forming tight rhombohedra mosaics (Figure 4.1 A). The dolomite is devoid of any fossils. The same characteristics are true for the dolomite marl.

The siliciclastic rocks from the various stratigraphic levels and the Upper Devonian carbonate marl and limestone contain detrital quartz, K-feldspar, biotite and plagioclase and are in some places enriched in white mica (illite, muscovite) and chlorite. The main grain size varies between 45 and 120 µm. Micas and chlorite are responsible for the occurrence of internal bedding stratifications. The siliciclastic rocks also contain micritic carbonate cements.

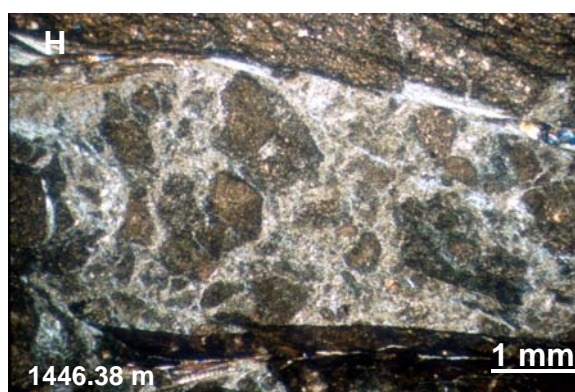
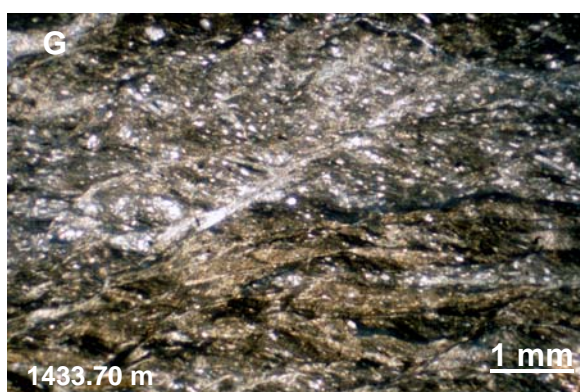
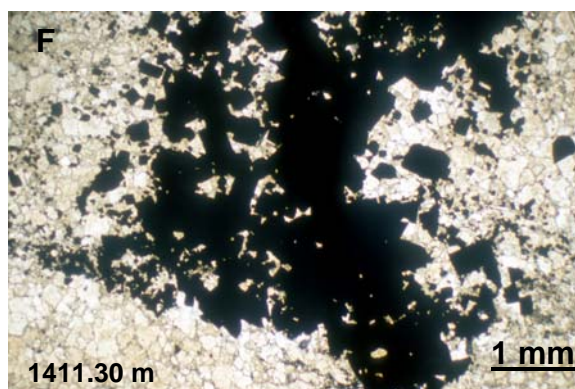
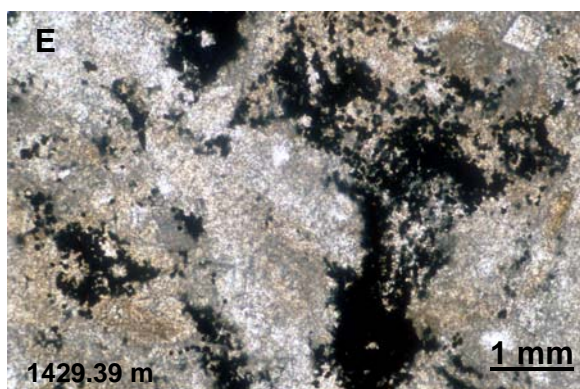
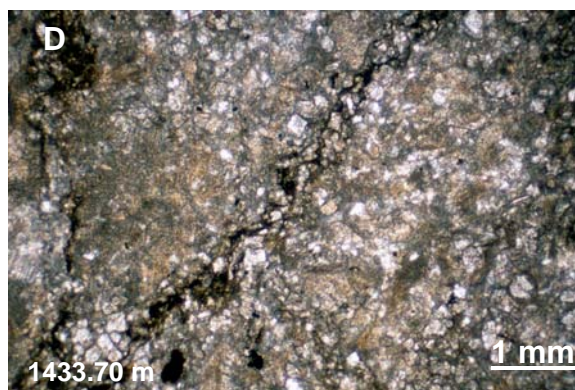
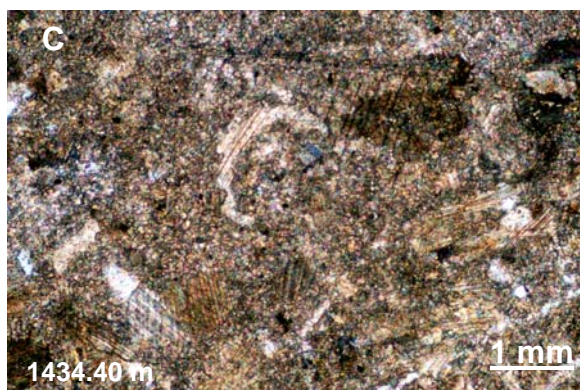
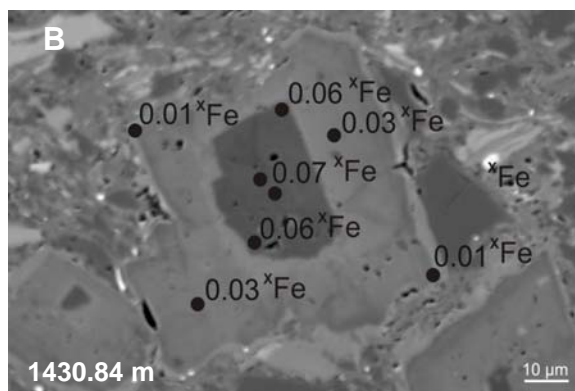
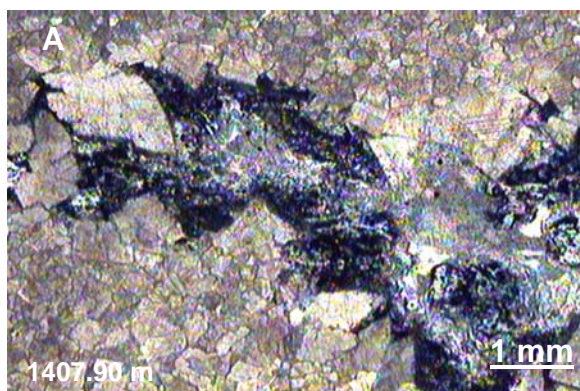
Partial pervasive dolomitisation of the rocks is ubiquitous. Where dolomitisation is more complete, the dolomite crystals form tight idiomorphic to hydriomorphic mosaics and are typically developed as grey matrix dolomite. The dolomite crystals have average diameters of 100 to 500 micrometers. The dolomite

crystals showing zonations due to their iron rich center with 0.7 mole % Fe, close to the classification of ankerite starting at 0.9 mole % Fe content (Figure 4.1 B). Where matrix dolomitisation was complete limestone nodules were overprinted with grey matrix dolomite (Figure 4.1 D). Differential matrix lithification (matrix-cements) also recrystallised the lime/dolo mud to micrite and microsparite. Anhydrite is rare and occurs mainly as cements in molds and vugs within the dolomite bank or where matrix dolomitisation is extensive. Framboidal pyrite grains can be partially observed in biorelic limestone matrix (Figure 4.1 E), but where matrix dolomitisation are extensive these pyrites are recrystallised to form cubic crystals (Figure 4.1 F).

Chemical compaction formed stylocumulates (Wanless, 1979), which are developed as less than 1 mm thick clay seem (dissolution seams) and stylolites, with average amplitudes between a few millimeters to about 1 cm (Figure 4.1 D). Stylolites have relatively sharp boundaries in partially dolomitised locations, but they are more diffuse in the pervasive dolomitised parts. Stylocumulates consist of clay minerals, i.e. illite, smectite, clinochlor, and pyrite. Shale parts present roughly the same mineral composition as stylocumulates. Chemical compaction and deformation formed a S_1 foliation. This foliation formed due to a compression aligned normal to bedding, reflecting the final stages of the burial history (Simpson, 1985). Late diagenetic features (e.g. micrite to microsparite cements) are overprinted by the S_1 foliation within the siliciclastic, argillaceous and calcareous rocks.

During the Variscian time the main deformation D_1 forming a S_2 foliation, crosscuts the S_1 foliation (Figure 4.1 G). The different rock types are partially brecciated. Brecciated zones are associated with the argillaceous intercalations (Figure 4.1 H), which played an important mechanical role during the deformation acting as preferred horizons for decoupling mechanisms with respect to shearing (see Mansy et al., 1999).

Figure 4.1: Photomicrographs of different structures within the lithologies: (A) idiomorphic matrix dolomite and saddle dolomite crystals at the vein margin embedded in smaller grains of dolomite and chalcopyrite, (B) dolomite zonations, note iron rich center (0.7 mole % Fe), (C) fossiliferous limestone nodule (D) dolomitised limestone with stylocumulates, (E) framboidal pyrite in limestone matrix, (F) euhedral pyrite in dolomitised limestone (G) S_1/S_2 foliation in pelites, (H) brecciation of siliciclastic rocks.



4.2 Vein Formation Mineralogy

One major thrust fault of the MAT intersects the drill core from 1516 m to 1391 m (Figure 2.3), indicated by the abundance of veins and cataclastic to mylonitic deformation structures. The textural and structural vein observation identified one major deformation event. Three vein types occurred synchronous with this event, the quartz-carbonate \pm chlorite veins, the carbonate \pm chlorite veins and the quartz \pm chlorite veins (Figure 4.3). These hydrothermal veins are a few millimetres to centimetres thick and make up \pm 20 Vol. % of the host rock. The vein minerals are accompanied by K-feldspar, plagioclase, chalcopyrite, smectite, sericite and pyrite (Figure 4.2). The main alteration minerals are chlorite and dolomite but also K-feldspar, smectite and illite. The voids and joints are sealed by quartz, carbonates and chlorite due to the precipitation from a hydrothermal fluid. These minerals completely fill the shear and extensional fractures (see chapter 4.3). Within each vein type the minerals, the structures and textures are different and are in detail described below.

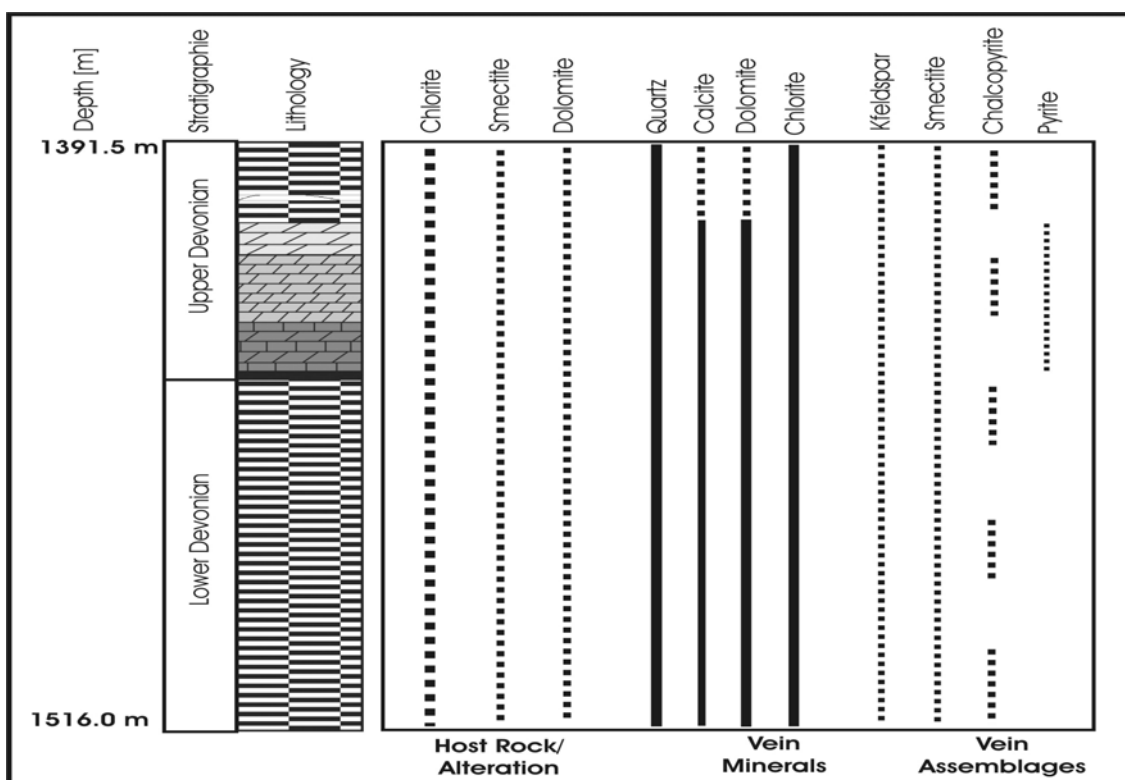


Figure 4.2: Distribution of the main hydrothermal minerals in the RWTH-1 drill core. Relative abundance of minerals is indicated by solid and dashed lines.

4.2.1 Quartz-carbonate \pm chlorite veins (D_1)

This abundant vein type is mineralised by quartz carbonate \pm chlorite assemblages. The quartz carbonate veins crosscut the Upper and Lower Devonian lithologies and textures (e.g stylolites, S_1 foliation). These veins vary in size from a few mm to >3 cm. They are composed of quartz coexisting with single calcite, or single dolomite and mixed calcite/dolomite grains (Figure 4.3 A and B). The carbonate grains mainly occur in the center of the vein as blocky, idiomorphic to hyidiomorphic crystals. Idiomorphic quartz grains mainly precipitated along the vein margins adjacent to the carbonate minerals. Quartz also precipitated as either single elongated crystals or as patches of blocky minerals intergrown with carbonates. Undulous extinction of quartz and carbonate grains, deformational twinning of carbonates and an initial stage of subgrain development in some of the quartz crystals can be observed. Where elongated chlorite occurs along the vein margins, the quartz and carbonates appear in the center of the veins. The larger fractures (up to 3 cm thick), which are filled with these mineral assemblages, are partially accompanied by k-feldspar and chalcopyrite.

4.2.2 Carbonate veins \pm chlorite (D_1)

The carbonate veins also crosscut the Upper and Lower Devonian textures (e.g stylolites, S_1 foliation) but are slightly smaller than the crosscutting quartz-carbonate veins. These veins vary in size from a few mm to >2 cm, composed of single calcite, or single dolomite and mixed calcite/dolomite grains. The calcite and/or dolomite crystals have idiomorphic to hyidiomorphic textures and also form xenomorphic (saddle-type, Figure 4.1 A) textures with the typical curved grain margins. The calcite and/or dolomite crystals show the development of twin planes. Under cathodoluminescent light, the carbonates are red to yellowish luminescent, due to their iron content. Undulous extinction of calcite and dolomite grains, syntaxial vein forming and deformational twinning can be observed. Where elongated chlorite occurs mainly on vein margins the carbonates appear in the center of the veins. Fractures up to 2 cm thick are filled with these blocky carbonates and coexisting chlorites (Figure 4.3 C, D, and E). They are partially accompanied by K-feldspar and chalcopyrite.

4.2.3 Quartz veins \pm chlorite (D_1)

The crosscutting relationships of quartz veins are similar to those of the other vein types. They are also slightly smaller than the crosscutting quartz-carbonate veins and variable in size from mm scale to >2 cm wide (Figure 4.3 F and G). The microstructure of quartz varies, depending on the intensity of deformation of the veins. The quartz veins are either composed of blocky, $\sim 200\ \mu\text{m}$ large crystals or of elongate < 500 to $200\ \mu\text{m}$ large crystals, irregular shaped crystals of $< 50\ \mu\text{m}$ and stretched crystal structure $\sim 200\ \mu\text{m}$ large (Figure 4.3 F). The latter subgrains are mainly developed at the grain boundaries of the elongated quartz minerals or along fibrous micro shears. An initial stage of subgrain development in some of the quartz crystals can be observed. The recrystallised quartz grains have straight grain boundaries and show subgrain rotations. Fractures up to 2 cm thick filled with these quartz assemblages and chlorites, partially accompanied by K-feldspar and chalcopyrite.

4.2.4 Chlorite paragenesis and alteration

Chlorite is widely distributed in the Upper and Lower Devonian formations and is the third most abundant mineral in the different veins. Chlorite is closely intergrown with quartz or carbonate and partial with K-feldspar and sericite in shear veins and slickensides. Chlorite occurs mainly on vein margins and coexisting quartz and carbonates grains appear in the center of the veins. These relationships indicate that quartz, carbonates and chlorite are formed contemporaneously. The chlorite crystals are up to $200\ \mu\text{m}$ long and have grown towards the center of the veins in a radial pattern, chlorite alteration halos of small crystals $< 5\ \mu\text{m}$ extending laterally a few millimetres into the host rock (Figure 4.3 C and E). Asymmetric pressure fringes of fibrous to elongated chlorites can be observed locally. The different crosscutting veins are associated with mm-scale alteration halo consisting mainly of chlorite, but also dolomite, K-feldspar, smectite and plagioclase. This mineral assemblage corresponds to an early alteration phase.

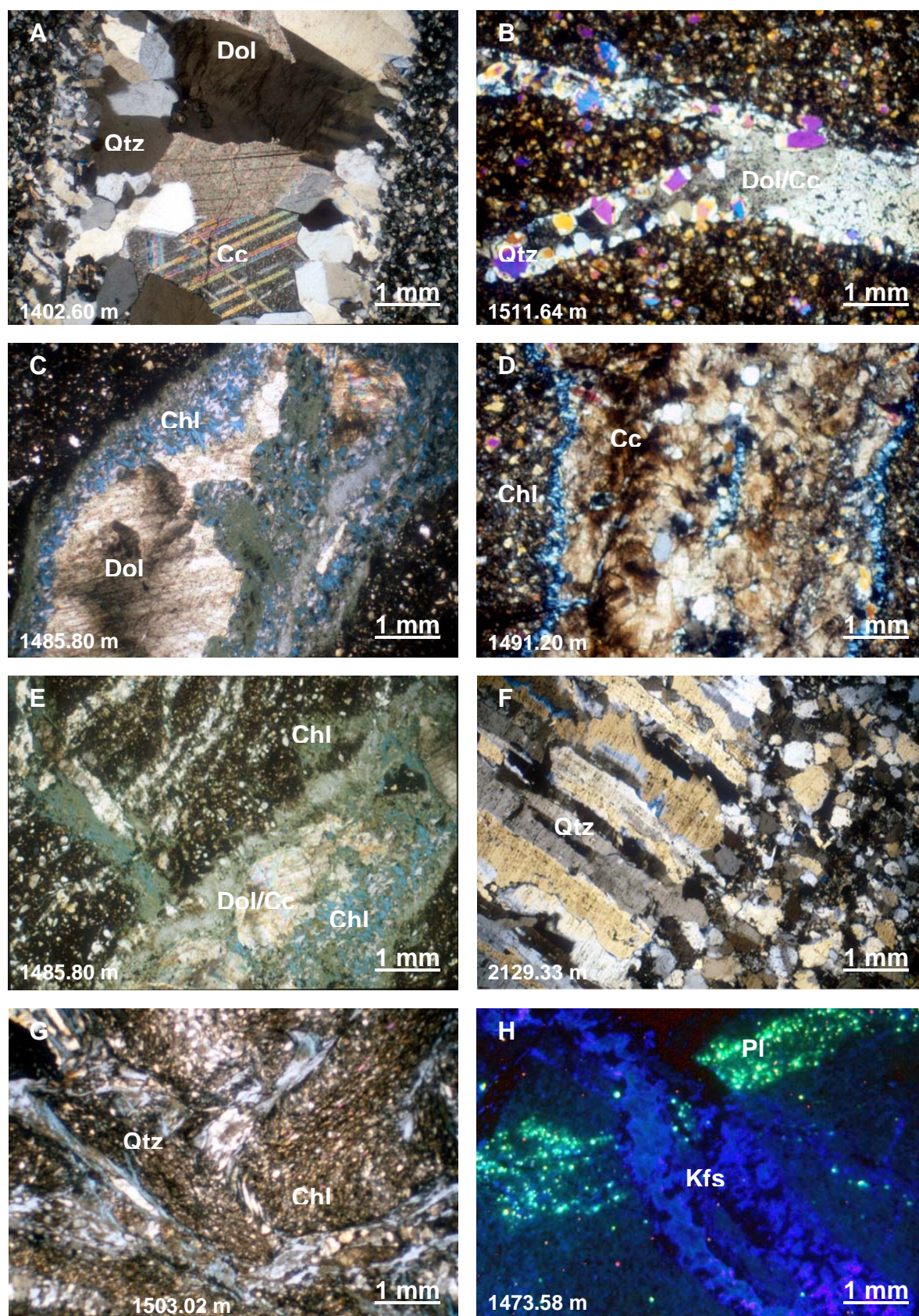


Figure 4.3: Photomicrographs of different vein types: (A) and (B) quartz-carbonate ± chlorite veins, (C), (D) and (E) carbonate ± chlorite veins, (F) and (G) quartz ± chlorite veins, and (H) K-feldspar vein under cathodoluminescent light.

4.2.5 Chlorite-sericite-K-feldspar paragenesis

Chlorite-sericite-K-feldspar-plagioclase paragenesis can locally be observed and occurs in shear veins, slickensides and filled micro-cracks, which are commonly deformed (Figure 4.4 G and H). The vein forming minerals consist of fine grained chlorite (maximal 60 wt. %), K-feldspar (maximal 40 wt. %) and sericite up to 10 wt. %. Additionally, small amounts of plagioclase and chalcopyrite are precipitated contemporaneously with the hydrothermal vein minerals. The chlorite crystals are up to 50 μm long and with respect to their optical characteristics and chemical composition similar to the chlorites associated with quartz-carbonate, carbonate and quartz veins. The K-feldspar grains are up to 100 μm long and clearly identifiable under cathodoluminescent light due to their distinct blue colouring (Figure 4.2 H). The very fine grained sericite is distributed between chlorite and K-feldspar. These assemblages are considered to reflect low fluid-rock interaction and have formed in close approach to equilibrium with the infiltrated hydrothermal fluid. This is supported by the petrological observation that alteration zones reach only a few millimeters into the host rock (Böhlke 1989; Mueller and Groves 1991).

4.3 Deformation Patterns

The thin veins (1mm – 3 cm) are developed in shear and extensional fractures within the compressional field of the Variscan thrust front. There are many indications that veins have formed during faulting and shearing of the rocks. They are very frequent in the bedded to massive Lower and Upper Devonian lithologies. The veins show a lenticular to sigmoidal shape and usually post-date bedding and stylolites (pressure solution seams). Extensional veins containing idiomorphic grains (Figure 4.3 A and B) and shear veins containing xenomorphic grains (Figure 4.3 E and G). Shear fractures show normal and reverse faulting. Extensional veins with syntaxial vein forming mechanisms, indicates different rates of opening versus crystal growth. The veins completely fill fractures and are commonly deformed (Figure 4.4). All veins mutually crosscut each other and show stretched crystals. Volumetrically the most important fractures system is characterised by a very regular and dense network, often displaying conjugate and sigmoidal vein systems (Figure 4.3 A,

4.6), which are linked with the (>1 cm) extension and thin (<1 mm) shear veins. The geometric features indicate that the fractures formed during faulting (see also Ramsay and Humber, 1987).

Vein structures are formed at the transition from brittle to ductile deformation. Brittle to ductile deformation is indicated by dilational jogs, tension gashes and pseudotachylites. Seismic activities lead to the abundance on dilational jogs and the development of pseudotachylites (Sibson, 2001). Asymmetric pressure fringes at shear veins on fibrous to elongated chlorite grains indicate later deformation. Subsequent shearing of these veins caused by deformation, followed by recrystallisation resulted in finer grain size or polymodal size distribution. Ductile deformation is also indicated by the undulous extinction of the quartz and carbonate grains, deformation twinning of carbonates and an initial stage of subgrain development in some of the quartz crystals. The undulatory extinction and the development of curved twinning of the carbonate minerals can be related to the onset of intracrystalline deformation mechanisms (Burkhard, 1993). Mylonitic structures can also be observed on reactivated veins. The curved shapes of the veins suggest also a brittle to ductile failure mode during precipitation of the veins. It is characteristic of these different veins that their textures usually indicate that vein formation took place cyclically. From crosscutting relationships and relationships to the vein textures and structures mentioned above, generally it seems that all vein types formed contemporaneously during progressive deformation and that deformation took place episodically. Such vein characteristics are common in many fold-and-thrust belts (e.g. Dunne, 1986) and have been recently described by Micarelli et al., (2005).

Veins in tension gashes show a fibrous structure (Figure 4.4 A and B), a characteristic of a crack seal origin (Ramsey, 1980). There are several types of microstructures, which are important for the understanding of the veining mechanism. Curved and fibrous crystals with growth surfaces, tension gashes (Figure 4.4 B and C) and dilational jogs (Figure 4.4 D) point to shearing during growth of the grains, while quartz and carbonates in other veins show recrystallised structures. Insoluble residuum forming selvages on the vein margin within pelitic rocks (Figure 4.4 A and B) can partially be observed, suggesting a diffusional mechanism of mass transfer out of the wall rock (Oliver and Bons, 2001). Multiple reopening of the fractures is documented by bands of rock

fragment along the vein margin. Stretched crystal veins (Figure 4.4 D) are of the crack seal type and crystals have a roughly constant width across the vein. All textural/structural features of this type of vein suggest shear and extensional regimes during their formation within brittle to ductile deformation processes (e.g. Sibson, 2000).

Cathodoluminescence analyses of these veins show a more intense yellow to red partly zoned luminescence than the more yellow-brown luminescence of the host rock cements. The different luminescence of veins and wall rock suggests a different content of CL-activation elements (e.g. Budd et al., 2000) and therefore more chemical fluid-rock disequilibrium.

4.3.1 Pseudotachylite

Pseudotachylites are generally found in regional-scale shear zones at the transition from brittle to ductile deformation. Pseudotachylites develop from melts resulting from temperatures of up to 1800 °C during periods of high frictional force. In this case the host rock consists of clay, silt sized pelites and detrital quartz and K-feldspar. The pseudotachylite (1512.95 m) varies in diameter from 2-4 mm and consists of a dark matrix which encloses angular to rounded fragments of wall rock (Figure 4.4 E and F). It shows a sharp contact to the wall rock and indications of melting of white micas, as well as the corrosion of these minerals. The micas are preserved as thin cataclastic layers at the margins of the pseudotachylite. Within the pseudotachylite-matrix the quartz and K-feldspar porphyroclasts are corroded, but show non-melting conditions. Crystallisation of long elongated minerals (microlithe) of muscovite and biotite also occur in the matrix. As indicated by the XRD analyses the fine crystalline matrix recrystallised from a glass containing mainly quartz, K-feldspar, clinochlor, siderite and muscovite. The pseudotachylite as well as the different vein types are deformed later on. The coexisting relationship and the possibility to date the pseudotachylite provide the important information of the maximum age of the deformation event and hydrothermal fluid activity. The potassium content of minerals in the pseudotachylite was analysed using the EMPA. Quantitative analyses were performed on muscovite, biotite and K-feldspar. The measurements indicate 9–11 wt. % potassium in muscovite minerals, 6-9 wt. % potassium in biotite and 17 wt. % potassium in K-feldspar minerals.

The element mapping of the matrix in context with the quantitative analyses shows a general distribution of the potassium content around 5 to 10 vol. %.

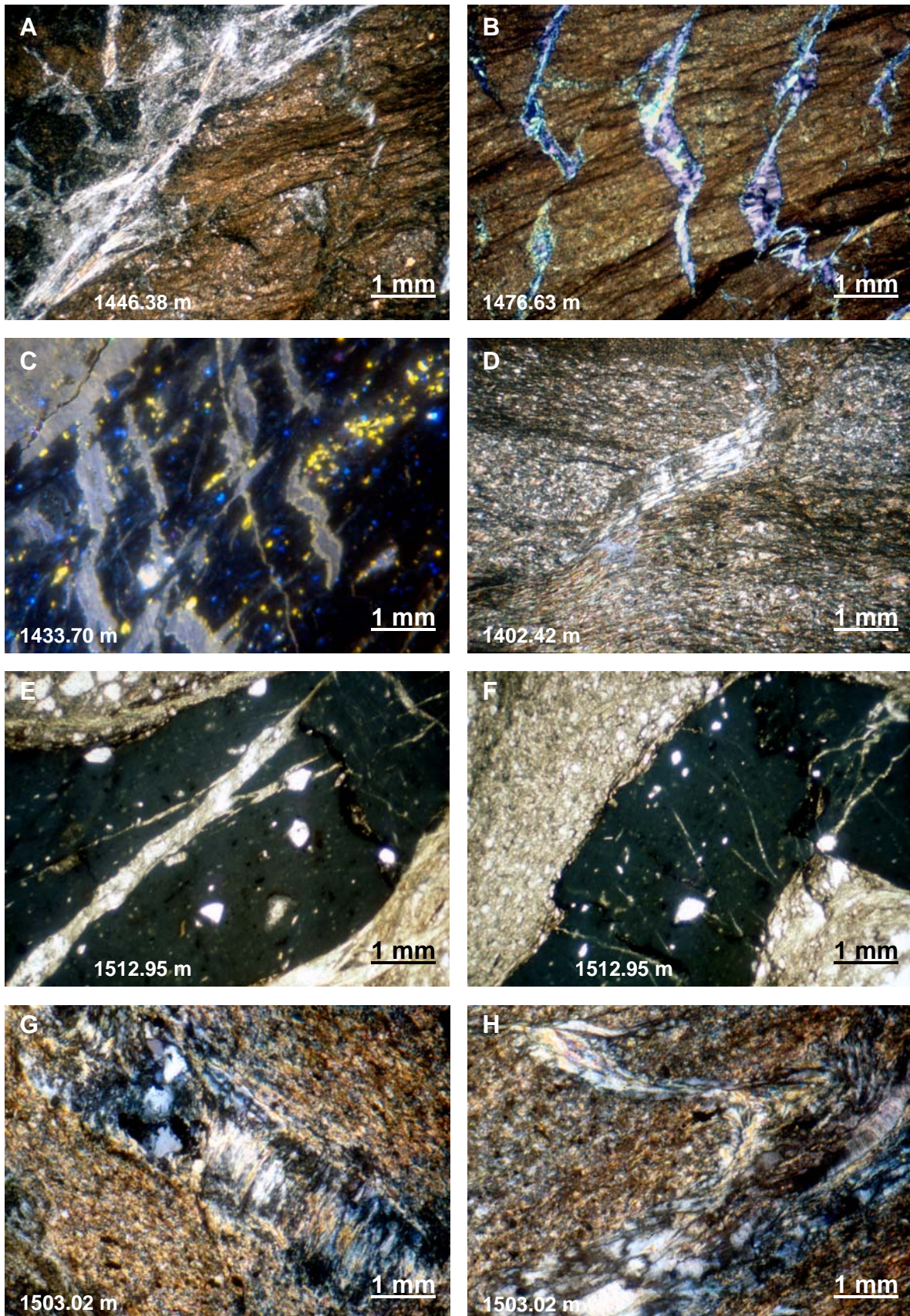


Figure 4.4: Deformation pattern within different lithologies: (A) shear veins consisting of quartz/K-feldspar/chlorite and brecciation crosscutting foliation, (B) tension gashes consisting of quartz/chlorite crosscutting foliation, (C) tension gashes consisting of quartz showing zonation under cathodoluminescent light, note also K-feldspar and calcite cements, (D) dilational jog consisting of stretched quartz grains, (E) and (F) pseudotachylites consists of a dark matrix which encloses angular to rounded fragments of the wall rock, and (G) and (H) shear veins of chlorite-sericite-K-feldspar-plagioclase paragenesis.

4.4 Variscan (D_1) Deformation and Post Variscan (D_2) Deformation

The textures of the veins usually indicate that vein formation took place episodically. Veins in some places form a very regular and dense network, often displaying conjugate systems (Figure 4.6). The veins studied here formed during the Variscan D_1 deformation. In contrast, post-Variscan (D_2) veins are undeformed and show fibrous mineral growth (Figure 4.7; pers. com. Ph. Muchez). Therefore the vein forming conditions of the hydrothermal overprint represent the situation during thrusting and hydrothermal fluid flow along the MAT at around 380 – 290 Ma (Walter, 1995).

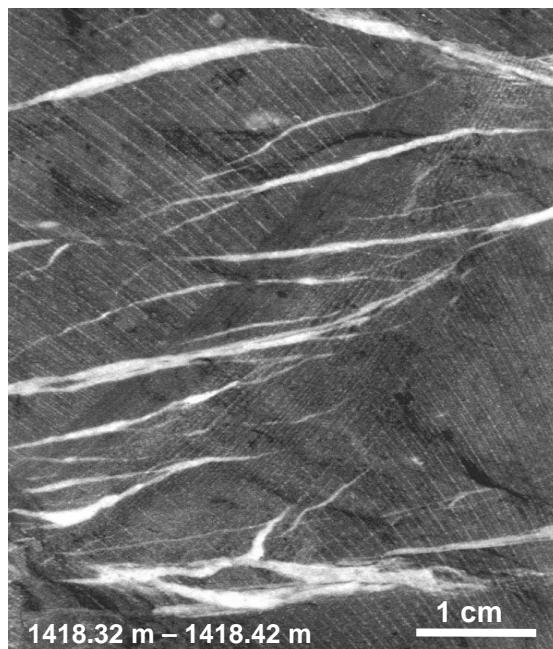


Figure 4.5: Photograph of clay-silt sized, grey pelites of the RWTH-1 drill core. Note the deformed quartz-carbonate \pm chlorite veins developed during Variscan (D_1) deformation.

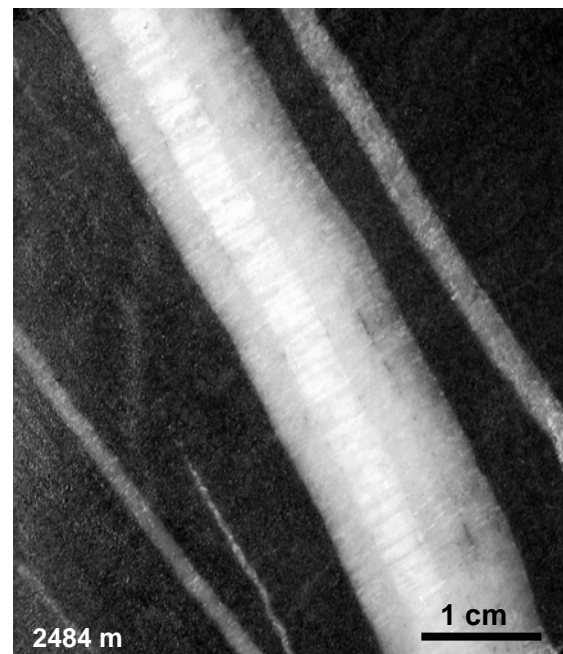


Figure 4.6: Photograph of siltstone matrix of the Bolland drill core. Note the undeformed fibrous mineral growth of the quartz vein developed during post Variscan (D_2) deformation.

4.5 Geothermometry

4.5.1 Calcite-dolomite and chlorite

Temperature calculations based on the mineral composition of the vein calcite-dolomite pairs were performed using the EMPA. The calcite-dolomite geothermometer was applied uses the Fe-Mg exchange between calcite and dolomite in the system CaCO_3 , MgCO_3 and FeCO_3 (Powell et al., 1984). The resulting temperatures range from 280-370 °C (Figure 4.5 A).

The chlorite geothermometers, after Walshe (1986), Chathelineau and Nieva (1985) and Zang and Fyfe (1995), were carried out on chlorite from the different vein types, slickensides, and alteration halos (Table 9.2). The mineral compositional data on chlorites were measured with the electron microprobe. Resulting temperatures are shown in Figure 4.5 B. In the thermodynamic model of Walshe (1986), the composition of the chlorites is described in a six-component solid solution system which allows the calculation of temperature at known pressures. Chathelineau and Nieva (1985) concluded that the number of Al-atoms in the tetrahedral positions in chlorites (Al^{IV}) is positively correlated with temperature. Calculated temperatures of the chlorites in the veins, slickenside, and alterations halos are all in the same range from 290 - 350 °C and in average about 310 °C. According to the classification scheme of Hey (1954), all chlorites plot in the ripidolite field. In the Bolland drill chlorite is closely intergrown with quartz in shear veins associated with the MAT (Schroyen and Muchez, 2000). The calculated precipitation temperature of the chlorite is around 310°C (Zhang et al., 1997); this temperature corresponds to the investigated geothermometers of the RWTH-1 drill.

Chlorite geothermometers are strongly dependent on other parameters, such as different temperatures, coexisting mineral assemblages, $\text{Fe}/(\text{Fe}+\text{Mg})$, or bulk rock composition/mineralogy (De Patrice et al., 1993). These authors found that chlorite geothermometers should be used with caution and only in combination with alternative methods of estimating palaeotemperatures. In this study further methods of estimating palaeotemperatures were used, such as fluid inclusion homogenisation temperatures (see chapter 5) and stable isotope geothermometers (see chapter 6).

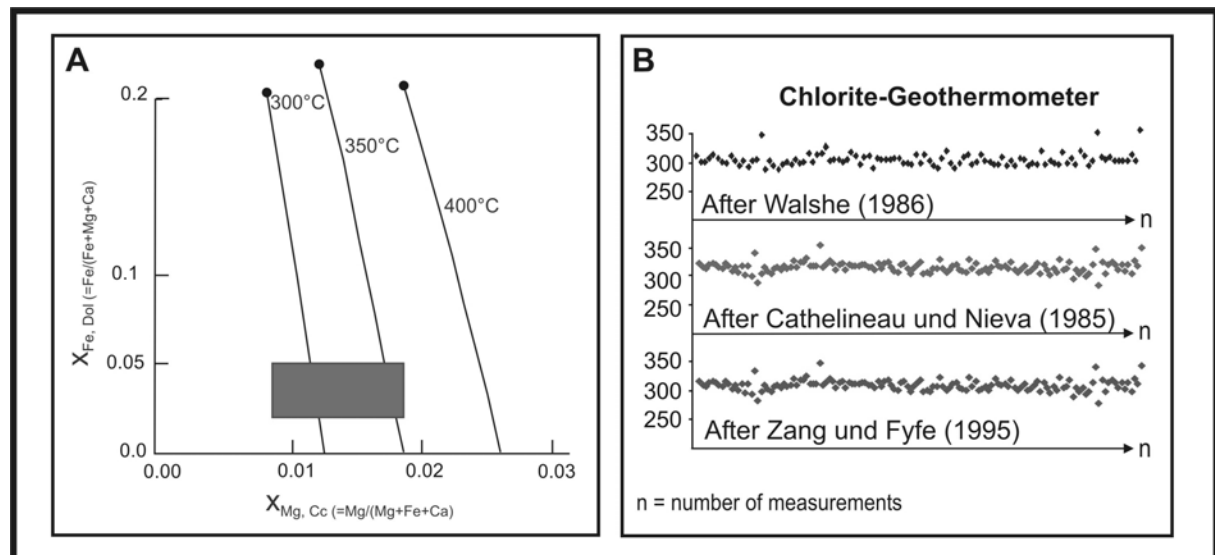


Figure 4.7: Diagram A, a plot of $X_{\text{Fe,Dol}}$ versus $X_{\text{Mg,Cc}}$ show the predicted curves for 300°C, 350°C, and 400°C, for equilibrium between calcite and dolomite (Powell et al., (1984)). The shaded field depicts the estimated calcite-dolomite thermometer in the system CaCO_3 , MgCO_3 and FeCO_3 . Diagram B, results of chlorite geothermometry with different calibrations.

4.6 Summary

The siliciclastic rocks from the various stratigraphic levels and the Upper Devonian carbonate marl and limestone contain detrital quartz, K-feldspar, biotite and plagioclase and are in some places enriched in white micas and chlorite. Partial pervasive dolomitisation of the rocks is ubiquitous. Chemical compaction formed dissolution seams and stylolites. Chemical compaction and deformation formed a S_1 foliation. Late diagenetic features are overprinted by the S_1 foliation within the siliciclastic, argillaceous and calcareous rocks. During the Variscian time the main deformation D_1 forming a S_2 foliation, crosscuts the S_1 foliation. The different rock types are partially brecciated.

One major thrust fault of the MAT intersects the drill core from 1516 m to 1391 m, indicated by the abundance of veins and cataclastic to mylonitic deformation structures. The textural and structural vein observation identified one major deformation event. Vein structures are formed at the transition from brittle to ductile deformation, indicated by dilational jogs, tension gashes and pseudotachylites. Seismic activities lead to the abundance of dilational jogs and the development of pseudotachylites. Subsequent shearing of these veins caused

by deformation, followed by recrystallisation resulted in finer grain size or polymodal size distribution.

Brittle deformation controlled the fluid transport and the hydrothermal alteration of the wall rocks. The different vein systems are characterised by shearing and are associated with a Variscan thrust fault. The vein forming conditions described here represented the situation during thrusting and hydrothermal fluid flow along the MAT, indicating a Variscan age.

Temperature calculations based on the mineral composition of vein chlorite and vein calcite-dolomite pairs were used in this study. The calculated temperatures from calcite-dolomite pairs range from 280 - 370°C. The chlorite geothermometers were carried out on vein chlorite, slickensides, and alteration halos. The estimated temperatures of the chlorites range from 290 - 350°C.

5 Fluid Inclusions

The principal aim of fluid inclusion studies is to determine the physicochemical parameters and the composition of palaeofluids. This data permits the identification and the characterisation of distinct fluid compositions and may provide implications for the fluid origin and the reconstruction of the thermal evolution. Fluid data in conjunction with hydrothermal vein, hydrothermal alteration and host rock data provide additional constraints on fluid rock interaction and accompanying P-T conditions. This investigation is concentrated on the fluid inclusions from the different vein types (i.e. quartz-carbonate, carbonate, and quartz veins; \pm chlorite), which are associated with the progressive deformation (D_1) process. Microthermometric measurements of fluid inclusions were performed on doubly polished, 60 to 100 μm thick sections using a modified USGS cooling-heating stage. A total of 45 doubly polished thick sections were examined, 15 of which were selected for further analyses by pyrolysis – gas-chromatography / mass-spectrometry (Py-GC/MS), the compositions of the fluid inclusions were then determined qualitatively and semi-quantitatively using an external one-point calibration generated from a reference gas mixture.

5.1 Fluid Inclusion Petrography

In all vein types, the fluid inclusions in quartz and carbonate grains are mainly transparent, H_2O -rich (Type I) inclusions. The classification of the fluid inclusion types following that of Roedder (1971). The majority of the inclusions are two phase liquid-vapour fluid inclusions. The volume fraction of the vapor phase was estimated at ambient P-T conditions and varies between 15 – 50 Vol. % with a mean value around 35 Vol. %. In quartz and carbonate grains, dark monophasic inclusions can also be observed and are associated with the aqueous inclusions. The darker inclusions are Type II vapour rich (i.e. low density) inclusions, but are too dark to be analysed by microthermometry. However, gas-chromatography identified CO_2 , CH_4 and N_2 gas bearing fluid inclusions within the vein minerals (Figure 5.6).

Fluid inclusion trapping were classified by their position within the different vein systems and minerals to fluid inclusion groups (i.e. primary fluid inclusions). The

fluid inclusion assemblages (FIA) of primary inclusions occur in growth zones (visible due to trapped fluid inclusions) and zonations (variation in the chemical composition) of carbonates and along grain boundaries in quartz grains. These fluid inclusions are dominant in the hydrothermal vein minerals. The FIA of pseudo-secondary inclusions were trapped as clusters and intra-granular trails within the minerals. Furthermore, secondary inclusions appear as trans-granular trails in quartz. Primary and/or pseudo-secondary fluid inclusions can locally be observed together with secondary inclusion. Most of the fluid inclusions are less than 15 μm in length, however, inclusions larger than 25 μm were only nearby observed.

5.1.1 Quartz-carbonate veins

Fluid inclusion in quartz-carbonate veins were investigated in quartz, dolomite, and calcite grains. The transparent, H_2O -rich inclusions are two phase liquid-vapour fluid inclusions. The fluid inclusions in quartz grains occur as primary fluid inclusions along grain boundaries and as pseudo-secondary inclusions trapped in clusters within the minerals (Figure 5.2 A, B and C). They are varying in size from 6 to 20 μm and have an irregular to negative crystal shape. The fluid inclusions in carbonate grains occur mainly as primary fluid inclusion along growth zones and zonations, but also as pseudo-secondary inclusions trapped as clusters within the minerals. In many cases dolomite and calcite grains show growth zones due to the abundance of trapped fluid inclusions within the grains (Figure 5.2 D and E). They vary in size from 4 to 15 μm and have an irregular to negative crystal shape. Secondary fluid inclusions appear as trails in recrystallised quartz grains at the vein margin and cross cut grain boundaries. They are varying in size from 6 to 20 μm and have an irregular to oval shape.

5.1.2 Carbonate veins

Fluid inclusions in carbonate veins were investigated in dolomite and calcite grains. The transparent, H_2O -rich inclusions are mainly two phase liquid-vapour fluid inclusions. The dark, monophasic inclusions are present in all of the different vein systems and appear to be particularly abundant here. The inclusions within the carbonate grains occur only as primary fluid inclusions

along grain boundaries, in growth zones and zonations. They are varying in size from 4 to 20 μm and have an irregular to negative crystal shape. Zonations were observed under cathodoluminescent light (Figure 5.1). In many cases growth zones can be observed due to the distribution of trapped inclusions within dolomite and calcite grains (Figure 5.2 D and E).

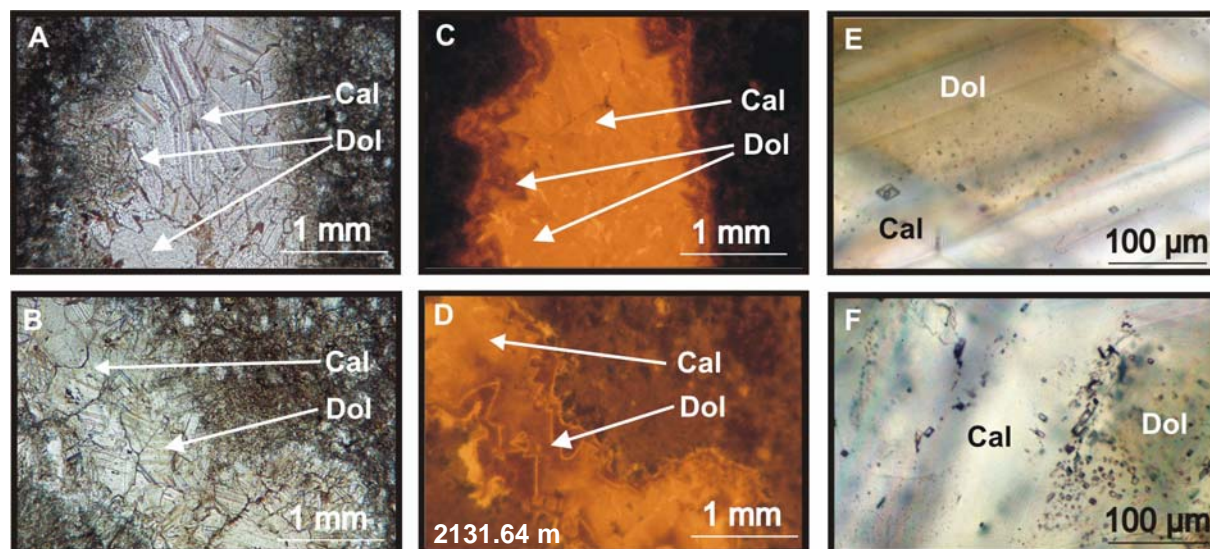


Figure 5.1: Photomicrograph (A+B) and cathodoluminescent-photomicrograph (C+D) of vein forming calcite and dolomite. Photomicrograph of primary fluid inclusions (E+F) distributed along zonation.

5.1.3 Quartz veins

Fluid inclusion in quartz veins are transparent, H_2O -rich inclusions. The majority of the inclusions are two phase liquid-vapour fluid inclusions. The fluid inclusions in quartz grains occur as primary fluid inclusion along grain boundaries (Figure 5.2 G). They are varying in size from 6 to 20 μm and have an irregular to negative crystal shape. The pseudo-secondary inclusions are trapped as clusters and intra-granular trails within the minerals. The intra-granular trails are orientated perpendicular or parallel to the elongation of the grains and occur in blocky/fibrous quartz veins (Figure 5.2 F). They are varying in size from 4 to 15 μm and have an irregular to oval shape. Secondary fluid inclusions appear as infrequent trans-granular trails (Figure 5.1 H). The trans-granular trails are randomly orientated containing small ($< 10 \mu\text{m}$) inclusions and occur in blocky to fibrous quartz veins or recrystallised quartz grains at the vein margin.

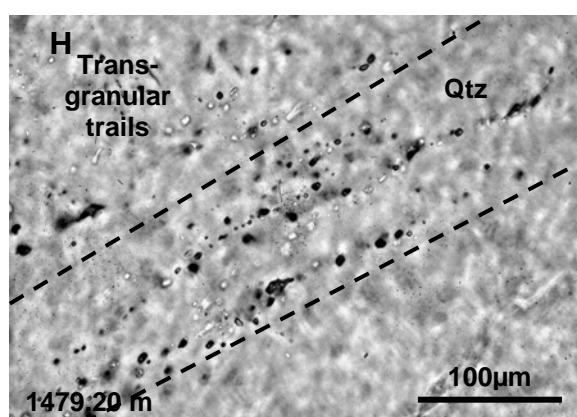
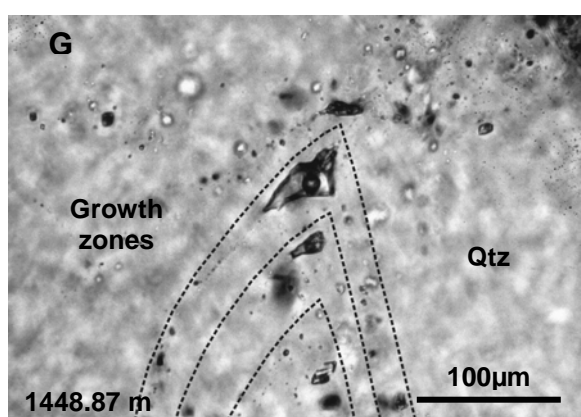
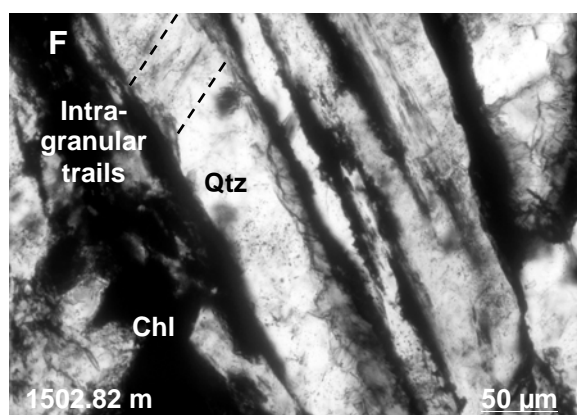
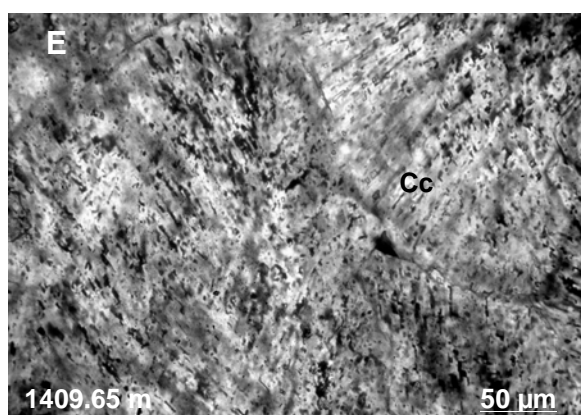
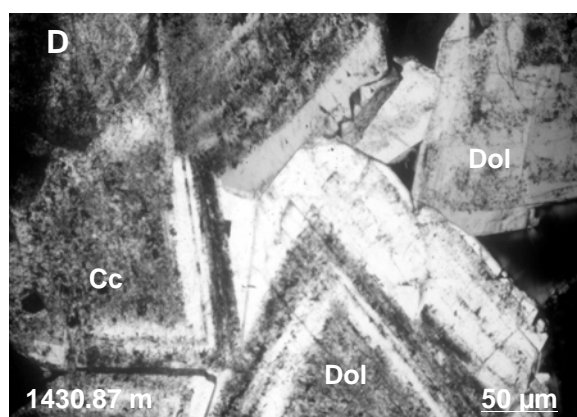
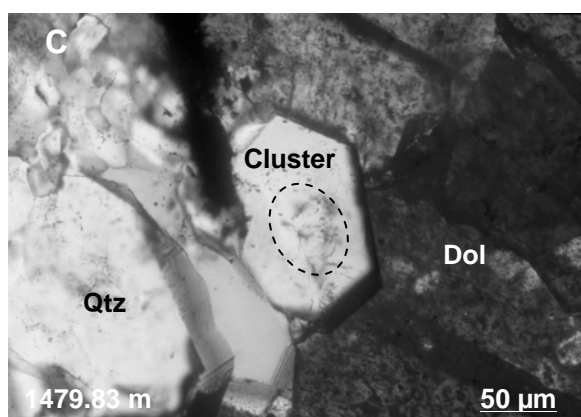
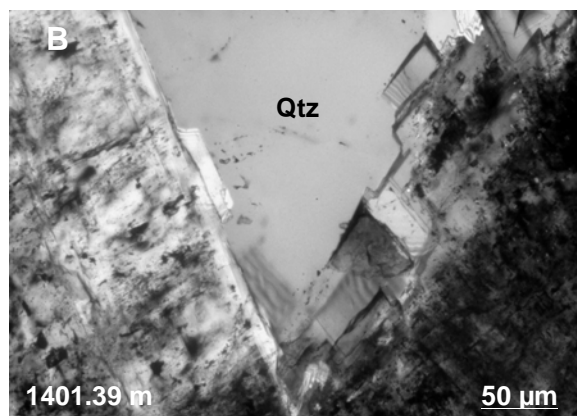
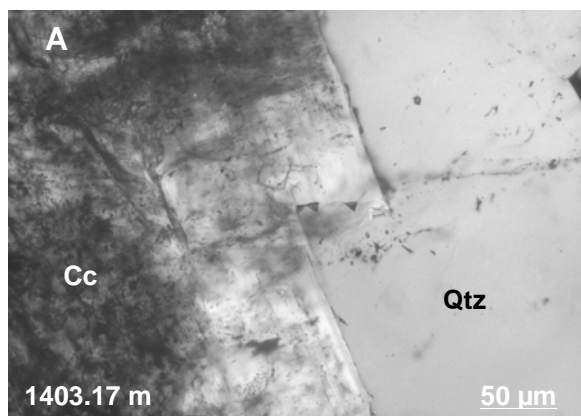


Figure 5.2: Photomicrographs of fluid inclusions from different vein types: (A) and (B) show quartz-carbonate veins with abundant primary FIA (dark specs) in calcite/dolomite grains and primary FIA along grain boundaries in quartz grains; (C) primary (growth zones) and pseudo-secondary (cluster) FIA in dolomite and quartz grains of a quartz-carbonate vein; (D) and (E) carbonate grains of carbonate veins with growth zones, visible due to the abundance of trapped primary fluid inclusions; (F) intra-granular trails of pseudo-secondary FIA perpendicular to a quartz grain surrounded by chlorite; (G) primary FIA along grain boundaries in quartz grains of a quartz vein; and (H) same vein type with secondary FIA along trans-granular trails in quartz grains.

5.2 Fluid Inclusion Microthermometry

The investigated two phase liquid-vapour fluid inclusions always homogenised to the liquid phase. The fluid inclusions assemblages (FIA) show no expansion during cooling (especially for fluid inclusions in carbonate grains). On samples only containing aqueous inclusions the homogenisation temperature [Th] was first measured, followed by eutectic temperature [Te] and final melting temperature [Tm]. Microthermometry analyses of the two phase (L-V) fluid inclusions, from the different vein systems and fluid inclusion positions were recalculated using the H₂O-Na-(K)-Cl equation of Bowers and Helgeson (1985). A summary of microthermometric results is shown in Appendices, Table 9.4, 9.5, 9.6.

5.2.1 Quartz-carbonate veins

The homogenisation temperatures and salinities of primary inclusions in quartz of the quartz-carbonate veins range from 270 - 390°C and <4 - 9 eq.wt% NaCl respectively (Figure 5.3). The homogenisation temperatures and salinities of primary inclusions in carbonates of the quartz-carbonate veins range from 275 - 390°C and >4 - 9 eq.wt% NaCl. The majority of salinities from primary fluid inclusions are higher than normal seawater with 3.3 eq.wt% NaCl. Temperatures and salinities of pseudo secondary inclusions in quartz and carbonate grains are in the range from 230 - 250°C and <2 - 5 eq.wt% NaCl. The homogenisation temperatures of secondary inclusions in quartz of quartz-carbonate veins show temperatures between 180 - 210°C and have salinities from <2 - 6 eq.wt% NaCl. The temperature of eutectic melting from different fluid inclusion groups is similar. The measured [Te] ranges from -20 to -24°C and in some cases around

-11°C, indicates that these fluids have a H₂O-Na-(K)-Cl composition. A total of 173 fluid inclusions were investigated.

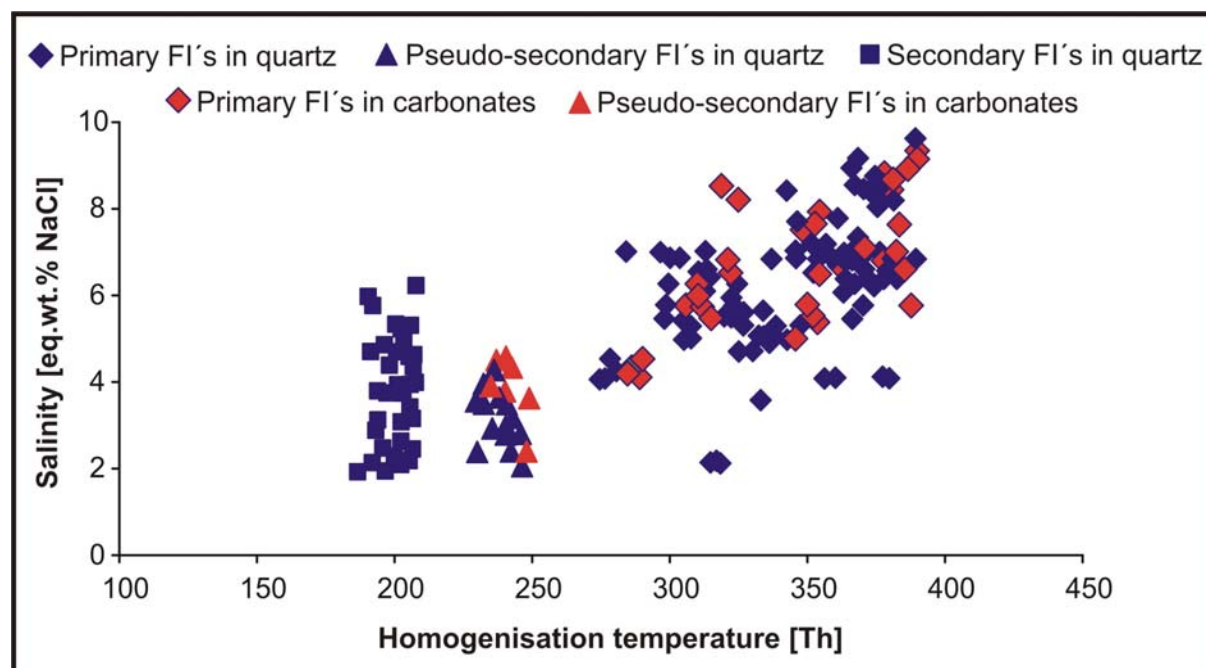


Figure 5.3: Diagram of salinity (eq.wt.% NaCl) versus homogenisation temperature (Th) of fluid inclusions in quartz and carbonate grains of the quartz-carbonate veins. Classified according to their position within the different minerals.

5.2.2 Carbonate veins

The homogenisation temperatures and salinities of primary inclusions in carbonates of the carbonate veins range from 200 - 370°C and <1 - 6 eq.wt% NaCl respectively (Figure 5.4). The majority of salinities from primary fluid inclusions in dolomite and calcite are higher than normal seawater with 3.3 eq.wt% NaCl. Temperatures and salinities of primary inclusions in dolomite from carbonate veins are measured at [Th] 260 - 370°C and >2 - 6 eq.wt% NaCl. The homogenisation temperatures of primary inclusions in calcite grains from carbonate veins have temperatures between 200 - 310°C and salinities from <1 - 6 eq.wt% NaCl. FIA within dolomite grains have higher max. temperatures up to 370°C as the FIA in calcite grains with max. [Th] up to 310°C. Homogenisation temperatures between 260 - 310°C were measured in dolomite and calcite grains. The arrangement of fluid inclusion temperatures and salinities bear a resemblance to growth zones and zonations of those minerals. Thereby the temperatures and salinities in dolomite grains increase towards the center of

the grain from one growth zone or zonation to the other. The same observation can be made for the calcite grains (Figure 5.2 D). The measured temperature of eutectic melting from the primary fluid inclusions of around -21°C , indicates that these fluids have a $\text{H}_2\text{O}-\text{Na}-(\text{K})-\text{Cl}$ composition. A total of 45 fluid inclusions were investigated.

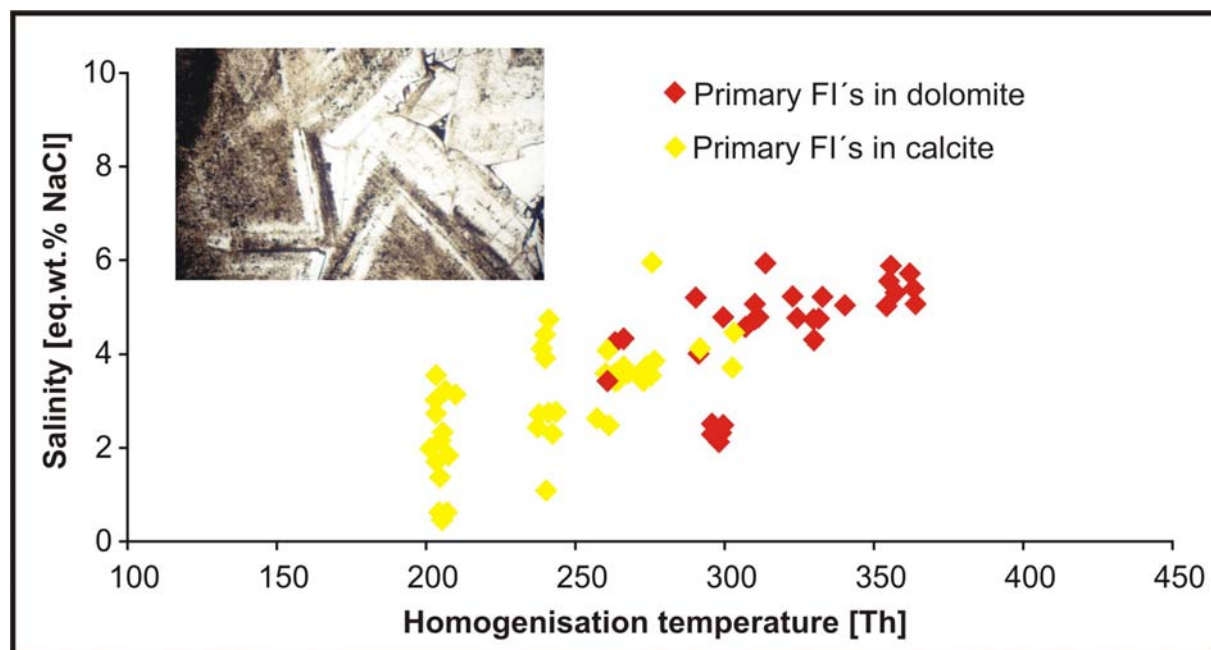


Figure 5.4: Diagram of salinity (eq.wt.% NaCl) versus homogenisation temperature (Th) of fluid inclusions in dolomite and calcite grains of the carbonate veins, classified according to their position within the different minerals. The picture in the upper left corresponds to Figure 5.2 D.

5.2.3 Quartz veins

The homogenisation temperatures and salinities of primary inclusions in quartz of the quartz \pm chlorite veins range from 270 - 390°C and >2 - 6 eq.wt% NaCl respectively (Figure 5.5). Temperatures and salinities of pseudo secondary inclusions in quartz grains are in the range from 250 to 260°C and <4 - 5 eq.wt% NaCl. The homogenisation temperatures of secondary inclusions in quartz grains show temperatures between 190 and 210°C and have salinities from 2 - 4 eq.wt% NaCl. The homogenisation temperatures and salinities of secondary inclusions in quartz grains of the quartz veins without chlorite in paragenesis range from 180 - 220°C and <4 - 8 eq.wt% NaCl. The measured temperature of eutectic melting from different fluid inclusion groups of around -

21°C, indicates that these fluids have a H₂O-Na-(K)-Cl composition. A total of 43 fluid inclusions were investigated.

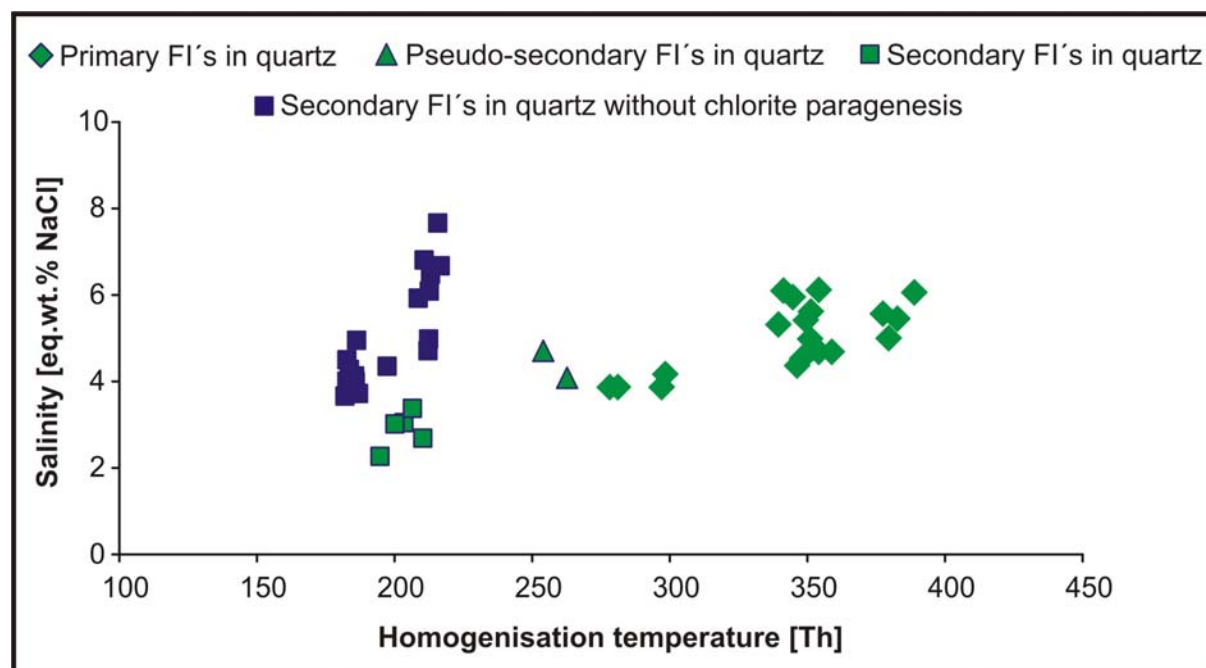


Figure 5.5: Diagram of salinity (eq.wt.% NaCl) versus homogenisation temperature (Th) of fluid inclusions in quartz grains of the quartz veins. Classified according to their position with in the different minerals.

5.3 Fluid Inclusion Pyrolysis-Gas Chromatography-Mass Spectrometry

Gas bulk composition of trapped fluid inclusions in quartz and carbonates from several depths of different vein types, were analysed by pyrolysis - gas-chromatography / mass-spectrometry (Py-GC/MS). A quadropul mass spectrometer linked with a gas chromatograph was online coupled with a pyrolysis unit. The pyrolysis unit was loaded with a quartz tube containing peaces (<2 mm) of fluid inclusion thick sections. Gas chromatographic separation was carried out on a Carboxen 1010 PLOT fused silica capillary column with Helium as carrier gas. The mass spectrometer was operated by scanning from 15 to 50 m/z at a scan rate of 1 s/decade with a source temperature of 200°. Fluid inclusion compositions were determined qualitatively and semi-quantitatively using an external one-point calibration generated from a reference gas mixture (CO₂, CH₄ and N₂; 1:1:1 v:v:v). The analytical results reveal that the main component of the solution is H₂O, with smaller amounts of CH₄ and N₂, relative to CO₂ (Figure 5.6). CO₂, CH₄ and N₂ are present in variable

ratios but carbon dioxide generally becomes the main volatile component. Therefore the fluids are H_2O -Na-(K)-Cl-dominant solutions containing the gases CO_2 , CH_4 and N_2 .

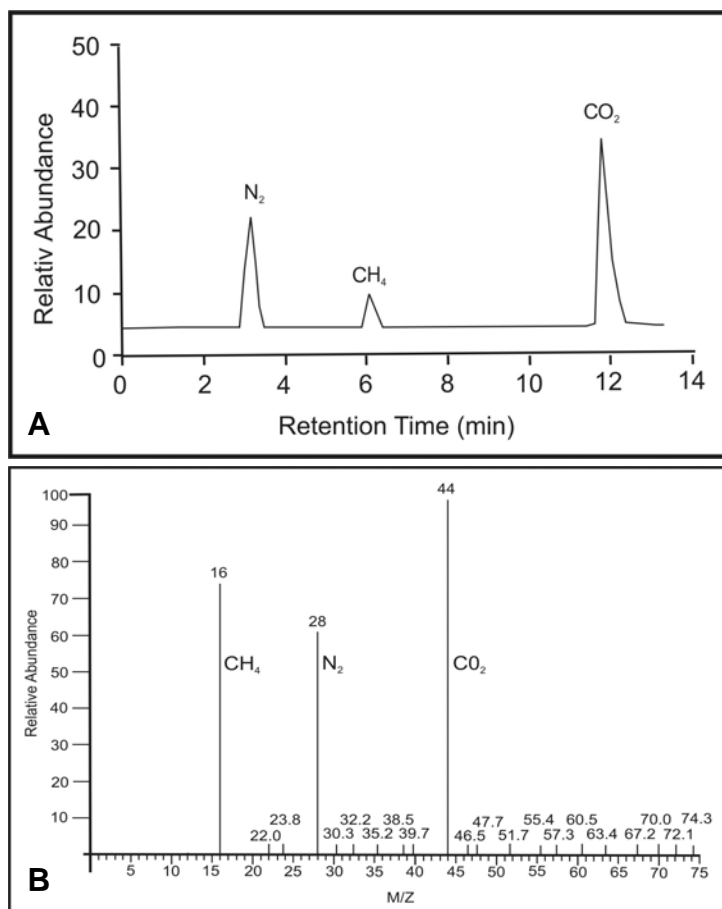


Figure 5.6: (A) Gas-chromatogram with retention time versus relative abundance of gases included in fluid inclusions of a quartz-carbonate vein, and (B) mass-spectrogram of the same sample.

5.4 Interpretation

5.4.1 Fluid inclusion trapping processes

The integration of the data obtained by petrographic, microthermometric and gas-chromatographic analyses of fluid inclusions describe a fluid trapped during progressive deformation. The hydrothermal fluid is characterised by the H_2O -(CO_2 - CH_4 - N_2)-Na-(K)-Cl water dominated system. The fluid inclusion groups occur from relatively high temperature and salinities (i.e. primary FI's) over intermediate (i.e. pseudo-secondary FI's) to relatively low temperature and salinities (secondary FI's).

Different stages of fluid inclusion trapping can be classified: Primary and pseudo-secondary inclusions display a fluid trapping during early/syn-vein

crystallisation and secondary fluid inclusions display a fluid trapping during late vein crystallisation, as indicated by the association of all different fluid inclusion groups within one crystal. Additionally, the values of homogenisation temperature fields around 200°C are found in secondary FI's in quartz grains and in primary FI's in calcite grains. The temperature range of 180 to 370 °C of primary fluid inclusions within the carbonate grains could be explained by the more ductile behaviour of carbonate minerals. In contrast, the lower temperatures of secondary fluid inclusions in quartz grains could be explained by the more brittle behaviour of quartz minerals and their trapped fluid inclusions. Based on composition and salinities, secondary fluid inclusion are very similar to primary and pseudo-secondary inclusions and trapping occurred during the same fluid flow episode (i.e. growth of veins and fracturing) during progressive deformation.

The relationship of the vapor fraction and gas composition of fluid inclusions can be related to a water-dominant system, indicating no boiling of the fluid. However, the narrow interval of homogenisation temperature and salinity suggest fluid unmixing conditions. In many cases the distinction between fluid unmixing and partial mixing is reported to be difficult and it is likely that both processes could take place almost simultaneously (e.g. Anderson et al. 1992, Touray 1987). An unrevised hydrothermal fluid is supported by the absence of post trapping modifications such as leakage or necking down features of the investigated fluid inclusions. Even the secondary inclusions show no modifications/or decrepitation during heating up to 400°C.

Real trapping P-T conditions for fluids are more difficult to obtain, since the homogenisation temperatures indicate only the minimum trapping conditions.

5.4.2 Fluid inclusion isochores and P-T-path

The relationship between pressure, temperature and bulk density of fluid inclusions can be calculated with the MacFlinCor software (Brown, 1989). This calculation is based on the equation of state for H₂O-Na-K-Cl, after Bowers and Helgeson (1985). Using the homogenisation temperature, the salinity, and the density a first estimate of the minimum and maximum trapping temperature and pressure of the fluid inclusions can be obtained. The densities of the fluid inclusions are the straight relationship to the pressure. Resulting isochores are

calculated from primary, pseudo-secondary and secondary fluid inclusions in different veins and minerals. Figure 5.7 presents the calculated P-T conditions for trapping of distinct fluid inclusion groups of the hydrothermal vein systems.

The homogenisation temperatures of primary fluid inclusions in quartz and carbonate grains of the quartz-carbonate veins range from 270 to 390°C, the densities varies (independent of degree of filling) between 0.57 and 0.86 g/cm³, and salinities range from 4 to 8 eq.wt% NaCl. Pseudo-secondary inclusions are trapped from 230 to 250°C, have densities between 0.75 and 0.89 g/cm³, and salinities from 2 to 5 eq.wt% NaCl. The temperatures of secondary fluid inclusions in quartz grains give trapping conditions from 180 to 210°C, a density about 0.90 g/cm³, and salinities from 2 to 6 eq.wt% NaCl (Figure 5.7 A).

The trapping temperatures of primary fluid inclusions in carbonate grains of carbonate veins given by the microthermometry are from 200 to 360°C, the densities varies between 0.69 and 0.88 g/cm³, and salinities from <2 - 6 eq.wt% NaCl (Figure 5.7 B).

The trapping temperatures of primary fluid inclusions in quartz grains of the quartz veins given by the microthermometry are from 270 to 390°C, the densities varies between 0.58 and 0.80 g/cm³, and salinities from >2 - 6 eq.wt% NaCl. Pseudo-secondary inclusions are trapped from 250 to 260°C, have densities between 0.81 and 0.83 g/cm³, and salinities from <4 - 5 eq.wt% NaCl. The temperatures of secondary fluid inclusions in quartz grains give trapping conditions from 180 to 220°C, densities from 0.90 to 0.93 g/cm³, and salinities from <4 - 8 eq.wt% NaCl (Figure 5.7 C).

Calculated bulk densities for the high temperature primary fluid inclusions in quartz and carbonate grains within the different veins are mainly between 0.7 and 0.9 g/cm³ and salinities between 3 and 7 eq.wt% NaCl. A trapping temperature of 250 - 500°C and trapping pressures between 0.5 and 2.5 kbar can then be calculated (Figure 5.7 D).

However, syn-vein (i.e. primary FI's) and late-vein (secondary FI's) fluid inclusion trapping conditions change the temperatures and salinity/density of the inclusions, causing the isochores of different inclusions to spread, leading to large temperatures and pressure ranges. Due to the co-eval entrapment of the different fluid inclusion groups (FIA), the high temperature primary inclusions are more suitable for a pressure correction, because the flat gradient of the isochores leads to a smaller error in terms of the entrapment pressure.

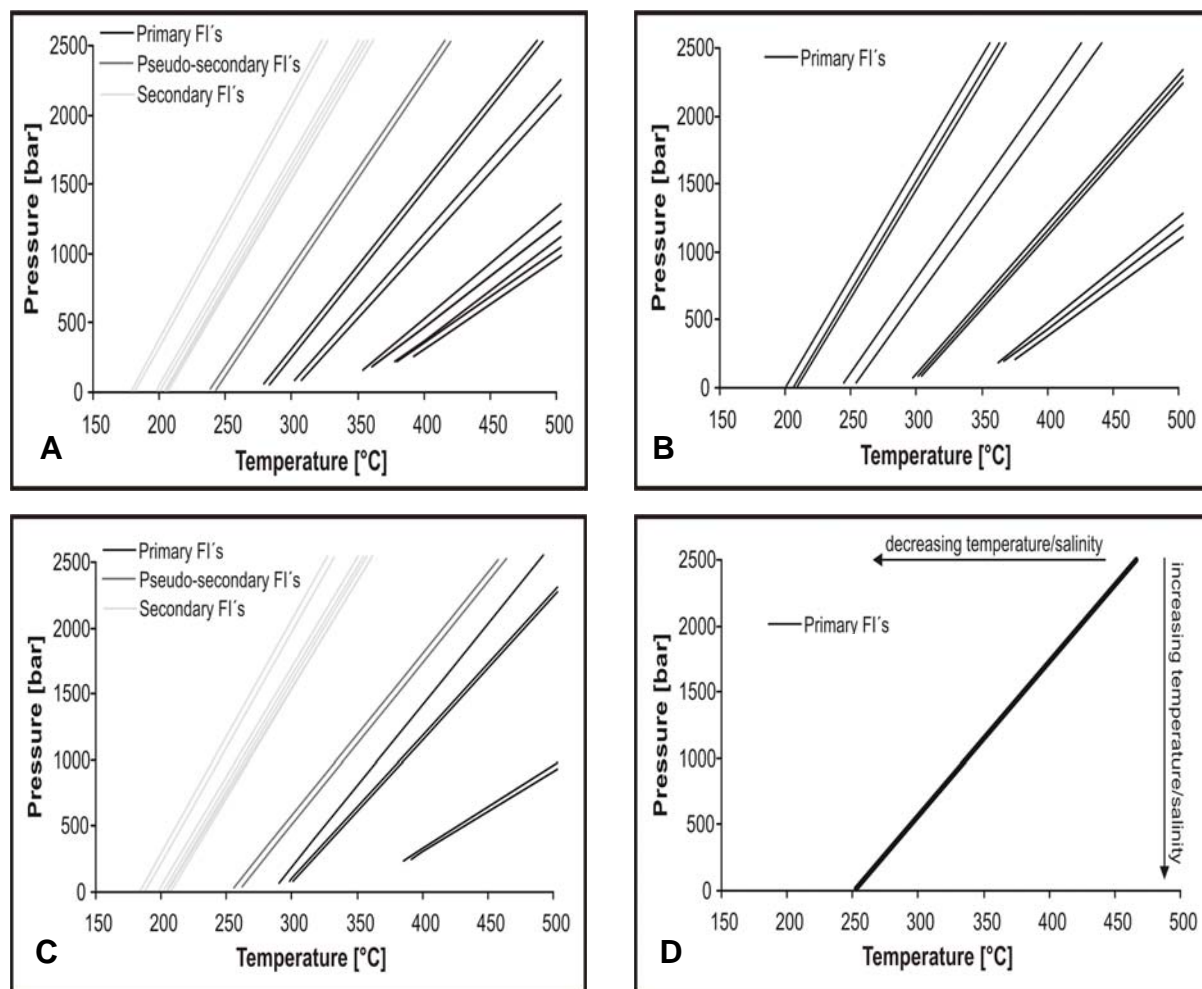


Figure 5.7: P-T diagrams show isochores with the minimum and maximum P-T conditions, calculated from fluid inclusion groups of (A) quartz-carbonate veins, (B) of carbonate veins, and (C) quartz veins. Note isochores of secondary inclusion have generally lower salinities/higher densities and lower temperatures leading to a higher gradient, whereas the primary FI's have higher temperatures and salinities/lower densities leading to flat gradients of the corresponding isochores. Diagram (D) show the isochore of the high temperature primary fluid inclusions of all the vein types.

The temperature calculated from the chlorite and calcite-dolomite geothermometers (see chapter 4.4) and stable isotope geothermometers of minerals (see Chapter 6.4.2), provide additional constraints if the minerals precipitated contemporaneously with the entrapment of fluid inclusions. If one fluid type is trapped at the same time and the same physicochemical conditions, the intersection of the isochores with another geothermometer gives the true P-T values of fluid trapping. The P-T correction of the isochores with the mineral geothermometers gives P-T values with pressures of up to 1.5 kbar and temperatures of up to 350°C of fluid inclusion trapping conditions. The P-T correction of the isochores with the oxygen isotope geothermometer give P-T

values with pressures of up to 2.5 kbar and temperatures of up to 450°C of fluid inclusion trapping conditions.

Finally, a further effort can be made by using estimates of the geothermal gradient. Comparison of isochores with reasonable geothermal gradients indicates that the fluid inclusions probably formed in a thermal regime with a locally confined (i.e. vein associated) geothermal gradient between 70°C/km and 80°C/km (Fig. 5.8). The estimated pressure in context with the geothermal gradient leads to maximum burial depths of up to 4 km.

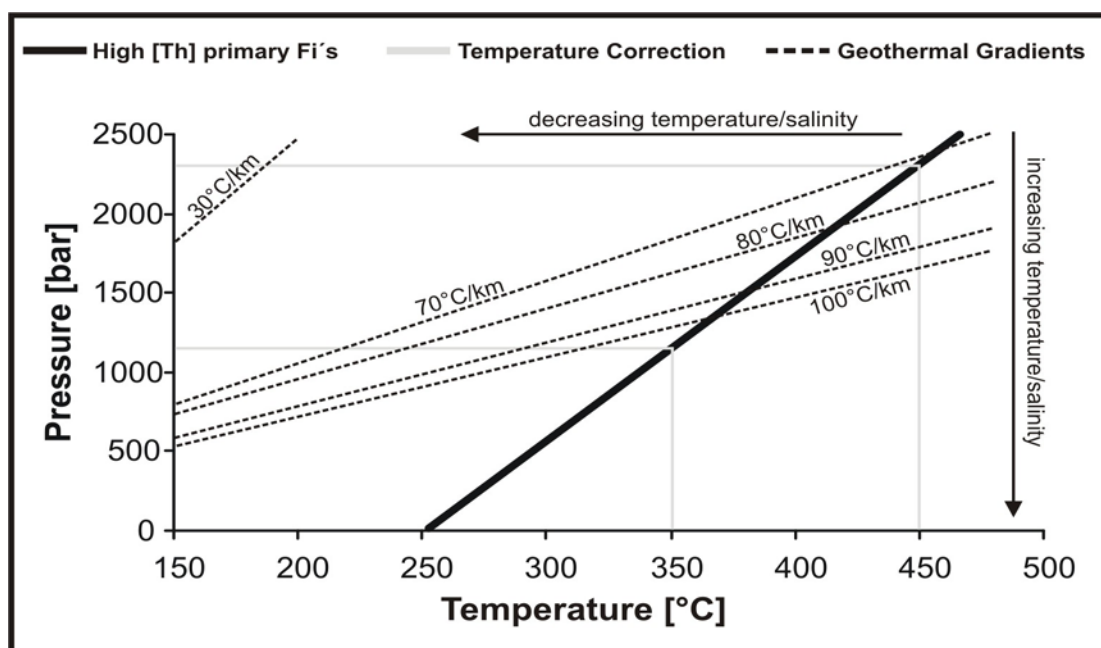


Fig. 5.8: P-T diagram show the isochore calculated from the high temperature primary fluid inclusions of different vein types. Note the intersection of the isochores with the chlorite and calcite-dolomite geothermometers at 350°C and 450°C of stable isotope geothermometers. Dashed lines represent lithostatic gradients of 30, 70, 80, 90 and 100°C/km, respectively.

5.4.3 Fluid evolution

The integration of the fluid inclusions, petrographic and textural/structural analysis of quartz and/or carbonate veins within the Aachen Shear Zone, provide important constraints about vein forming mechanisms, fluid flow, and P-T evolution during shear zone activity. The fluids present during the precipitation of the shear zone fill were aqueous-carbonic (and locally aqueous-methanic/or nitrogenic) and trapped under unmixing conditions. As a consequence of unmixing it can be ruled out that temperature and pressure conditions of

trapping are directly derived from H₂O-dominated (temperature of trapping) and CO₂/CH₄-dominated (pressure of trapping) fluid inclusions. The slight pressure fluctuations could be a consequence of recurrent pressure fluctuations during mineral growth in the vein.

The retrograde evolution of the hydrothermal fluid trapped in quartz and carbonate grains is characterised by decrease in temperature and pressure from primary, over pseudo-secondary to secondary fluid inclusions. The maximum homogenisation temperatures of 390°C of primary fluid inclusions and the calculated pressures of up to 2.5 kbar derived from fluid inclusions formed during the progressive deformation; reflect the maximum P-T conditions during the hydrothermal overprint. More specifically, pseudo-secondary and secondary fluid inclusions were trapped one after the other at slightly decreasing P-T conditions during shear zone activity and growth of different vein minerals and are considered co-genetic to primary fluid inclusions.

Taking all evidences into account the fluid inclusions recorded two stages of fluid circulation based on specific homogenisation, eutectic, and ice melting temperatures. The fluid inclusion groups display a retrograde P-T path from primary over pseudo-secondary to secondary fluid inclusions, with progressively decreasing temperature and pressure (Figure 5.9) related to the progressive deformation within the Aachen fold and thrust belt. Therefore, the relatively high temperature and salinity of primary fluid inclusions represent the maximum P-T conditions of the vein forming fluid. The low temperature (>180°C) fluid inclusions marked the end of the hydrothermal fluid activity and vein formation.

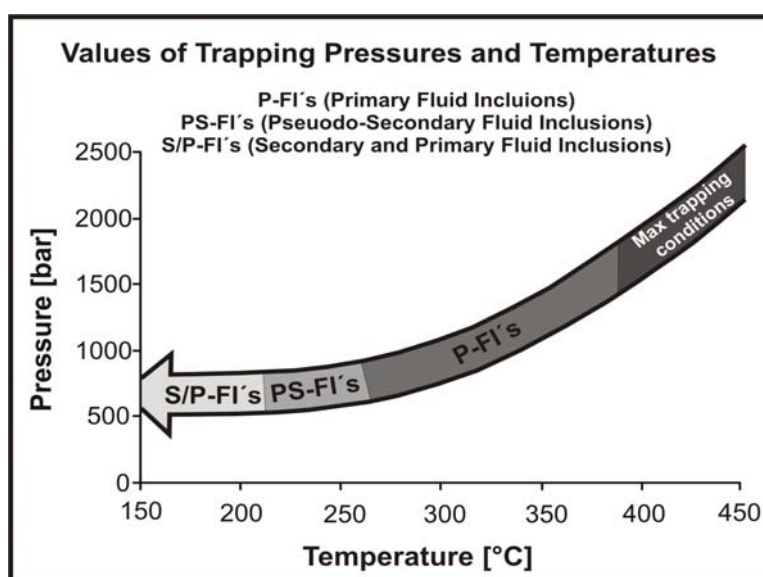


Figure 5.9: Diagram showing the evolution of P-T path inferred for early to late stage fluid inclusion trapping conditions within the RWTH-1 shear zone.

5.4.4 Palaeotemperature and fluid composition within the regional scale

During the Variscan orogeny in the Rhenoharzian terrane, synkinematic fluid flow generated the fluid-system of the so-called "Tectonic Brines" (Behr et al., 1993). These brines represent a H_2O -Na-(K)-Cl-dominated fluid of low to intermediate salinity with CO_2 , CH_4 and N_2 and a homogenisation temperature of $\leq 350^\circ\text{C}$. The post-Variscan hydrothermal ore deposits of the Rheinisches-Schiefergebirge are derived from so-called "Basement Brines" (Behr et al., 1993). This fluid is a H_2O -Ca-Na-Cl-dominated solution of high salinity and homogenisation temperatures of $[\text{Th}] \leq 200^\circ\text{C}$ (Figure 5.10).

Previous investigations on regional-scale microthermometric analysis in the Aachen region were mainly obtained from post-variscian Pb-Zn vein deposits (Figure 5.10). The homogenisation temperatures $[\text{Th}]$ of different fluid systems with NaCl- CaCl_2 -bearing solutions range around 70°C and lower salinities to fluid systems with $[\text{Th}]$ around 190°C and high salinities (Redecke, 1992; Stroink, 1993; and Glasmacher, 1995; Figure 5.10).

Fluid inclusion studies within the Variscan fold and thrust belt of eastern Belgium also characterised different fluid systems. Homogenisation temperatures $[\text{Th}]$ of syn-Variscan fluid flow with Na-(K)-Cl-bearing solutions range around 250°C and have low salinities (Figure 5.10). Furthermore, fluid inclusion studies in the Variscan fold and thrust belt near Brussels, Belgium show a syn-Variscan H_2O - CO_2 -NaCl-dominated fluid of low to intermediate salinity and a homogenisation temperature of $[\text{Th}] \leq 380^\circ\text{C}$ (Schroyen et al., 2000). Post-variscian Pb-Zn vein deposits in eastern Belgium consist of NaCl- CaCl_2 -bearing solutions with homogenisation temperatures ranging around 70°C and low salinities and fluid systems with $[\text{Th}]$ around 190°C and high salinities (Muechez et al., 1994). Secondary fluid inclusions in quartz grains of shear veins in the Bolland drill indicate trapping temperatures of 250°C (Muechez et al., 1998, Piessens et al., 2002). Secondary and pseudo-secondary fluid inclusions in quartz grains of shear veins in the RWTH-1 drill indicate trapping homogenisation temperatures of $180 - 210^\circ\text{C}$ in secondary and of $230 - 250^\circ\text{C}$ in pseudo-secondary inclusions. Fluid inclusion studies at the southern margin of the Anglo Brabant fold belt along the MAT-System (Dewaele et al. 2004) identified H_2O -Na-K-Cl composition of low salinities and homogenisation temperatures between $189 - 377^\circ\text{C}$, with the gases CH_4 and CO_2 . In the northern Variscan front (northern France), Kenis et

al., (2000) defined P-T conditions of a progressive deformation by studying Variscan fluids with [Th] 200 – 260°C and post Variscan fluids with [Th] 50 – 85°C.

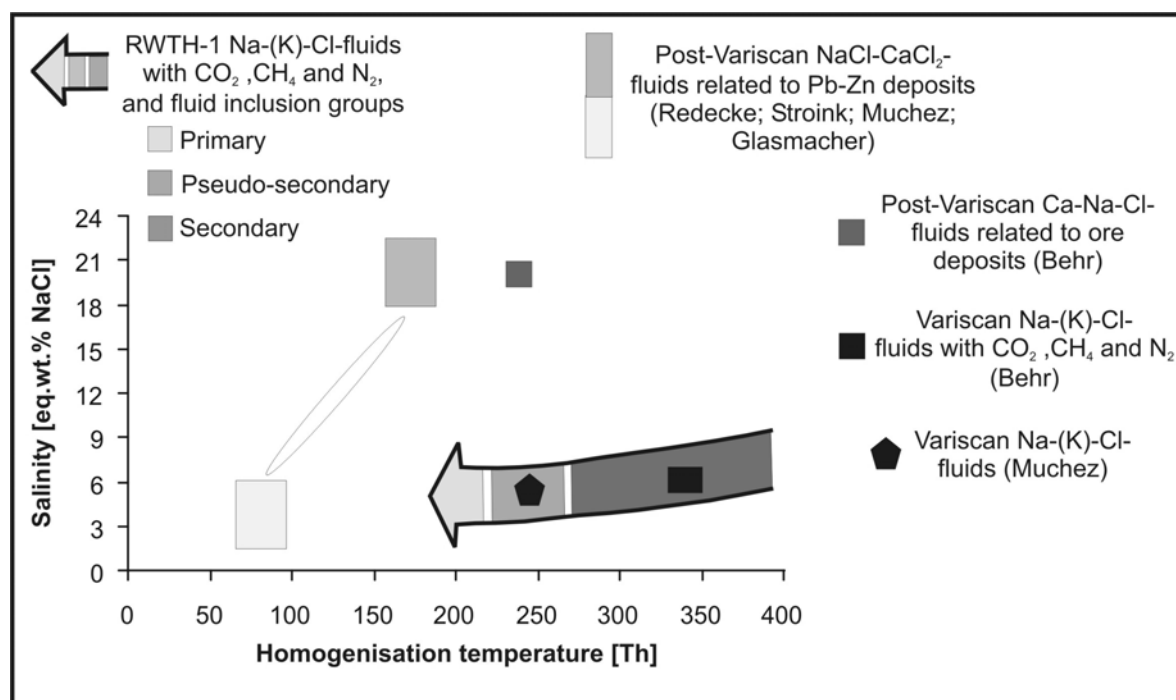


Figure 5.10: Diagram of salinity (eq.wt.% NaCl) versus homogenisation temperature (Th) of investigated fluid inclusions of the RWTH-1 well. Additionally, regional scale fluid inclusion studies classified in the order of different authors within the Ardennes of Western Germany (east and west of the river Rhine and the Ardennes of Eastern Belgium).

The high temperatures of <390°C from primary fluid inclusions of vein minerals within the RWTH-1 drill have not been reported for the German Variscides west of the river Rhine before. The recorded high temperatures and low to intermediate salinities of the Variscan hydrothermal overprint in Palaeozoic rocks from Belgium and western Germany (RWTH-1) close to the MAT indicate rather low-metamorphic conditions than diagenetic temperatures. The hydrothermal fluids were probably released during Variscan metamorphism from deeper crustal source. The fluids are H₂O-Na-(K)-Cl-dominant solutions of low salinities containing the gases CO₂, N₂ and CH₄. The temperature and fluid composition of these fluids is equivalent to those of the "Tectonic Brines" in the Variscan basement of the Rhenohercynian terrain east of the river Rhine (Behr et al., 1993).

Within the RWTH-1, the presence of liquid-rich inclusions, the relationship between [Th] and salinity of primary, pseudo-secondary and secondary

inclusions, indicate that the minerals precipitated at least at a temperature between 180 – 390°C and a pressure of 0.5 – 2.5 kbar from a hydrothermal fluid. The isochores indicate that the fluid inclusions probably formed in a regime with a high geothermal gradient. The fluid inclusion groups point to a hydrothermal fluid activity during the Variscan tectonic period.

5.5 Summary

In all vein types, the fluid inclusions in hydrothermal quartz and carbonates are mainly transparent, H₂O-rich inclusions. The majority of the inclusions are two phase liquid-vapour fluid inclusions.

The [Te] from all the various fluid inclusion groups is around -21°C, indicating that these fluids have a H₂O-Na-(K)-Cl composition. The inclusions always homogenise into the liquid phase. The estimated salinities of the fluid inclusion groups within the different veins are higher than normal seawater conditions.

The homogenisation temperature and salinities of primary fluid inclusions in quartz and carbonate grains of the quartz-carbonate ± chlorite veins range from 270 - 390°C, fluid inclusions in quartz and carbonates have low to intermediate salinities from <4 - 9 eq.wt% NaCl. Temperatures and salinities of pseudo secondary inclusions in quartz and carbonate grains are range from 230 - 250°C and <2 - 5 eq.wt% NaCl. The homogenisation temperatures of secondary inclusions in quartz of quartz-carbonate veins varies between 180 and 210°C and have salinities from <2 - 6 eq.wt% NaCl.

The homogenisation temperatures and salinities of primary inclusions in carbonates of the carbonate veins range from 200 - 370°C and <1 - 6 eq.wt% NaCl, respectively. FIA within dolomite grains have higher temperatures <370°C as the FIA in calcite grains with [Th] <310°C.

The homogenisation temperatures and salinities of primary inclusions in quartz of the quartz ± chlorite veins range from 270 - 390°C and >2 - 6 eq.wt% NaCl respectively. Temperatures and salinities of pseudo secondary inclusions in quartz grains are range from [Th] 250 - 260°C and <4 - 5 eq.wt% NaCl. The homogenisation temperatures of secondary inclusions in quartz grains show temperatures between 190 - 210°C and have low salinities from 2 - 4 eq.wt% NaCl.

The integration of the data obtained by petrographic, microthermometric and gas-chromatographic analyses of fluid inclusions describe a fluid inclusion trapping during progressive deformation. The hydrothermal fluids are H₂O-Na-(K)-Cl-dominant solutions of low salinities with the gases CO₂, N₂ and CH₄. The fluid inclusion assemblages (FIA) represent several pulses of fluid circulation associated with the deformation processes during vein growth. Different stages of fluid inclusion trapping can be classified: Primary and pseudo-secondary inclusions display a fluid trapping during early/syn-vein crystallisation and secondary fluid inclusions display a fluid trapping during late vein crystallisation, as indicated by the association of all different fluid inclusion groups within one crystal. The fluid inclusion groups do not show evidence of subsolvus trapping (they exhibit a near constant degree of filling), although the textural characteristics indicate an association of the fluid inclusion groups within the different veins and minerals.

The combination of the fluid inclusion data, petrographic and textural/structural analysis of quartz and/or carbonate veins within the Aachen Shear Zone, provide important constraints about vein forming mechanisms, fluid flow, and P-T evolution during shear zone activity. The maximum homogenisation temperatures of 390°C of primary fluid inclusions and the calculated pressures of up to 2.5 kbar derived from fluid inclusions formed during the progressive deformation; reflect the maximum P-T conditions during the hydrothermal overprint. More specifically, pseudo-secondary and secondary fluid inclusions were trapped one after the other at slightly decreasing P-T conditions during shear zone activity and growth of different vein minerals and are considered co-genetic.

Taking all evidences into account the fluid inclusion recorded two stages of fluid circulation. The fluid inclusion groups display a retrograde P-T path with progressively decreasing temperature and pressure conditions; related to the progressive deformation within the Aachen fold and thrust belt. Therefore, the relatively high temperature and low to intermediate salinity of primary fluid inclusions represent the maximum P-T conditions of the vein forming fluid.

The high temperatures <390°C from primary fluid inclusions have not been

reported for the German Variscides west of the river Rhine before. The recorded high temperatures and low salinities of the Variscan hydrothermal overprint in Palaeozoic rocks from Belgium and western Germany close to the MAT indicate rather low-metamorphic conditions than diagenetic temperatures. The hydrothermal fluids were probably released during Variscan metamorphism from deeper crustal source. The temperature and fluid composition of these fluids is equivalent to those of the "Tectonic Brines" in the Variscan basement of the Rhenohercynian terrain east of the river Rhine (Behr et al., 1993). The fluid inclusion assemblages point to a hydrothermal fluid activity during the Variscan tectonic period.

6 Stable Isotopes

The stable isotope study was carried out using quartz-carbonate \pm chlorite, carbonate \pm chlorite, and quartz \pm chlorite veins. Several samples of alteration halos around the veins as well as unaltered whole rocks were selected. Chlorite mineral-separates were analysed for oxygen and hydrogen isotopes. Mineral-separates of quartz-carbonate pairs in quartz-carbonate veins were analysed for oxygen isotopes. Calcite and dolomite minerals were analysed for oxygen and carbon isotopes of the carbonate veins and quartz veins were analysed for oxygen isotopes. Whole rock samples from different stratigraphic levels and lithologies were analysed for oxygen, hydrogen, and carbon isotopes, respectively. The samples taken for stable isotopes are listed in Appendices, Section 9.4, and Table 9.7. The oxygen isotopes of silicate mineral-separates from different vein types and alteration zones, as well as powdered samples of the siliciclastic rocks were analysed, using the laser-based micro-analytical method described by Rumble and Hoering, 1994 (Appendices, Section 9.4.1). For the hydrogen isotopes of silicates the Thermo-Chemical Elemental Analyser (TCEA) described by Sharp et al., 2001 (Appendices, Section 9.4.2) was chosen. Carbonate samples of 100 - 200 μg were analysed in the Gas Bench II (Thermo-Finnigan) with 100% orthophosphoric acid (H_3PO_4) digestion technique at 70°C (Spötl and Vennemann, 2003). The isotopes were normalised against the V-SMOW (Vienna standard mean ocean water) and PDB (Belemnite of the cretaceous Pee Dee Formation South Carolina, USA), using the δ notation in parts per mil [‰]. A summary of stable isotopic results are shown in Appendices, Section 9.4.

6.1 Oxygen (VSMOW) and Hydrogen (VSMOW) Isotopy of Chlorites

The oxygen isotopes of chlorite from different vein types, as well as chlorite separates of chlorite slickensides and chlorite alteration were analysed. The vein chlorite separates of the coexisting quartz-chlorite minerals have $\delta^{18}\text{O}$ values between 17.7 and 18.5 ‰ and δD values between -53 and -56 ‰. Chlorite separates of coexisting dolomite-chlorite vein minerals have $\delta^{18}\text{O}$ values between 17.9 and 18.3 ‰ and δD values between -65 and -66 ‰.

The alteration zone of chlorite is isotopically heavier with $\delta^{18}\text{O}$ values between 14.9 and 16.2 ‰ and similar δD values between -60 and -66 ‰ (Table 6.1). Whole rock samples of the siliciclastic rocks, taken from red and grey pelites are heavier in isotopic composition with $\delta^{18}\text{O}$ values lying between 14.4 and 14.9 ‰ and δD values between -49 and -53 ‰ (Appendices, Section 9.4.2, Table 9.9)

Depth [m]	Sample	Vein and Alteration Mineralogy	δD VSMOW	$\delta^{18}\text{O}$ VSMOW
1399,63	¹⁾ 52a	Chlorite/Quartz Vein	-53	18.50
1435,50	¹⁾ 23	Chlorite/Quartz Vein	-59	18.45
1436,90	¹⁾ 37a	Chlorite/Quartz Vein	-59	18.45
1479,20	¹⁾ 56	Chlorite/Quartz Vein	-52	17.67
1488,25	¹⁾ 62a	Chlorite/Quartz Vein	-58	17.98
1503,25	¹⁾ 35	Chlorite/Quartz Vein	-56	17.82
1403,17	²⁾ 24a	Chlorite/Dolomite Vein	-65	18.33
1486,70	²⁾ 30a	Chlorite/Dolomite Vein	-66	17.86
1399,63	³⁾ 53	Chlorite Alteration	-62	15.91
1435,50	³⁾ 25	Chlorite Alteration	-66	14.90
1459,24	³⁾ 51	Chlorite Alteration	-61	15.04
1479,20	³⁾ 57	Chlorite alteration	-64	15.27
1485,80	³⁾ 29	Chlorite alteration	-60	15.16

Table 6.1: Results of stable isotope analyses of chlorite (δD) and ($\delta^{18}\text{O}$) in ¹⁾ quartz-chlorite veins, ²⁾ carbonate-chlorite veins, and ³⁾ chlorite alteration.

6.2 Oxygen Isotopy (VSMOW) of Vein Minerals and Whole Rock

6.2.1 $\delta^{18}\text{O}$ of quartz-carbonate veins

For the veins containing quartz and carbonate minerals it is necessary to separate these two minerals manually to analyse the oxygen isotopes of the silicate (quartz) and the carbonates individually. In order to calculate the isotopy of the carbonate separations (calcite and/or dolomite), XRD and the applied Rietveld method were used to qualify and quantify the mineral phases present. The vein quartz separates of the coexisting quartz-carbonate minerals have $\delta^{18}\text{O}$ values between 17.9 and 19.2 ‰. Coexisting calcite-dolomite minerals have $\delta^{18}\text{O}$ values between 16.2 and 17.1 ‰. Coexisting single calcite minerals have $\delta^{18}\text{O}$ values between 16.0 and 16.4 ‰ and coexisting single dolomite minerals have $\delta^{18}\text{O}$ values of 16.0 ‰. The $\delta^{18}\text{O}$ values are always lower for calcite and dolomite compared to quartz (Table 6.2; Figure 6.1).

Depth [m]	Sample	Vein Mineralogy	$\delta^{18}\text{O}$	$\delta^{18}\text{O}$
			Qtz	Cc/Dol
1399,63	52b	Quartz-Carbonate (Calcite)	18,50	16,38
1402,60	54	Quartz-Carbonate (Calcite/Dolomite)	19,02	17,10
1403,17	24b	Quartz-Carbonate (Calcite)	18,33	16,03
1417,16	60a	Quartz-Carbonate (Calcite/Dolomite)	19,24	16,55
1430,69	58	Quartz-Carbonate (Calcite/Dolomite)	18,02	16,20
1436,90	37b	Quartz-Carbonate (Calcite)	18,45	15,95
1486,70	30b	Quartz-Carbonate (Dolomite)	17,86	16,00
1488,25	62b	Quartz-Carbonate (Dolomite)	17,98	15,97

Table 6.2:
Oxygen
isotopy
(VSMOW)
of quartz-
carbonate
pairs.

6.2.2 $\delta^{18}\text{O}$ of single quartz and single carbonate veins

The quartz veins have $\delta^{18}\text{O}$ values between 16.3 and 17.8 ‰. The calcite veins have $\delta^{18}\text{O}$ values around 16 ‰, whereas vein dolomite has $\delta^{18}\text{O}$ values between 16.4 and 18.3‰ (Section 10; Table X; Figure 6.1).

6.2.3 $\delta^{18}\text{O}$ of siliciclastic rocks, dolostone and limestone

Whole rock samples of the siliciclastic rocks, taken from red and grey pelites have $\delta^{18}\text{O}$ values between 14.4 and 14.9 ‰. This value is slightly heavier compared to the $\delta^{18}\text{O}$ isotopy of chlorites. Dolomite, taken from the dolomite bank has a $\delta^{18}\text{O}$ composition of 22.1 ‰ that differs strongly from the veins, alteration zones, limestones and siliciclastic rocks. Limestone samples of the limestone nodules have a $\delta^{18}\text{O}$ composition of 16.6 ‰. This isotopy is similar to the $\delta^{18}\text{O}$ values of the carbonate veins and quartz-carbonate veins (Figure 6.1).

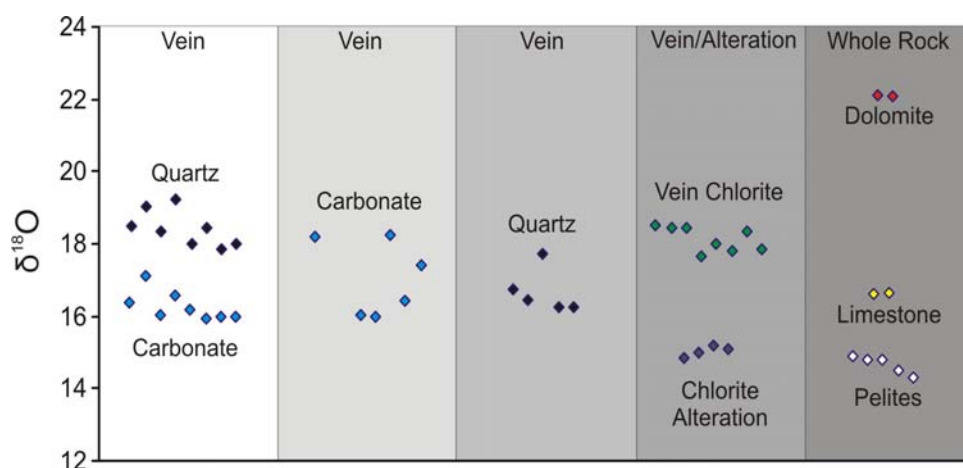


Figure 6.1:
 $\delta^{18}\text{O}$ (VSMOW)
values of
different vein
types and
chlorite
assemblages,
chlorite
alteration and
whole rock
samples.

6.3 Oxygen (PDB) and Carbon (PDB) Isotopy of Carbonates

In carbonates, oxygen and carbon isotopes were analysed simultaneously (Appendices, Section 9.4.3). Mineral-separates of quartz-carbonate veins, single carbonate veins, and whole rock samples of limestone nodules and the dolomite bank were taken (Figure 6.2). The oxygen isotopy of the carbonates within quartz-carbonate and carbonate veins range from $\delta^{18}\text{O}$ -12.3 to -14.5 ‰. The carbon isotopy in quartz-carbonate veins (calcite/dolomite) have values lying between -0.4 and -1.5 ‰, the quartz-carbonate veins with single calcite have values lying between -4.6 and -9.2 ‰, and with single dolomite $\delta^{13}\text{C}$ values are between -17.3 and -19.9 ‰.

The analysed whole rock samples of the dolomite bank have a $\delta^{18}\text{O}$ isotopy of -8.6 ‰, and $\delta^{13}\text{C}$ of -0.05 to -0.06‰. The analysed nodular limestone has a $\delta^{18}\text{O}$ isotopy of -13.8 ‰, and $\delta^{13}\text{C}$ of -1.04 ‰. The oxygen and carbon isotopes values of the limestone nodules are similar compared to the $\delta^{18}\text{O}$ and $\delta^{13}\text{C}$ isotopy of the surrounding quartz-carbonate veins.

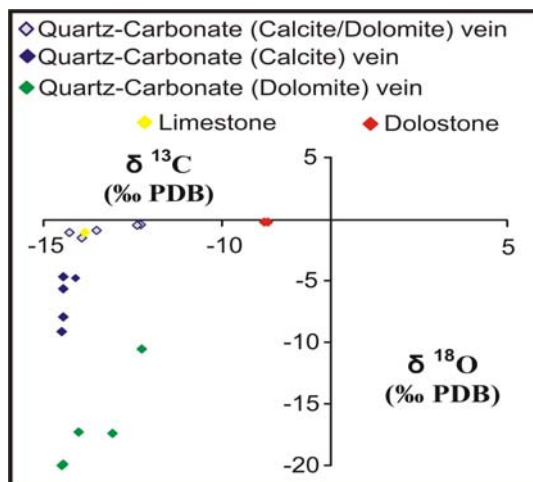


Figure 6.2: Oxygen and carbon isotopic (PDB) composition of the mineralised veins (n=15), limestone nodules (n=2) and the dolomite host rock (n=2). Note, the limestone nodules have a similar isotopy compared to the surrounding mixed calcite/dolomite vein cements of the quartz-carbonate veins.

6.4 Interpretation

6.4.1 Fluid composition and source

The isotopic composition of δ D and $\delta^{18}\text{O}$ from chlorite minerals was measured to determine the fluid composition with respect to the origin of the vein forming fluid (i.e. fluid source). There are two ways to determine the isotopy of the fluid: (1) calculation from the isotopic analysis of coexisting hydrothermal minerals, in conjunction with the precipitation temperature and (2) direct analysis of the fluid by decrepitating fluid inclusions (Ridley and Diamond, 2000). Both methods are used in this study, concerning way (2) see section 6.5.

The isotopic composition of a fluid in equilibrium with a mineral can be calculated from the mineral $\delta^{18}\text{O}$ and δ D values, applying a mineral water fractionation factor ($10^3 \ln \alpha$). In this study the $\delta^{18}\text{O}$ and δ D isotopic composition of an aqueous fluid in equilibrium with the mineral separates and the alteration zones of chlorites were calculated (Table 6.3), using the equation of Graham et al. (1984b). The calculations were carried out for a temperature of 350°C as this is the main homogenisation temperatures of the primary fluid inclusions in the coexisting quartz or dolomite minerals. The temperature of 350°C is supported by calcite/dolomite and chlorite geothermometers (s.f. Geothermometry).

Table 6.3: Results of calculated mineral-water fractionation of chlorite (δ D) and ($\delta^{18}\text{O}$) in ¹⁾ quartz-chlorite veins, ²⁾ carbonate-chlorite veins, and ³⁾ chlorite alteration. Factors of fractionation after Graham et al. (1984b).

Depth [m]	Sample	Vein and Alteration Mineralogy	δ D to Fluid	$\delta^{18}\text{O}$ to Fluid
1399,63	¹⁾ 52a	Chlorite/Quartz Vein	-19.5	18.83
1435,50	¹⁾ 23	Chlorite/Quartz Vein	-25.5	18.78
1436,90	¹⁾ 37a	Chlorite/Quartz Vein	-25.5	18.78
1479,20	¹⁾ 56	Chlorite/Quartz Vein	-18.5	18.00
1488,25	¹⁾ 62a	Chlorite/Quartz Vein	-24.5	18.31
1503,25	¹⁾ 35	Chlorite/Quartz Vein	-22.5	18.15
1403,17	²⁾ 24a	Chlorite/Dolomite Vein	-31.5	18.37
1486,70	²⁾ 30a	Chlorite/Dolomite Vein	-32.5	18.19
1399,63	³⁾ 53	Chlorite Alteration	-28.5	16.25
1435,50	³⁾ 25	Chlorite Alteration	-32.5	15.23
1459,24	³⁾ 51	Chlorite Alteration	-27.5	15.37
1479,20	³⁾ 57	Chlorite alteration	-30.5	15.61
1485,80	³⁾ 29	Chlorite alteration	-26.5	15.49

Information on the H-isotope composition of the fluid could only be obtained from chlorite since it is the only hydrous mineral occurring in veins and alterations zones. The chlorite separates of the coexisting quartz-chlorite minerals have $\delta^{18}\text{O}$ values lying between 18.0 and 18.8 ‰ and δD values between -20 and -26 ‰. Chlorite separations of coexisting dolomite-chlorite minerals have slightly lighter $\delta^{18}\text{O}$ values lying between 18.1 and 18.4‰ and δD values between -31 and -33 ‰. The alteration zone of chlorite is isotopically heavier as the vein minerals with $\delta^{18}\text{O}$ values lying between 15.3 and 16.2 ‰ and similar δD values between -27 and -30 ‰. In general metamorphic fluids have δD values within the range -20 to -75‰ (e.g., see Taylor, 1974a). Therefore in a $\delta^{18}\text{O}$ versus δD diagram the isotopic values of the hydrothermal fluid plot in the metamorphic water field (Figure 6.3).

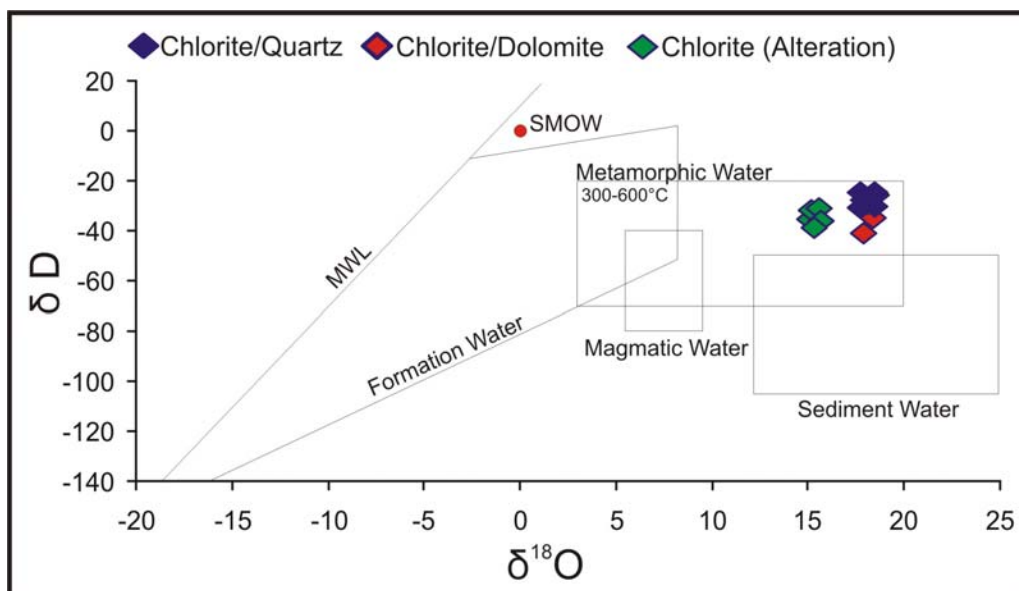


Figure 6.3: Mineral/water fractionation calculated after Graham et al. (1984b) of $\delta^{18}\text{O}$ values versus δD values (VSMOW) of chlorite in veins and alteration zones. The field of metamorphic water combines the values of Taylor (1974) and Sheppard (1986), the field of magmatic water is from Taylor (1974), and the meteoric water line (MWL) from Epstein (1970).

6.4.2 Stable isotope composition of quartz/carbonate veins

If vein filling resulted from the precipitation of the metamorphic fluid, the isotopic composition of quartz carbonate pairs should be in equilibrium with the

same fluid. Calcite, dolomite, and mixed calcite/dolomite are present as blocky and scattered grains in textural equilibrium with silicate phases.

The equation of Zheng (1993a) was used in order to calculate fractionation factors for quartz. For calcite and for dolomite the equation of Zheng (1999) was chosen. The calculations were carried out for a temperature of 350°C as this is the main homogenisation temperatures of the primary fluid inclusions in the coexisting quartz or carbonate minerals. The quartz of the coexisting quartz-carbonate minerals has $\delta^{18}\text{O}$ values between 12.3 and 13.6 ‰ (Table 6.4). Cogenetic calcite-dolomite minerals have $\delta^{18}\text{O}$ values between 11.6 and 12.5 ‰. Cogenetic single calcite minerals have $\delta^{18}\text{O}$ values between 11.3 and 11.8 ‰ and cogenetic single dolomite minerals have $\delta^{18}\text{O}$ values between 11.2 and 11.3 ‰.

Table 6.4: Results of calculated mineral-water fractionation of oxygen isotope (VSMOW) of quartz-carbonate pairs (Zheng, 1993a/Zheng, 1999). Results of oxygen isotope thermometry in shaded fields (Sharp & Kirschner, 1994).

Depth [m]	Sample	Vein Mineralogy	$\delta^{18}\text{O}$ Qtz to Fluid	$\delta^{18}\text{O}$ Cc/Dol to Fluid	Isotope T [°C]
1399,63	52b	Quartz-Carbonate (Calcite)	12,91	11,82	399 °C
1402,60	54	Quartz-Carbonate (Calcite/Dolomite)	13,43	12,47	433 °C
1403,17	24b	Quartz-Carbonate (Calcite)	12,74	11,47	373 °C
1417,16	60a	Quartz-Carbonate (Calcite/Dolomite)	13,65	11,92	324 °C
1430,69	58	Quartz-Carbonate (Calcite/Dolomite)	12,43	11,57	455 °C
1436,90	37b	Quartz-Carbonate (Calcite)	12,86	11,25	347 °C
1486,70	30b	Quartz-Carbonate (Dolomite)	12,27	11,30	445 °C
1488,25	62b	Quartz-Carbonate (Dolomite)	12,39	11,24	417 °C

Since the isotopic fractionation between cogenetic quartz and calcite/dolomite minerals is large enough to be used for oxygen isotope thermometry, it was possible to calculate temperatures for quartz-carbonate pairs. The temperatures are calculated after Sharp & Kirschner (1994) this calculation was chosen because it is based on isotope studies of cogenetic quartz-carbonate vein minerals. The results are listed in shaded fields of Table 6.4. In all cases, the $\delta^{18}\text{O}$ values of the quartz and carbonate (Table 6.4/Figure 6.4) were similar within individual veins, regardless of whether textural equilibrium was apparent or not. The calculated temperature of quartz and cogenetic calcite/dolomite minerals ranges from 324 to 355°C. Calculated temperatures of quartz and

cogenetic calcite are lying between 347 and 399°C, and the temperatures of quartz and cogenetic dolomite are lying between 427 and 445°C. The fractionation between these two phases indicates average temperatures of 350°C (Figure 6.4). This temperature is similar to the homogenisation temperatures obtained from the investigated fluid inclusions, suggesting that quartz and carbonate may well have precipitated contemporaneously from the same fluid.

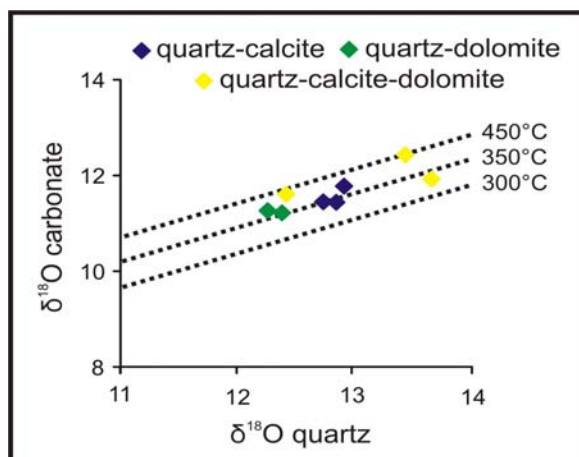


Figure 6.4: Oxygen (VSMOW) isotope fractionation of coexisting quartz-calcite, quartz-dolomite, and quartz-calcite-dolomite pairs within the quartz-carbonate veins. Factors of fractionation after Zheng (1993a & 1999). Temperatures calibrations after Sharp & Kirschner (1994).

6.4.3 Carbonate composition and source

A combined study of carbon and oxygen isotopes (PDB) in carbonates was used to distinguish between carbonates of different origins, especially in relation to the process of limestone and dolostone diagenesis. The study of carbon isotopes allows the origin of the carbon in the carbonate to be determined and the distinction between marine, organic (i.e. methane-related) carbon (Coleman and Raiswell, 1981). A study of oxygen isotopes in sedimentary carbonates can also be used to determine the origin of fluids in equilibrium with the carbonates.

The range of the stable isotopic composition of the carbonate minerals from the quartz carbonate veins is similar to the limestones. In a $\delta^{18}\text{O}$ versus $\delta^{13}\text{C}$ diagram they plot close to the field of hydrothermal carbonates (Figure 6.5). This may be due to the precipitation of carbonate cements from a fluid in which isotopic composition was buffered by the surrounding rock. Since the vein carbonates are not restricted to the limestone and dolostone the isotopic composition of the limestone was overprinted by the hydrothermal fluid. However, the $\delta^{13}\text{C}$ and $\delta^{18}\text{O}$ values of the veins and limestone differentiate from

those of the dolostones (Figure 6.5). The negative oxygen (PDB) isotope values of the uniform dolomite bank are more compatible with a burial origin or with a re-equilibration during further burial. Petrographic evidence, however, indicates a diagenetic origin of the dolostone in conjunction with a process of re-equilibration during further burial and deformation. These process has been widely recognised and reflects a common discrepancy between petrographic and geochemical data in carbonates (see also Land, 1980; Hardie, 1987; Machel and Mountjoy 1987; Peeters et al., 1993).

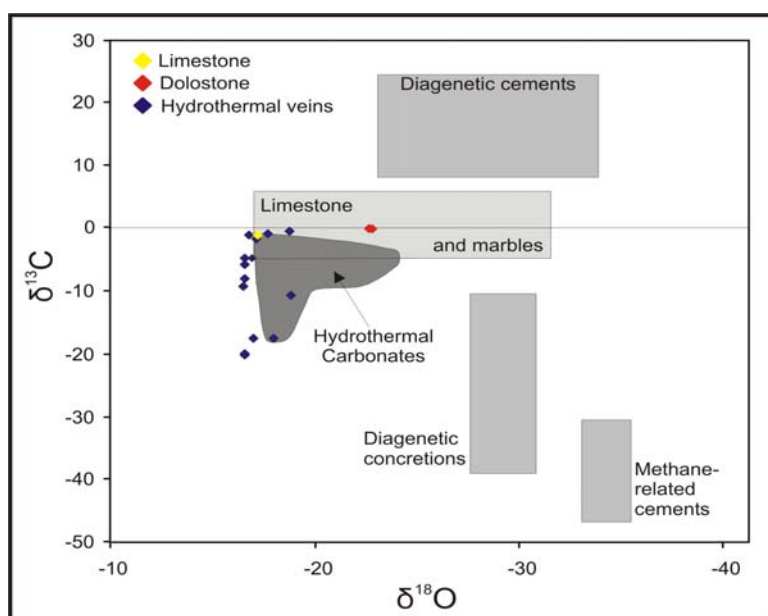


Figure 6.5: $\delta^{18}\text{O}$ (PDB) versus $\delta^{13}\text{C}$ (PDB) plot showing the composition of a variety of carbonate environments. Note the calculated $\delta^{18}\text{O}$ values and $\delta^{13}\text{C}$ values of limestone, dolostone and carbonate veins, plot close to the field of hydrothermal carbonates.

Within the geological context, the low $\delta^{13}\text{C}$ values of the vein carbonates could be due to the incorporation of light carbon derived from adjacent Lower Devonian shales during oxidation and thermal decarboxylation of the organic matter in these sediments (Irwin et al. 1977; Mullis et al. 1994). The $\delta^{13}\text{C}$ and $\delta^{18}\text{O}$ values of the limestone are too low for marine or diagenetic carbonates. During burial, the carbon and oxygen isotopic ratios normally decrease due to intense water/rock interaction (Longstaffe and Ayalon 1987, 1988, 1991).

In this study the process of siliceous limestone decarbonation occurs when the high temperature fluid reacts with the limestone. The decreasing $\delta^{18}\text{O}$ isotopic composition is therefore due to the hydrothermal overprint of the metamorphic fluid. The $\delta^{13}\text{C}$ values vary between the different lithological units and within the units. In contrast to the $\delta^{18}\text{O}$ isotopic composition, where rather uniform values point to a process active over the whole scale of vein filling, the varying $\delta^{13}\text{C}$ values indicate rather local controls on C-isotopy (e.g. clay content/pelites).

At temperatures of 300 - 350°C, ferroan carbonates with a $\delta^{18}\text{O}$ value between -15 and -20‰ PDB would have precipitated from a fluid with an oxygen isotopic composition up to 18.0‰ PDB. Such values are in agreement with a fluid whose oxygen isotopic composition changed due to interaction with carbonates (Clayton et al. 1966; Hitchon and Friedman 1969) or which is of metamorphic origin (Taylor 1974; Sheppard 1986).

6.5 δD and $\delta^{13}\text{C}$ Values of Water from Fluid Inclusions

Water contained in fluid inclusions of quartz, calcite and dolomite grains of the different vein types were extracted by mechanical/crushing decrepitation in a vacuum extraction line. Released H_2O and CO_2 were trapped under vacuum in a liquid nitrogen-cooled U-tube. CH_4 was separated from H_2O and CO_2 by careful expansion into an isolated part of the vacuum line and in turn oxidized to H_2O and CO_2 . A summary of these stable isotopic results are given in Appendices, Section 9.5

6.5.1 H- and C-isotope composition of water in fluid inclusions and C-isotope composition of methane from fluid inclusions

The δD values of water extracted from fluid inclusions range between -89 and -113‰ VSMOW. The analysed quantities of CO_2 from fluid inclusions are always lower than 5 μmol , with $\delta^{13}\text{C}$ values from -13 and -22.3‰. The $\delta^{13}\text{C}$ compositions of methane from fluid inclusions range from -26.9 and -28.7‰.

6.5.2 Evolution of isotopic composition of the fluid and fluid source

The δD values of the fluids responsible for vein formation were determined from water trapped as fluid inclusions, and from measured δD values of chlorite minerals (Chapter 6.4.1). The δD values of water were measured directly on the bulk composition extracted from fluid inclusions in separated quartz and carbonate grains from quartz carbonate \pm chlorite veins (Figure 6.6). The range of values determined in this study is compatible with 1) metamorphic waters with δD values higher than -50‰ that have equilibrated with clay minerals, and 2) water with δD values less than -90‰ formed by the breakdown and

oxidation of organic matters, as well as waters representing mixtures of these two sources (Tarantola et. al., 2007). The low δD values of the fluid are out of the range of the host rock silicates, which have δD values between -49 and -53‰. The decrease of water δD values relates to a H_2O - CO_2 - CH_4 composition of the metamorphic fluid. However, with increasing metamorphism of the fluid source there is a tendency towards isotopic equilibrium with illite - muscovite mixtures, reflected by an increase in δD values of the measured chlorite minerals. Otherwise the decrease of δD values of water could be related to the process occurring within CH_4 and H_2O bearing fluids. The decrease of δD values of water may thus be related to the incorporation of deuterium depleted methane-derived water (Tarantola et. al., 2007). This process leads to changes in chemical composition of the fluid inclusions. Therefore the isotopic data suggest the following oxidation reaction:



This reaction is then more or less simultaneously preserved in fluid inclusions trapped during the growth of quartz and carbonate crystals.

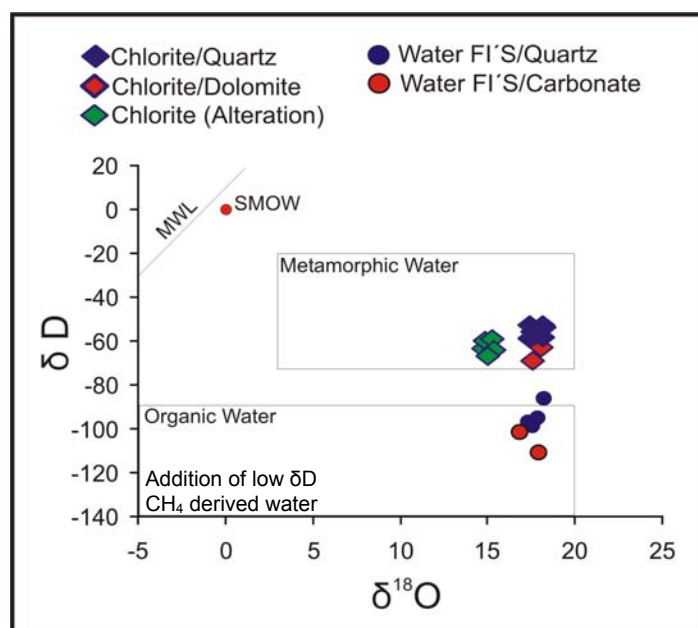


Figure 6.6: Isotopic compositions ($\delta^{18}O/\delta D$ / VSMOW) of vein chlorite and chlorite alteration compared to the isotopic composition of fluid inclusion waters that formed vein quartz and carbonates. The δD values of waters were measured from fluid inclusions and $\delta^{18}O$ were measured from the minerals hosted the fluid inclusions (FI's).

6.5.3 Relations between methane and carbon dioxide

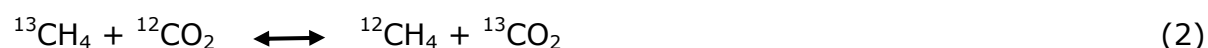
The H_2O - CO_2 -(CH_4)- $NaCl$ -(KCl) composition of the metamorphic fluid precipitating calcite, dolomite, and quartz crystals, as well as chlorite contemporaneously. Methane extracted from water in fluid inclusions in

quartz/calcite/dolomite grains and their C-isotope fractionation (calculated after the calibration of Bottinga, 1969) suggest that CH₄ and the minerals reached isotopic equilibrium at the respective maximum temperature conditions (350 to 450°C). During cooling and vein formation the fluid inclusion water of different minerals have preserved this equilibrium composition (Vrolijk et. al., 1988; Sharp, 1999). The decrease in $\delta^{13}\text{C}$ (CH₄) is correlated with increasing CO₂ content in the fluid (Table 6.5).

Table 6.5: Carbon isotopy (VSMOW) of water extracted from quartz-carbonate pairs.

Depth [m]	Sample	Vein Mineral	CH ₄ mbar	CO ₂ mbar	$\delta^{13}\text{C}$ CH ₄	$\delta^{13}\text{C}$ CO ₂
1403.68	P5	quartz- calcite ± chlorite	4	8	too small	-22,3
1408.75	P11	quartz- dolomite ± chlorite	6	28	too small	-12,8
1417.03	P8	quartz -carbonate ± chlorite	20	39	-28,9	-13,3
1430.69	P9	quartz -carbonate ± chlorite	6	7	too small	-13,0
1436.68	P4	quartz- calcite ± chlorite	17	6	-28,5	-19,9
1436.90	P7	quartz -carbonate ± chlorite	13	33	-26,9	-17,4
1459.24	P12	quartz- dolomite ± chlorite	15	74	-28,3	-17,8
1479.20	P2	quartz -carbonate ± chlorite	2	33	too small	-21,0
1486.7	P6	quartz -carbonate ± chlorite	2	33	too small	-23,3
1503.25	P3	quartz- dolomite ± chlorite	3	8	too small	-18,0

One possible explanation is an isotopic exchange between the methane and carbon dioxide trapped together at peak temperature conditions as fluid inclusions in quartz and carbonate grains. This process might be explained with the formula:



During cooling, isotopic equilibration between CO₂ and CH₄ may have lead to increasing $\delta^{13}\text{C}$ (CO₂) values and decreasing $\delta^{13}\text{C}$ (CH₄) values (Bottinga, 1969; Horita, 2001). Two different sources of carbon can be proposed for CO₂ within the different vein minerals: 1) carbon derived from a decarbonation reaction within the wall rocks (i.e. limestone, micrite cements, dolomitisation), or 2) methane derived carbon through the oxidation reaction (2) within the fluid. For the setting 1) $\delta^{13}\text{C}$ (CO₂) = $\delta^{13}\text{C}$ (CaCO₃) the fractionation factor is +1.7‰ at 270°C and for the methane derived setting 2) $\delta^{13}\text{C}$ (CO₂) = $\delta^{13}\text{C}$ (CH₄) the fractionation factor is +27‰ at 270°C (Tarantola et. al., 2007), and offers a better correlation with the obtained data.

However, in a carbonate-rich host rock, the range of negative $\delta^{13}\text{C}$ values for the isotopic composition of CO_2 measured in the fluid inclusions of different vein minerals suggest that this CO_2 is probably of mixed origin. The smaller part of the total CO_2 is derived from the wall rock and the larger part of the CO_2 is obtained from the oxidation of the methane within the fluid.

6.6 Fluid-Rock Interaction

The oxygen isotope (VSMOW) data for mineral-separates from the veins are different compared to isotopic composition of alteration halos and host rock samples. If fluid-rock ratios had been low, then fluids streaming through the fractures would have an isotope composition, independent of the host rock (Conrad, 1992 and 1995). In this study the oxygen isotopic composition of different veins, alteration halos and host rock varies from 14 to 22 ‰ (Figure 6.1). The isotopic compositions of different vein minerals range in $\delta^{18}\text{O}$ values between 16 and 19 ‰, whereby the quartz and chlorite isotopy is always heavier compared to the isotopic composition of the coexisting carbonate minerals. The dolomite host rock has $\delta^{18}\text{O}$ values of 22 ‰ and the pelites have $\delta^{18}\text{O}$ values between 14 and 15 ‰. Therefore, host rock isotopy compared to the isotopic composition of the vein minerals indicates low fluid rock interactions (i.e. low fluid-rock ratios). The fluid in equilibrium with the alteration zones of chlorite with $\delta^{18}\text{O}$ values around 15.5 ‰ varies more compared to the vein isotopy than correlate to the pelites and lead to intermediate fluid-rock ratios. The dolomitised limestones have $\delta^{18}\text{O}$ values of around 16.5 ‰, which is in the range of the isotopic composition of vein forming carbonates and different to the isotopic composition of the dolomite host rock (Figure 6.1). The similar isotopic composition of dolomitised limestones providing that dolomitisation took place during the hydrothermal overprint. This is also in agreement with the petrological observation that dolomitisation can be related to a hydrothermal alteration.

In open fluid systems the isotopic composition of a fluid may be out of equilibrium with the solid phases of the host rock. Consequently, the isotopic composition of the veins does not reflect that of the host rock (Burkhard and Kerrich, 1988). The presented isotopic variations of the minerals compared to

host rock reflect mineral-water fractionation rather than a mineral-rock fractionation.

To quantify the water-rock ratios an equation for an open system through which the water travels only once (single pass) is given by Taylor (1977). The $\delta^{18}\text{O}$ values of quartz-carbonate-chlorite assemblages related to the host rock isotopy of surrounding carbonate marls and red to grey pelites requires relatively low fluid-rock ratios (<0.5). The variations between chlorite vein assemblages, chlorite alteration and the pelitic host rock can be related to the variation in temperatures from the fluid to the host rock during vein formation and alteration. The low fluid-rock ratios suggest an independent, focused fluid, unable to achieve equilibrium with the host rocks; this is supported with the petrological observation of cm-sized veins and mm-sized alteration halos.

The hydrogen isotopy of the calculated vein chlorite is higher compared to the hydrogen isotopy of water extracted from the fluid inclusions within vein quartz and carbonates, which have low δD values between -89 and -113‰ . These significantly lower δD values relate to the actual fluid and the higher δD values of -53 and -66‰ to the fluid from which the chlorites precipitated. This suggests isotopic fractionation from the fluid to the vein forming minerals during precipitation, independent of the host rock (s.f. chapter 6.5.2). This is supported by the isotope composition of host rock pelites with δD values lying between -49 and -51‰ . Most hydrous minerals contain relatively small amounts of hydrogen relative to the infiltrating fluid; they are therefore particularly sensitive to the fluid that had interacted with the minerals; unless fluid-rock interactions are very small (Graham et. al., 1987). The fact that the vein minerals and the host rock have different hydrogen isotope compositions supports that fluid-rock ratios were low.

Fluid-rock interaction can especially be influenced by fluids containing CO_2 . When the fluid-rock ratio is small the $\delta^{13}\text{C}$ in the rocks/minerals dominates the system and the $\delta^{13}\text{C}$ of the fluid composition is changed. When the fluid-rock ratio is higher and the $\delta^{13}\text{C}$ of the CO_2 dominates, the $\delta^{13}\text{C}$ of the rock/minerals is modified. The latter process can be related to the isotopic composition of the limestone due to the pervasive dolomitisation. Generally the fractionation of carbon isotopes is controlled by both equilibrium and kinetic processes. Equilibrium fractionations are illustrated in Figure 6.7. The isotopic fractionation

values of measured $\delta^{13}\text{C}/\text{CO}_2$ of water and methane extracted from fluid inclusions plot in the field of methane fractionated fluids at 350 to 450°C. This isotopic composition is close to the graphite equilibration relative to CO_2 . The diagram shows that the fluid is not in equilibrium with typical dolomite ($\text{CaMg}(\text{CO}_3)_2$) or limestone (CaCO_3). These correlations also indicate low fluid-rock interaction (i.e. low fluid-rock ratios). Additionally, considering the dolomitised limestone isotopy, it can be proved that dolomitisation is controlled by the hydrothermal activity.

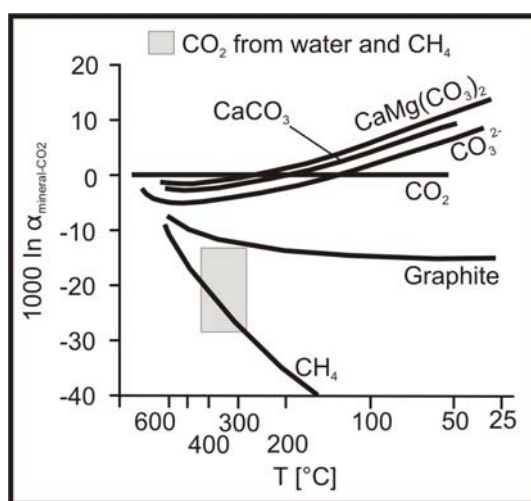


Figure 6.7: Fractionation of carbon species relative to CO_2 (redrawn from Ohmoto and Rye, 1979). Note the field of isotopic composition of water from fluid inclusions in quartz and carbonates related to the fractionation of CH_4 versus CO_2 .

However, it should be noted that one common equilibrium process – that of dissolution and precipitation – does not substantially fractionate carbon isotopes. Kinetic fractionation is important in biological systems such as the fixing of CO_2 in organic carbon and the evolution of methane from anaerobic fermentation of organic matter during diagenesis. Additionally, metamorphic fluids buffered at 300 to 500°C by graphite could have considerably lower values for $\delta^{13}\text{C}$, with $\delta^{13}\text{C}(\text{CH}_4) - 34 \pm 4 \text{ ‰}$ and $\delta^{13}\text{C}(\text{CO}_2) - 13 \pm 2 \text{ ‰}$ at equilibrium, respectively (Bottinga, 1968; Valley and O’Neil, 1981; Ohmoto and Kerrick, 1977).

The estimated temperature of 350 to 450°C (Figure 6.8) corresponds to the calculated temperature of $\delta^{13}\text{C}$ (PDB) values of carbonate minerals compared to CO_2 in fluid inclusions of coexisting vein quartz. The $\delta^{13}\text{C}$ values for carbonate versus $\delta^{13}\text{C}$ of CO_2 are approximately 1.9 to 2.0, corresponding to a temperature of equilibrium of ~425°C (Bottinga, 1968).

6.7 Summary

The stable isotopes of oxygen, hydrogen and carbon were used to constrain the origin of the fluids as well as to evaluate the extent of fluid-rock interaction and the P-T conditions at the time of hydrothermal veining.

The isotopic composition of δ D and $\delta^{18}\text{O}$ from chlorite minerals was measured to determine the fluid composition with respect to the origin of the vein forming fluid (i.e. fluid source). The calculations were carried out at 350°C, which is the assumed temperature of precipitation. The calculated $\delta^{18}\text{O}$ and δ D isotopic composition of chlorite from vein assemblages and the alteration plot in a $\delta^{18}\text{O}$ versus δ D diagram in the field of metamorphic water.

Additionally, the δ D values of water were measured directly from fluid inclusions in quartz and carbonate grains of the quartz carbonate \pm chlorite veins, whereby the $\delta^{18}\text{O}$ values were calculated assuming isotopic equilibrium between aqueous fluids and their minerals. In a $\delta^{18}\text{O}$ versus δ D diagram the isotopic values of this hydrothermal fluid plot also in the metamorphic water field.

The oxygen and carbon isotope values (PDB) of the nodular limestone are similar compared to the $\delta^{18}\text{O}$ and $\delta^{13}\text{C}$ isotopy of the surrounding quartz-carbonate veins. In a $\delta^{18}\text{O}$ versus $\delta^{13}\text{C}$ diagram they plot close to the field of hydrothermal carbonates. Since the vein carbonates are not restricted to the limestone and dolostone the isotopic composition of the limestone was changed by the hydrothermal fluid; this could be correlated to the hydrothermal overprint occurring as pervasive dolomitisation.

The fluid responsible for the precipitation of coexisting quartz-carbonate vein minerals has similar $\delta^{18}\text{O}$ values, whereby the $\delta^{18}\text{O}$ values are always lower for calcite and dolomite compared to quartz. The used oxygen isotope thermometer of vein quartz and cogenetic calcite/dolomite requires temperatures from 350 to 450°C. This temperature is similar to the homogenisation temperatures obtained from the fluid inclusion studies, suggesting that quartz and carbonate may well have precipitated contemporaneously from the metamorphic fluid.

Host rock isotopy compared to the isotopic composition of the vein minerals indicate low fluid-rock ratios. The low fluid-rock ratios suggest an independent, focused fluid, unable to achieve equilibrium with the host rock; this is supported with the petrological observation of cm-sized veins and mm-sized alteration halos.

The isotopic fractionation values, of measured $\delta^{13}\text{C}/\text{CO}_2$ of water and methane from extracted fluid inclusions, plot in the field of methane fractionated fluids at 350 to 450°C, further evidencing the low fluid-rock interaction.

On the basis of isotopic analysis, the different vein minerals were precipitated from one fluid type. The fluid that precipitated vein forming minerals has a much lighter $\delta^{18}\text{O}$ and δD than the host rock. Therefore, one major origin for this fluid can be proposed. It could have been derived from the metamorphic zone to the south of the area studied. The combination of microthermometry, stable-isotopes and the regional geological setting indicate that the fluid most likely originated from metamorphic rocks within the Stavelot-Venn-Massive and interacted with the Devonian strata along its migration path.

7 Discussion

The RWTH-1 geothermic well situated within the nappe tectonic setting of the outer Variscan fold-and-thrust belt have undergone a complex history of diagenesis, Variscan deformation and fluid activity. With respect to the undertaken investigations, the presented findings will be critically examined and discussed. Special emphasis will be put on the tectono-sedimentary evolution of the fault belt within the regional geological setting, with special reference to the fluid infiltration and precipitation mechanisms for the quartz and/or carbonate \pm chlorite veins and vein alteration assemblages.

7.1 Tectono-Sedimentary Evolution

The Wurm Synclinorium within the Ardennes of western Germany, west of the River Rhine and the corresponding Namur Synclinorium within the Ardennes of eastern Belgium comprise the marginal facies of the Rhenish-Ardennes outer Variscan Orogen (Walter, 1995). In the study area, regional-scale synclines, anticlines and locally developed thrusts trend NE – SW related to the Variscan deformation (D_1). The Wurm Synclinorium and the Aachen Anticlinorium are one of these structures. In Aachen, the Variscan thrust front is represented by the Aachen thrust, which continues to the west in the Midi Thrust in eastern Belgium (see Figure 2.1).

The Midi-Aachen-Thrust is the northernmost large scale thrust fault of the Variscan orogen (Oncken et al., 1999). The high strain zones at the southern margin of the Anglo-Brabant fold belt were reactivated and form part of a larger zone, the Midi-Aachen-Thrust fault zone (Legrand 1967; André et al., 1981, André and Deutsch, 1985; Debacker et al., 2003). This fault zone has often been identified along the Anglo-Brabant fold belt in eastern Belgium by the presence of brecciated rocks in boreholes (Legrand 1968).

The nappe setting and the related stacking patterns of the lithostratigraphic units were confirmed by the Bolland and Soumage drills in eastern Belgium (Graulich, 1984). Recently the RWTH-1 drill supported the nappe tectonic setting. The extension of these structures of the outer Variscan front were interpreted by seismic processing (e.g. Behrmann et al., 1991; Betz et al., 1988; Dejonghe et

al., 1989; DEKORP Research Group, 1991). These authors described a slightly south dipping reflector which is interpreted as the basal detachment fault separating the Devonian rocks from the Old Palaeozoic basement. This corresponds to the Midi-Aachen-Thrust system.

The study describes the Devonian evolution of the eastern segment of the Wurm Synclinorium to be related to the south-eastern marginal facies of the Brabant Massiv and their adjacent tectono-sedimentary units. This interpretation can be considered analogous to the facies distribution found in the Bolland and Soumage core. All the Palaeozoic rocks in the study area have been affected by the Variscan orogeny.

7.1.2 Pre-tectonic / burial-diagenetic evolution

The Upper and Lower Devonian near shore depositional successions are developed under restricted sedimentation conditions. The lithostratigraphy is characterised by rapid facies variations, irregular, non-stratified dolomitisation, erosion, brecciation and depositional gaps (Stroink, 1993, see chapter 2).

The RWTH-1 siliciclastic rocks from the various stratigraphic levels and the Upper Devonian carbonate marl and limestone contain detrital quartz, K-feldspar, biotite and plagioclase and are in some places enriched in white micas and chlorite. The presence of angular and non-recrystallised biotite and K-feldspar detritus suggest a short transport distance from the Brabant Massive and the preservation of these minerals propose rapid burial conditions.

The rocks are partially pervasive dolomitised. Where dolomitisation is more complete, the dolomite crystals form tight idiomorphic to hyidiomorphic mosaics and are typically developed as grey matrix dolomite, sometimes completely replacing limestone nodules (Figure 3.1 D). Differential matrix lithification (matrix-cements) also recrystallised the lime/dolo mud to micrite and microsparite. The varying luminescence colour of the dolostone and replacive dolomites (i.e. dolomite alteration) crystals suggest that the major part of the dolomites formed during precipitation of a fluid with variable chemical composition.

Chemical compaction formed stylocumulates, which are developed as dissolution seams and stylolites. Chemical compaction and deformation formed a S_1 foliation. This foliation formed due to a compression aligned normal to bedding, reflecting the final stages of the burial history. Late diagenetic features (e.g. micrite to microsparite cements, stylocumulates) are overprinted by the S_1 foliation within the siliciclastic, argillaceous and calcareous rocks. During the Variscan time the main deformation D_1 forming a S_2 foliation, crosscuts the S_1 foliation (Figure 4.1 G). The different rock types are partially brecciated. Brecciated zones are associated with the argillaceous intercalations (Figure 4.1 H), which played an important mechanical role during the deformation acting as preferred horizons for decoupling mechanisms with respect to shearing (see Mansy et al., 1999).

7.1.3 Tectonic evolution

Variscan tectonic led to an intense fracturing of the Palaeozoic rocks in the Wurm Synclinorium and initiated fluid migration through the rock sequences. The rocks of the RWTH-1 drill and their late burial diagenetic features are overprinted by hydrothermal veining and several cataclastic to mylonitic deformation processes (Figure 7.1).

The textural and structural vein observations identified one major deformation event (D_1). Three vein types occurred synchronously with this event, the quartz-carbonate \pm chlorite veins, the carbonate \pm chlorite veins and the quartz \pm chlorite veins. The vein minerals are accompanied by K-feldspar, plagioclase, smectite, sericite, chalcopryrite, and pyrite (see chapter 4). These minerals completely fill the shear and extensional fractures and commonly deformed (see chapter 4.3). The main alteration minerals are chlorite but also dolomite, K-feldspar and smectite. Within each vein type the minerals, the textures and the structures are different and are in detail described in Section 4.

It is characteristic of these veins that their textures usually indicate that vein filling took place episodically. In some places the veins form a very regular and dense network, often including conjugate systems (Figure 7.1; see also figure 4.7). The different vein types can be divided in shear and extensional fractures

with respect to their tectonic and geometric appearance. Shear fractures show normal and reverse faulting.

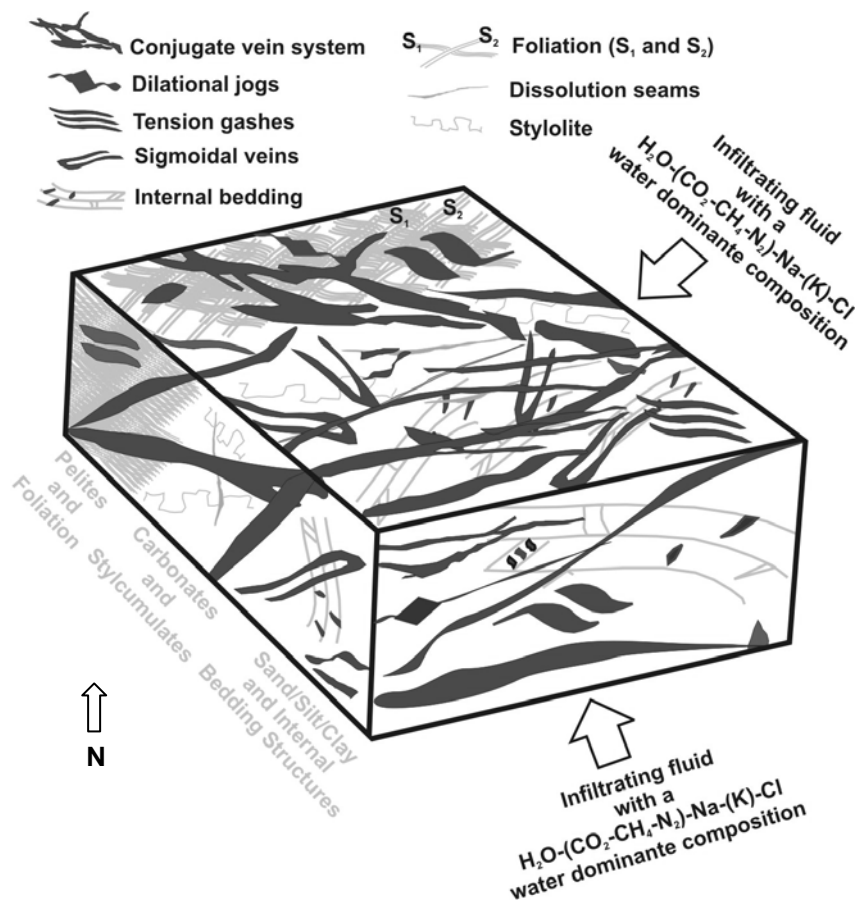


Figure 7.1: Schematic 3D block of the different lithologies during the D₁ stage, illustrating the structural fabrics, hydrothermal veining as well as the infiltrating fluid and its physicochemical conditions during convective fluid flow.

Vein structures are formed at the transition from brittle to ductile deformation indicated by dilational jogs, tension gashes and pseudotachylites. Pseudotachylites are generally found in regional-scale shear zones at the transition from brittle to ductile deformation and give strong evidence for seismic activity (e.g. shallow earthquakes; Sibson, 2001). Asymmetric pressure fringes at shear veins on fibrous to elongated chlorite grains indicate the progressive deformation processes. Subsequent shearing of these veins caused by deformation, followed by recrystallisation resulted in finer grain size or polymodal size distribution. Ductile deformation is indicated by the undulous extinction of the quartz and carbonate grains, deformation twinning of carbonates and an

initial stage of subgrain development in some of the quartz crystals. The undulatory extinction and the development of curved twinning of the carbonate minerals can be related to the onset of intracrystalline deformation mechanisms (Burkhard, 1993). Increasing pressure plays an important role in dissolving rock forming minerals (carbonate cements) and possibly on the redistribution of fluid into open fractures. Such vein characteristics are common in many fold-and-thrust belts (e.g. Dunne, 1986) and have been described by Micarelli et al., (2005). From crosscutting relationships and relationships to the vein structures mentioned above, generally it seems that all vein types formed contemporaneously during progressive deformation and that deformation took place episodically.

The several types of micro-textures are important for understanding the vein forming mechanisms. Curved and fibrous textures with growth surfaces, tension gashes and dilational jogs point to shearing during growth of the grains, while quartz and carbonates in other veins show recrystallised textures. Insoluble residuum forming selvages on the vein margin within pelitic rocks (Figure 4.4 A and B), suggesting a diffusional mechanism of mass transfer out of the wall rock (Oliver and Bons 2001). Multiple reopening of the fractures is documented by bands of rock fragments along the vein margin, which is one crack-seal indicator (Figure 4.4 G and H). The fibrous texture of veins in tension gashes (Figure 4.4 B) is also a characteristic of a crack seal origin (Ramsey, 1980). Additionally, the stretched crystal veins are of the crack seal type and the crystals have a roughly constant width across the vein. All textural/structural features of this type of vein suggest fairly pure extensional regimes during their formation within brittle deformation processes (e.g. Sibson, 2000).

Therefore, brittle deformation focused the fluid transport and the hydrothermal fluid led to mm-scale alteration of the wall rock. The different vein systems are associated with a Variscian thrust fault, indicating a Variscian age. Therefore the vein forming conditions of the hydrothermal overprint represented the situation during Variscan thrusting and fluid flow along the MAT-System at around 360 – 290 Ma.

7.2 Palaeotemperature and Fluid Composition

The integration of the physicochemical data describes a heterogeneous fluid and a heterogeneous fluid trapping (temperature/pressure) during progressive deformation (D_1). The hydrothermal fluids are H_2O -(CO_2 , CH_4 , N_2)-Na-(K)-Cl-dominant solutions of low to intermediate salinities (<2 to 9 eq.wt.% NaCl) and have homogenization temperatures of up to 390°C. The fluid inclusion assemblages (FIA) represent pulses of fluid circulation associated with the deformation processes during vein growth. Different stages of fluid inclusion trapping, based on petrographic criteria can be classified: Primary and pseudo-secondary inclusions display a heterogeneous trapping during early/syn-vein crystallisation and secondary fluid inclusions display a contemporaneously heterogeneous trapping during late vein crystallisation.

The pH of the fluid can be read from Figure 7.2 where the paragenesis sericite-K-feldspar-plagioclase indicates a pH of ca. 5.5 at 6 eq.wt.% NaCl. Contours of pH are calculated using NaCl° constants of Eugster and Baumgartner (1987). These calculations suggest that the fluid responsible for vein filling was at approximately stable pH throughout the P-T conditions of vein formation and alteration. Potassium is added to the shear vein minerals as expected for fluids with a decreasing temperature, whose composition was initially buffered by equilibrium with K and Na bearing minerals (Yardely, 1986). The fluid composition may be modified by chemical reactions during fluid dispersion and infiltration into the adjacent wall-rock (Ridley et al., 1996).

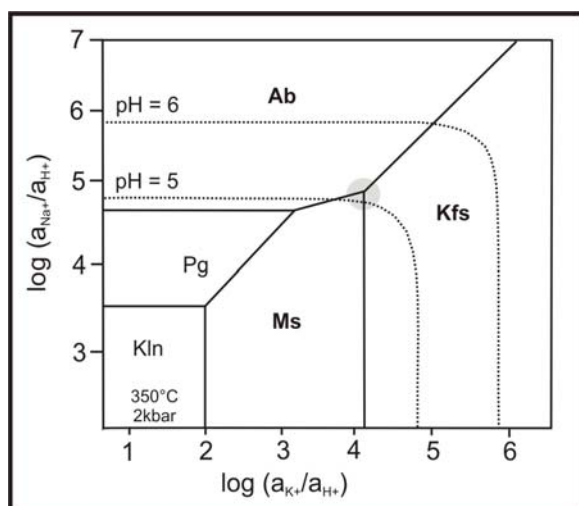


Figure 7.2: Stability relationships for Na-K aluminosilicates as a function of fluid composition at 350°C and 2 kbar. The pH conditions are for 6 eq.wt.% NaCl. Data from Bowers et al. (1984), Eugster and Baumgartner (1987), and Shock and Helgeson (1988).

The apparent constant content of major fluid components, including CO₂, CH₄, N₂, total salinity, and Na and K, suggest that concentrations of the fluid components were buffered by the fluid, and that low fluid-rock ratios existed within the fluid conduits. Under less strongly fluid-buffered conditions and low fluid rock-ratios, strong metasomatic effects would be expected only from near fluid source regions within metamorphic rocks (e.g. McCaig et al., 1990). This can be immediately ruled out as the rocks of the RWTH-1 are not metamorphic.

The occurrence of iron-rich chlorites and the zoning of the dolomite crystals with an iron-rich center indicate a variation in the supply of Fe, and Ca becoming more enriched towards late stage of fluid activity and vein filling. A reduction in Ca/Mg concentration of the fluid can be explained by precipitation of carbonates. Ca/Mg- and CO₂-bearing fluids will reach saturation with respect to dolomite and calcite at temperatures from 350 to 600°C (Mikucki and Ridley, 1993). This is a temperature at which carbonates become an ubiquitous vein phase. The iron-rich dolomite usually precipitates at higher temperatures. A fluid should generally become more acidic as it cools through the dissociation of neutral associated aqueous acid species such as HCl^o and H₂CO₃^o (e.g. Heinrich et al., 1989). At lower temperatures, carbonate precipitation reactions will also lead to fluid acidification (e.g. Kishida and Kerrich, 1987). That the pH values of the fluid stay constant at neutral values speaks for fluid-rock interaction as an important control on fluid pH. Hydrolysis reactions involving hydrothermal fluids and wall rocks (i.e. chloritisation and sericitisation), provide a convenient removal mechanism for the excess H⁺ produced by acid dissociation and carbonate precipitation. Vein mineral assemblages resulting from fluid buffering reactions during cooling of the fluid are also described by Wall (1987). The broad similarities in the fluid composition of the various fluid inclusions and the high homogenisation temperatures point to a single fluid movement through the upper crust from a fluid source outside of the outer zone of the Variscan fault and thrust belt.

The temperature and fluid composition of this fluid correspond to those of the "Tectonic Brines" in the Variscan basement of the Rhenohercynian terran east of the river Rhine (Behr et al., 1993). These fluid parameters are also in agreement with fluid inclusion studies on Variscan fault and thrust belts in eastern Belgium (see chapter 5.4.4).

7.3 Fluid Origin

The recorded high temperatures and low to intermediate salinities of the Variscan hydrothermal overprint in Palaeozoic rocks from Belgium and western Germany close to the MAT indicate rather low-metamorphic conditions than diagenetic temperatures (i.e. $\leq 150^{\circ}\text{C}$). A metamorphic fluid has high temperatures and low to intermediate salinities (e.g. Sheppard and Taylor, 1974; Taylor, 1974). The calculated $\delta^{18}\text{O}$ and δD isotopic composition from chlorite separates of vein assemblages as well from the alteration zone, and the $\delta^{18}\text{O}$ values of quartz, calcite and dolomite in conjunction with the δD isotopic composition of fluid inclusions therein have a metamorphic signature (Taylor 1974, 1979; Yardely and Graham 2002; see for detail section 6.5.1). However, Cline and Bodnar (1991) demonstrated that the salinity of the fluids released is strongly dependent on the pressure during precipitation and that high saline fluids are not common at pressure greater than about 1.3 kbar. The estimated low to intermediate salinity of the fluid inclusions from quartz carbonate vein minerals within the RWTH-1 indicates pressures >2.0 kbar (see chapter 7.6). The influx of fluids from shallower levels is unlikely at deeper crustal levels, as $P_{\text{fluid}} \approx P_{\text{lithostatic}}$ and P_{fluid} gradients are normally a few hundred bars or less (Etheridge et al., 1983). Fluid pressures at mesothermal depths of vein formation are likely to be close to lithostatic; the fluid flow is therefore constrained to an upward movement (Ridley, 1993). Indeed, the high temperature/pressure and the mostly unaltered host rock require large-scale fluid focussing over a km scale and therefore a deeper source.

The investigated fluid inclusions consist of CO_2 , CH_4 and N_2 . This gaseous composition occurs abundantly in the metamorphic zone of the Stavelot-Venn-High in eastern Belgium and western Germany (Darimont 1986; Schroyen and Muchez 2000; Kenis et al., 2002). The N_2 in the fluid type is probably due to the progressive metamorphism, which resulted in a further release of nitrogen that is bound in organic material and/or progressive maturation of NH_4 -substituting minerals in the wall rock pylosilicates of the Stavelot-Venn High. In addition, the presence of CH_4 in the fluid inclusions, resulting from the breakdown of organic material, is a good indication of this metamorphic origin. The combination of microthermometry, stable-isotopes and the regional geological setting indicate that the fluid most likely originated from metamorphic rocks

within the Stavelot-Venn-Massive and interacted with the Devonian strata along its migration path.

The enrichment of K and Na of the paragenesis sericite-K-feldspar-plagioclase associated with micro-shear veins released from an external source. However, a ready supply of K and Na exists in the host rocks, having a high mobility, in the presence of H₂O and CO₂, where differential pressures and shearing prevail (Ridley and Diamond 2000). This suggests that fluid composition could have changed during fluid-rock interactions along the fluid pathway. The isotopic composition of vein minerals compared to the isotopic composition of the host rocks also rejects the possibility of a fluid originated from the dehydration of metamorphic rocks; consequently an external fluid source is necessary. Fluid mixing would be reflected in the isotopic composition, due to the uniform $\delta^{18}\text{O}$ values of the investigated vein minerals, fluid mixing is unlikely (McCuaig and Kerrick, 1998). Stable isotopes show that no signatures of magmatic, meteoric, sedimentary or formation waters influenced the isotopy of the metamorphic water. A short-term hydrothermal convection of a fluid migrating along the MAT-System from the metamorphic area of the Stavelot-Venn-Massive represents a potential fluid emplacement mechanism. The complexity of the fluid system provides a single pure fluid to be chemically and isotopically identified. This fluid was originated from one fluid source. However, the infiltration of the high temperature fluid has produced different vein assemblages during progressive deformation and implies a reactivation of the same fluid source. Related to tectonic brines, the fluid changed in temperature, pressure and salinity as indicated from P-T fluctuations and variation in salinity during migration and fluid trapping.

7.4 Fluid-Rock Interaction

Fluid data in conjunction with hydrothermal vein, hydrothermal alteration and host rock data provide additional constraints on fluid rock interaction and accompanying P-T conditions. The low fluid-rock ratios suggest an independent fluid, unable to achieve equilibrium with the host rocks; this is supported with the petrological observation of cm-sized veins and mm-sized alteration halos. The style of the veins and alteration is indicative of fracture controlled

permeability, this is in agreement with studies of Knipe and McCaig (1994) and McCaig (1997), who concluded that micro-fracturing is the dominant mechanism for the formation of permeabilities in a brittle regime and the formation of porosities in a ductile regime. The alteration zone itself implies that fluid movement at the site of vein formation was only restricted to narrow intervals and non equilibrium conditions existed between the fluids and the host rock, aside from the tectono-sedimentary deformation factors such as porosity and permeability. The non equilibrium conditions between the wall rock and the fluid can be proved with the variation in the mineral geochemistry. The fluid and vein forming minerals associated with the D₁ deformation have a much lighter $\delta^{18}\text{O}$ and δD than the host rock, further evidencing the low fluid-rock interaction (i.e. low fluid-rock ratios).

Eppel and Abart (1997) noted that an open system within a deformational setting is related to structural and lithological discontinuities, which is the case for the situation within the RWTH-1 drill. The fluid most likely migrated along the detachment faults into the MAT-System originated from the Stavelot-Venn-Massive, where several reservoirs contributed to the fluid flow system. Moreover, open systems are associated with higher permeabilities of the rocks (e.g. Gray et al., 1991; Marquer and Burkhard 1992; Losh 1997), which is the case with the extensional regime of the veins. Open systems are often reported from extensional tectonic regimes (Conti et al., 2001), and convection is a dominant fluid flow mechanism for such systems (Jamtveit and Yardley, 1997; Oliver and Bons, 2001). Convection as a mechanism for mass transfer of fluids occurs later in the deformation history of the rock, although during early phases, diffusion is more important (Gray et al., 2001). The intensive vein formation of quartz and carbonate \pm chlorite changes to a mineral chemistry of the chlorite-sericite-k-feldspar-plagioclase paragenesis in micro shear veins, which can be related to diffusion mechanisms. Initial modelling of quantitative diffusion-reaction show that alteration halos may develop around vein forming minerals in time spans as short as several tens to hundred years (Diamond and Steefel 1993). The mm-scale chlorite alteration represents low fluid-rock ratios associated with the vein mineralisation, developing from a more focused fluid, chemically and isotopically independent of the surrounding host rock. The mineral paragenesis reflects fluid dominant (fluid buffered) reactions. The fluid component concentration (e.g. CO_2 ,

CH₄, N₂, Cl, and \pm K) also support that the fluid was buffered by vein forming minerals and that low fluid rock ratio were apparent.

7.5 Transport and Precipitation

Vein formation, alteration and deformation occurred largely during the same progressive deformation event, post-dating the development of the stylolites and the S₁ foliation. The evolution of the fluid flow system could be positively compared with the general deformation history of orogens which are often related to a late extensional phase and characterised by an opening of fluid pathways (Conti et al., 2001; Gray et al., 2001). Thermometric data of fluid inclusions and stable isotopes may well indicate the lateral and upward migration of hot fluids. The temperatures during vein filling are much higher than the temperatures of surrounding host rocks.

The fluids present during the precipitation of the shear zone veins were aqueous-carbonic (methanic/nitrogenic) and trapped under unmixing conditions. As a consequence of unmixing it can be indicated that temperature and pressure conditions of trapping are directly derived from H₂O-dominated (temperature of trapping) and CO₂/CH₄-dominated (pressure of trapping) fluid inclusions. The slight pressure fluctuations could be a consequence of recurrent pressure fluctuations during mineral growth in the vein.

Temperatures of vein formation, estimated using fluid inclusion microthermometry and mineral equilibria, cover a range of 390 down to 180°C. The earliest high temperature growth of the quartz carbonate veins occurred at temperatures from 350 to 450°C determined from oxygen isotope thermometry using quartz-carbonate pairs. The cogenetic idiomorphic quartz grains and hydromorphic carbonate grains possibly could be explained in a simplified manner if quartz is assumed to be crystallising in an infinite carbonate "solution". This is supported by the findings of Sharp and Kirschner (1994) that the diffusion rate of oxygen in quartz is significantly slower than in carbonates.

After H₂O, CO₂ is the most abundant volatile in the Earth's crust (Symonds et al., 1994), the significance of a CO₂-H₂O fluid phase is well known for metamorphic systems, and CO₂-H₂O immiscibility is explicit in fluid inclusion literature. Supercritical CO₂ and liquid H₂O coexists in the shallow crust (Kaszuba et al., 2006). They conclude that supercritical CO₂ produces acidity, carbonate

saturation, and silica supersaturation in the brine. In this state the fluid possesses properties of both gas and liquid. Pure H₂O is a supercritical fluid above 374.2°C and 0.22 kbar; whereas pure CO₂ is a supercritical fluid at much lower P-T conditions (31.1°C and 0.074 kbar). Several studies examine the effect of NaCl on the CO₂-H₂O system (Anovitz et al., 2004; Duan et al., 2006, and references therein). In general, NaCl (and other salts) in the fluid, shift the supercritical point of CO₂ and H₂O to higher temperatures and pressures (Bowers and Helgeson, 1983; Joyce and Holloway, 1993). The theoretical work of Bowers and Helgeson (1983) evaluates both NaCl and pressure effects on the interactions between silicate reactions and CO₂-H₂O equilibria at temperatures in excess of 400°C and 0.2 kbar. In the case of hydrothermal fluids, quartz precipitates in veins because silica solubility decreases in the fluid that cools and depressurises along a fracture flow path (Fyfe et al., 1978). Phase separation and subsequent emplacement of an acidic, carbonate saturated, and silica supersaturated brine into a rock-dominant system buffered to more neutral pH may enhance precipitation of carbonates and quartz as veins or cements (Kaszuba et al., 2006), depending on the permeability structures of the rocks.

The smaller amount of CH₄ could be explained by methane oxidation to carbon dioxide and water (Tarantola et al., 2007). This is supported by: 1) the higher amounts of CO₂ in the trapped volatiles, 2) the extreme decrease for δD values of water trapped within fluid inclusions at the CH₄/H₂O-CO₂ transition, and 3) the heterogeneous and low $\delta^{13}C$ values of the CO₂ within fluid inclusions (see chapter 6.5.3).

Experimental calibrations of Clayton, (1981) conclude that significant retrograde exchange occurs in the majority of quartz-carbonate bearing veins, and the degree of retrograde resetting varies regularly as a function of the peak metamorphic temperature and continues down to temperatures as low as 100°C. Vein quartz formed by saturated SiO₂ water becoming supersaturated by cooling from 450 to 400 °C (Ague, 2005). The decrease in temperature causes supersaturation of the fluid during passage through the vein channelway. Quartz can reach supersaturation by either changing fluid composition (Newton and Manning, 2000) or reducing pressures (Fournier and Potter, 1982; Etheridge, 1984), or in response to pressure-induced or strain-induced concentration gradients (Fisher and Brantley, 1992; Oelkers, 2000). A simple explanation of pressure variation within a vein is vein dilation. The fluid pressure drop caused

by fracturing and vein dilation must be small enough to keep the vein open, as indicated by free growth of idiomorphic crystals (Fisher and Brantley, 1992), but large enough to cause supersaturation and quartz precipitation. On the other hand, if the vein would close after fracturing, quartz growth and idiomorphic crystals such as those in Figure 4.3 A, would not survive. If the fluid is saturated with respect to silica at the onset of vein opening, then even a minimal reduction in pressure will result in supersaturation and growth within the vein (Sharp et al., 2005). Findings by Mroczek and Christenson (2000) have shown that at 450°C a pressure drop from only 100 kbar within a NaCl-solution lead to rapid precipitation of about one half of the dissolved silica as quartz. Increase in fluid pressure will result in the opening of micro-fractures and growth of extension veins. The opening will lead to significant localised reduction in fluid pressure. This pressure drop will result in rapid deposition of quartz. Partially collapse of the vein space and repressurisation provides a mechanism for episodic movement of low density fluids toward the MAT-System in the Aachen region.

At vein formation temperatures up to 450°C and neutral pH of around 5.5 (Mikucki, 1998), the most significant mineral complex is quartz-carbonate-chlorite, with the assemblages of sericite, k-feldspar, plagioclase and chalcopryrite. The minimal interaction with the wall rock (see above) suggests that the D₁ vein formation was triggered by a factor other than fluid rock interaction. The veins are typical shear fill veins, a common vein type in orogenic systems (Hanmer and Passchier 1991).

The mechanism for the dilation and opening of these shear fill veins are readily established, some methods are reviewed in Hodgson (1989). The author found mainly two reasonable mechanisms: (1) dilation, which occurs at internal bedding structures and jogs, at a low angle to a shear fracture or fault, during slip (Koehn and Passchier 2000) and (2) crack-seal slip, where dilation results from repeated episodes of extensions of a shear fracture (Petit et al., 1999). The brecciated vein minerals, and hydraulic fault gouge observed at the vein margin illustrates the variations in fluid pressure. Furthermore, the pressure fringes on minerals are described as a common feature of decompression textures in high pressure rocks (Klemd et al., 1994, Kisters et al., 2000). These fluctuations in fluid pressure resulting from the operation of this fault-valve mechanism may consequently induce near complete segregation of the fluid and subsequent mineral precipitation (Sibson 1990).

7.6 Genetic Model for the Vein Formation

The combination of the fluid inclusion data, petrographic and structural analysis, as well as oxygen isotope thermometry of quartz carbonate veins within the Aachen Shear Zone, provide important constraints about veining mechanisms, fluid flow and P-T evolution during veining and shear zone activity. The fluid inclusions were trapped one after the other at decreasing P-T conditions during progressive deformation and growth of the different vein minerals and are considered co-genetic. The homogenisation temperatures of up to 390 °C from primary fluid inclusions, the application of oxygen isotope fractionation between quartz-carbonate pairs and the resulting maximum temperature of 450°C, and calculated maximum pressures of up to 2.5 kbar; reflect the maximum P-T conditions during the hydrothermal overprint of the metamorphic fluid. Comparison of isochores with reasonable geothermal gradients indicates that the fluid inclusions formed in a thermal regime with a geothermal gradient between 70°C/km and 80°C/km (Figure 7.3). The estimated pressures in context with the geothermal gradient lead to maximum burial depths of up to 4 km.

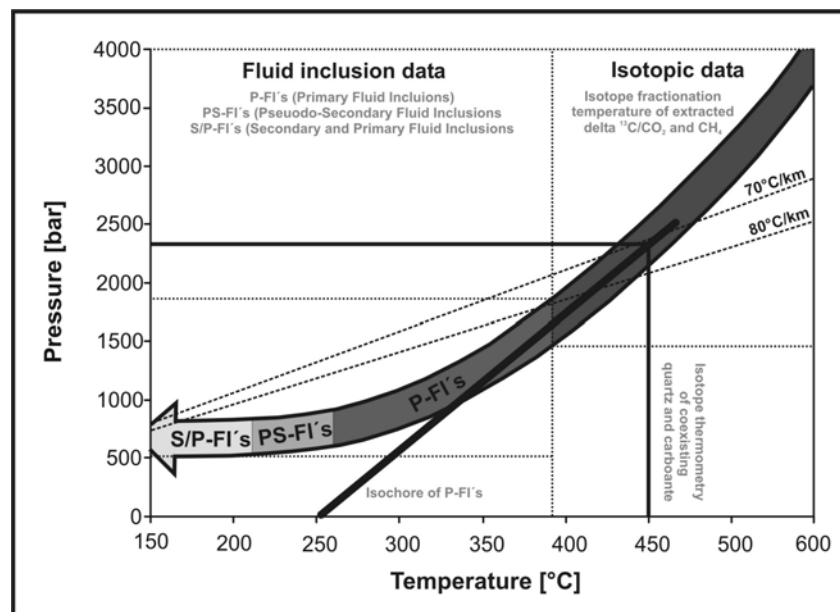


Figure 7.3: Retrograde P-T path from fluid inclusion temperatures and salinities in conjunction with higher temperatures of isotope geothermometry.

Taking all evidences into account the fluid inclusion recorded several stages of fluid circulation. The different fluid inclusion groups display a retrograde P-T path from primary over pseudo-secondary to secondary fluid inclusion trapping, with progressively decreasing temperature and pressure conditions; related to the progressive deformation within the Aachen fold and thrust belt. The low temperature ($>180^{\circ}\text{C}$) fluid inclusions marked the end of the hydrothermal fluid activity and vein formation.

The individual shear zones are associated with textural and geochemical anisotropies in the Lower and Upper Devonian rocks. The variation in the geometry of this shear zone may have resulted in dilational jogs at which regional fluid flow will have focussed (Cox et al., 2001; Sibson 2001). Therefore the P-T conditions of the hydrothermal overprint calculated here represents the situation during Variscan thrusting and hydrothermal fluid flow along the MAT at around 360 – 290 Ma. Regarding the structural setting, the south-dipping shear zone of the MAT-System forms an ideal structural feature in focussing the upward migration of the vein filling fluid. The migration of the metamorphic fluid was accompanied by progressive deformation along a low angle reverse shear zone (Figure 7.4). The shear zones essentially act as a conduit, channelling and focusing the fluid as it is driven upward. Retrograde temperatures in shear zones in general are considered a fundamental feature of metamorphic flow pattern (e.g. Etheridge 1983). The veins of the RWTH-1 drill were formed at a maximum temperature of 450°C down to 180°C and a pressure of approximately 2.5 kbar down to 1 kbar. The recorded high temperatures compared to the low temperature of the host rock represent open system behaviour and correspond to the tectono-metamorphic fluid event.

The structural and petrological reconstruction supported the Variscan stress field, and clearly identified one single fluid influx: 1) retrograde fluid trapping originated from deep metamorphic conditions, were released into the shallow crust levels of the RWTH-1 drill and 2) a thermal anomaly, positioned to the south of the MAT-System, which initiated widespread metamorphic fluid activity by fluid pumping along the detachment faults.

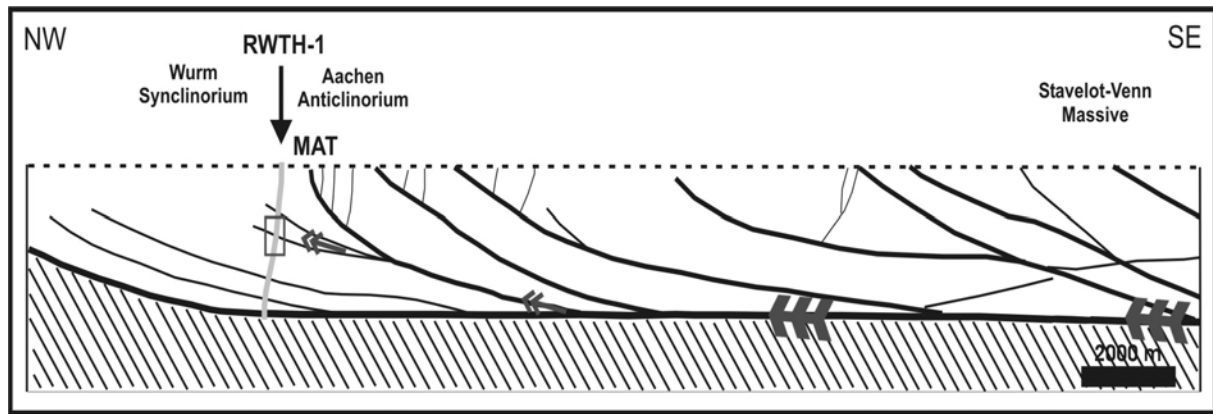


Figure 7.4: Schematic tectonic scetch along the seismic profile in the Aachen Region.

A larger-scale structural and geochemical study of vein formation associated with the MAT shear zone in the Aachen region and the Eifel High is necessary to resolve the question if a common fluid flow system is present. Such a study will eventually allow the results of the current study to be put into a broader perspective of the tectonic-sedimentary history at the southern extremity of the Anglo-Brabant fold belt and the adjacent Variscan MAT-System.

7.7 Geothermal Anomalies and Fluid Flow at the Variscan Thrust Front

The study demonstrates that the RWTH-1 and the Bolland drill show similar lithologies, similar physicochemical parameters of palaeo-fluids and a similar geothermal evolution (see CAI chapter 2.5.2, geothermometry chapter 4.4 and microthermometry chapter 5.4.4). The temperatures range of 200°C – 350°C in the Variscan hydrothermal overprint in Palaeozoic rocks from Belgium and western Germany close to the MAT are similar to each other but different compared to other studies in the Aachen region (see chapter 2.4). The high palaeo-geothermal gradient of about 70°C/km is likely the result of convective heat transport by hydrothermal fluid flow along permeable pathways during the Variscan orogeny. The recently measured temperature of 86°C stored in the RWTH-1 drill (Lundershausen, 2006) suggests a recent geothermal gradient of 30°C/km. This slightly increased geothermal gradient and the fact that all porosity in the rocks is destroyed by the Variscan hydrothermal overprint points to heat flow dominated by more conductive transport processes. However, recent seismic activity (e.g the 1992 Roermond earthquake) and hot springs suggest a

contribution by fracture-controlled hydrothermal heat transport restricted to post-Variscan D₂ structures in the Aachen region.

The close association of the palaeo-geothermal anomaly within the MAT suggests that the northward and upward migration of hot fluids along this fault modified the palaeo-temperature during the Variscan orogeny. However, fault controlled, episodic expulsion of deep fluids can easily explain such temperature anomalies. Higher temperature anomalies found by modelling of the palaeotemperature field at the MAT are most likely due to northward migrating of hydrothermal fluids along thrust faults (Luenenschloss et al., 1997; Luenenschloss, 1998). The expulsion and migration of fluids from the metamorphic area of the Stavelot-Venn-Massif along faults towards the MAT represents a simple explanation for the palaeo-geothermal anomaly and the hydrothermal vein formation. Brittle deformation of the fault and shear zones formed the permeability, which led to the precipitation of hydrothermal minerals from a metamorphic fluid. Numerical experiments on a wide range of geological environments show that permeability is usually the primary controlling factor on fluid flux and, therefore effective heat transport to lower crustal levels (Manning and Ingebritsen, 1999).

Primary fluid inclusions in quartz and carbonate grains of the hydrothermal veins, their homogenisation temperature of up to 390°C and pressures of up to 2.5 kbar, in conjunction with the CAI host rock temperatures, between 245°C and 320°C (see chapter 2.5.2), provide a small-scale fluid/rock interaction within the system. The minor hydrothermal alteration into the host rock point to a focused fluid flow. These fluid rock interactions imply a short-term, episodic fluid transport due to tectonic opening movements along shear zones. The abundance of extensional fractures (e.g. dilatancy structures and pseudotachylites) in the core can be related to shallow earthquakes during the time of hydrothermal veining. A consequence of the dilatancy and fluid-diffusion mechanism (e. g. shallow earthquakes) is that considerable volumes of fluids are rapidly redistributed in the crust via the reactivation of fault systems (Sibson, 1990). Seismic energy and the resulting brittle deformation are responsible for the development of permeabilities along the shear zones and seismic pumping controlled the hydrothermal fluid flow. This mechanism provides an explanation for the textures of the hydrothermal veins along the MAT, within the vicinity of the RWTH-1 geothermic drill. This model is generally accepted as a viable and

important mechanism of hydrothermal fluid transport (Cox et al., 2001; Sibson, 2001).

This study demonstrates the importance of fluid inclusion research for the reconstruction of palaeo-geothermal gradients, the palaeo-fluid flow and the recognition of multiple fluid flow periods during the evolution of the Devonian strata in the Variscan fold-and-thrust belt. The possible influence of metamorphic fluids on the temperature regime along thrust faults at the Variscan front zone has been discussed. The results obtained from the RWTH-1 drill suggest a rapid upward fluid flow along the MAT in a nappe tectonic setting. The high palaeo-geothermal gradient suggests dominant convective heat transport during the Variscan orogeny. During large-scale tectonics large amounts of fluids can be expelled (Vrolijk et al., 1988). Such a fluid migrated along the detachment faults into the MAT-System. However, during the compressional tectonic activity only small amounts of the fluid were active in the Wurm Synclinorium in the studied part of the MAT-System.

The fluids released during Variscan metamorphism relate to a deeper crustal source as they are H₂O-Na-(K)-Cl-dominant solutions of low to intermediate salinities with CO₂, N₂ and CH₄. During seismic activities this fluid was pumped into the system. The fluid inclusion homogenisation temperatures of up to 390°C within the vein minerals are several tens of degrees higher than the temperature of the host rock and are several hundred degrees higher than the reservoir temperatures at the time of exploitation, indicating that the system was heated up during the Variscan Orogeny and no more than conductive heat flow is retained.

8 References

- Ague, J.J.**, (2005): Fluid flow in the deep crust, in Rudnick, R.L., editor, *Treatise on Geochemistry, The Crust*: Amsterdam, Elsevier, pp. 195-228.
- Anderson, M.R., Rankin, A.H., Spiro, B.**, (1992): Fluid mixing in the generation of mesothermal gold mineralisation in the Transvaal Sequence, Transvaal, South Africa. *Eur. J. Mineral.* 4, 933-948.
- André, L., Deutsch, S., Michot, J.**, (1981): Données géochronologiques concernant le développement tectono-métamorphique du segment Calédonien Brabancon. *Ann. Soc. Geol. Belg.* 104, 241-253.
- André, L., Deutsch, S.**, (1985): Very low grade Sr isotopic resetting of magmatic rocks and minerals: evidence for the late Givetian strike-slip division of the Brabant Massive, Belgium. *Journal of the Geological Society London.* 142, 911-923.
- Anovitz, L.M., Labotka, T.C., Blencoe, J.G., Horita, J.**, (2004): Experimental determination of the activity-composition relations and phase equilibria of H₂O-CO₂-NaCl fluids at 500°C and 500 bars, *Geochim. Cosmochim. Acta*, 68, 3557-3567.
- Ayalon, A., and Longstaff, F.J.**, (1988): Oxygen isotope studies of diagenesis and pore water evolution in the western Canada sedimentary basin: evidence from the Upper Cretaceous basal Belly River sandstone, Alberta. *J. Sediment. Petrol.*, 58, 489-505.
- Behr, H. J., Gerler, J., Hein, U. F. & Reutel, C. J.**, (1993): Tectonic Brines und Basement Brines in den mitteleuropäischen Varisziden: Herkunft, metallogenetische Bedeutung und geologische Aktivität. *Goettinger Arb.Geol.Paläont.*, 58, 3-28.
- Behrmann, J., Drozdowski, G., Heinrichs, T., Huch, M., Meyer, W., Oncken, O.**, (1991): Crustal-scale balanced cross section through the Variscan fold belt, Germany: the central EGT-segment. *Tectonophysics*, 196, 1-21.
- Betz, D., Durst, H., Grundlach, T.**, (1988): Deep structural seismic reflection investigations across the North-eastern Stavelot-Venn Massiv. *Annales de la Société géologique de Belgique*, 111, 217-228.
- Bigeleisen, J., and Mayer, M.**, (1947): Isotopic exchange reactions. *J. Chem. Physics.* 15, 261-267.
- Böhlke, J.K.**, (1989): Comparison of metasomatic reactions between a common CO₂-rich vein fluid and diverse wall rocks: intensive variables, mass transfers, and Au mineralisation at Alleghancy, California. *Economic Geology.* 84, 291-327.
- Bottinga, Y.**, (1968): Calculation of fractionation factors for carbon and oxygen exchange in the system calcite-carbon dioxide-water: *J. Phys. Chem.* 72, pp. 4338-4340.
- Bottinga, Y.**, (1969): Calculated fractionation factors for carbon and hydrogen isotope exchange in the system calcite-carbon dioxide-graphite-methane-hydrogen-water vapour. *Geochim. Cosmochim. Acta* 33, 49-64.
- Bottinga, Y., and Javoy, M.**, (1973): Comments on oxygen isotope geothermometry. *Earth Planet. Sci. Lett.* 20, 250-265.

- Bowers, T.S., and Helgeson, H.C.,** (1983): Calculation of the thermodynamic and geochemical consequences of nonideal mixing in the system $\text{H}_2\text{O}-\text{CO}_2-\text{NaCl}$ on phase-relations in geological systems: Equation of state for $\text{H}_2\text{O}-\text{CO}_2-\text{NaCl}$ fluids at high pressures and temperatures. *Geochim. Cosmochim. Acta* 47, 1247-1275.
- Bowers, T.S., Jackson, K.J., Helgeson, H.C.,** (1984): Equilibrium Activity Diagrams for Coexisting Minerals and Aqueous Solutions at Pressures and Temperatures to 5 kb and 600°C. Springer, Berlin Heidelberg New York, 397 pp.
- Bowers, T.S., and Helgeson, H.C.,** (1985): Fortran programs for generating of fluid inclusions and fugacity coefficients for the system $\text{H}_2\text{O}-\text{CO}_2-\text{NaCl}$ at high pressures and temperatures. *Computer and Geosciences* 11, 203-213.
- Brown, E.B.,** (1989). Flincor: a microcomputer program for the reduction and investigation of fluid inclusion data. *Am. Mineral.* 74, 1390-1393.
- Browne, P.R.L., Roedder, E., Wodzicki, A.,** (1974): Comparison of past and present geothermal waters from a study of fluid inclusions, Broadlands field, New Zealand. *Proceedings of the International Symposium on Water-Rock Interaction*, pp. 43-47.
- Budd, D.A., Hammes, U., Ward, W.B.,** (2000): Cathodoluminescence in calcite cements: New insight on Pb and Zn sensitising, Mn activation, and Fe quenching at low trace-element concentrations. *Journal of Sedimentary Research*. 70, 217-226.
- Burkhard, M., Kerrich, R.,** (1988): Fluid regimes in the deformation of the Helvetic nappes, Switzerland, as inferred from isotopic data. *Contributions to Mineralogy and Petrology* 99, 416-429.
- Burkhard, M.,** (1993): Calcite twins, their geometry, appearance and significance as stress-strain markers indicates of tectonic regimes: a review. *J. Struc: Geol.*, 15: 351-368.
- Campbell, A.R., and Larsen, P.,** (1998): Introduction to Stable Isotope Application in Hydrothermal Systems. *Techniques in Hydrothermal Ore Deposits. Geology. J. Richardson and P. Larsen, Reviews in Economic Geology*. 10: 173-193.
- Cartwright, I., Buick, I.S.,** (2000): Fluid generation, vein formation and the degree of fluid-rock interaction during decompression of high-pressure terranes: the Schists Lustrés, Alpine Corsica, France. *Journal of Metamorphic Geology*, 18, 607-624.
- Cathelineau, M., Nieva, D.,** (1985): A chlorite solid solution geothermometer in the Los Azufres (Mexico) geothermal system. *Contrib. Mineral. Petrol.* 91, 235-244.
- Clayton, R.N., Friedman, I., Graf, D., Mayeda, T.K., Meents, W.F., Shimp, N.F.,** (1966): The origin of saline formation waters, 1. Isotopic composition. *J. Geophys. Res.* 71: 3869-382.
- Clayton, R.N.,** (1981): Isotopic thermometry. In *Thermodynamics of Minerals and Melts* (ed. R.C. Newton et al.), pp. 85-109. Springer Verlag.
- Cline, J.S., and Bodnar, R.J.,** (1991): Can Economic Porphyry Copper Mineralisation Be Generated by a Typical Calc-Alkaline Melt? *Journal of Geophysical Research* 96: 8113-8126.

- Cole, D.R., and Ripley, E.M.,** (1998): Oxygen isotope fractionation between chlorite and water from 170 to 350°C: A preliminary assessment based on partial exchange and fluid/rock experiments. *Geochim. Cosmochim. Acta* 65 (4), 449-457.
- Coleman, L.M. and Raiswell, R.,** (1981): Carbon, oxygen and sulphur isotope variations in concretions from the Upper Lias of N.E. England. *Geochim. Cosmochim. Acta* 45, 329-340.
- Conrad, M.E., and Chamberlain, C.P.,** (1992): Laser-based, in situ measurements of fins-scale variation in the $\delta^{18}\text{O}$ values of hydrothermal quartz. *Geology*, v. 20, p. 812-816.
- Conrad, M.E., O'Neil, J.R., and Peterson, U.,** (1995): The relation between widespread $\delta^{18}\text{O}$ depletion patterns and precious metal mineralisation in the Tayolita Mine, Durango, Mexico: *Economic Geology*, v. 90, p. 322-342.
- Conti, A., Turpin, L., Polino, R., Mattei, M., Zuppi, G.M.,** (2001): The relationship between evolution of fluid chemistry and the style of brittle deformation: Examples from the Northern Apennines (Italy). *Tectonophysics*, 330, 103-117.
- Cox, S.F., Knackstedt, M.A., Braun, J.,** (2001): Principles on Structural Control on Permeability and Fluid Flow in Hydrothermal Systems. *Structural Controls on Ore Genesis*. J.P. Richards and R.M. Tosdal, *Reviews in Economic Geology*, 14, 1-24.
- Darimont A.,** (1986): Les inclusions fluides de quartz filoniens d'Ardenne. *Annals de la Société Géologiques Belge*. 109, 587-601.
- Debacker, T.N., Herbosch, A., Sintubin, M., Verniers, J.,** (2003): Palaeozoic deformation history of the Asquempont-virginal area (Brabant Massive, Belgium). *Memoirs of the Geological Survey of Belgium*. 49, 1-30.
- DEKORP-Research-Group,** (1991): Results of the DEKORB 1 (BELKORP-DEKORP) deep seismic reflection studies in the western part of the Rhenish Massiv. *Geophys. J. Int.*, 106, 203-227.
- Dejonghe, L., Graulich, J.M., Hance, L.,** (1989): Les enseignements d'une campagne sismique conduite entre Liège et Verviers. *Bulletin de la Société belge de Géologie*, 98, 29-36.
- De Vos, W., Verniers, J. Herbosch, A., Vanguetstaine, M.,** (1993): A new geological map of the Brabant Massive, Belgium. *Geol. Mag.* 130, 605-611.
- Dewaele, S., Muchez, Ph., Banks, D.,** (2004): Fluid evolution along multistage composite fault systems at the southern margin of the Lower Palaeozoic Anglo-Brabant fold belt, Belgium. *Geofluids* 4, 1-16.
- Diamond, L.W., and Steefel, C.I.,** (1993): Geochronometry of Fluid-Rock Interaction in Hydrothermal Ore Deposits: Results of Diffusion Reaction Modelling of Gold-Quartz Veins in Brusson, NW Italian Alps [Abs.]. *Terra Nova*, 1 (5), 455.
- Duan, Z.H., Sun, R., Zhu, C., Chou, I.M.,** (2006): An improved model for the calculation of CO_2 solubility in aqueous solutions containing Na^+ , K^+ , Ca^{2+} , Mg^{2+} , Cl^- , and SO_4^{2-} , *Mar. Chem.*, 98, 131-139.
- Dunne, W.M.,** (1986): Mesostructural development in detached folds: an example from West Virginia. *Journal of Geology*. 94, 473-488.

- Eppel, H., and Abart, R.,** (1997): Grain-scale stable isotope disequilibrium during fluid-rock interaction; 2, An example from the Penninic-Austroalpine tectonic contact in eastern Switzerland. *American Journal of Science*. 297, 707-728.
- Epstein, S.,** (1970): Antarctic Ice Sheet: Stable Isotope Analysis of Byrd Station Coves and Interhemispheric Climatic Implications. *Science* 168: 570-572.
- Epstein, A.G., Epstein, J.B. & Harries, L.D.,** (1977): Conodont Colour Alteration, an index to organic metamorphism. U.S. Geological Survey Prof. paper, Washington, 995, 27 p.
- Etheridge, M.A., Wall, V.J., Vernon, R.H.,** (1983): The role of the fluid phase during regional metamorphism and deformation. *Journal of Metamorphic Geology*, 1, 205-226.
- Etheridge, M.A., Wall, V.J., Cox, S.F.,** (1984): High fluid pressure during regional metamorphism and deformation: implication for mass transport and deformation mechanisms. *Journal of Geophysical Research*, 89, 4344-4358.
- Eugster, H.P., and Baumgartner, L.,** (1987): Mineral solubilities and speciation in supercritical metamorphic fluids. In: Carmichael, I.S.E., Eugster, H.P., (eds.) *Thermodynamic Modelling of Geological Materials. Minerals, Fluids and Melts*. Mineralogical Society of America, Rev. Mineralogy. 17, 367-404.
- Ferry, J.M.,** (1994): A historical review of metamorphic fluid flow. *Journal of Geophysical Research*, 99, 15487-15498.
- Fisher, D.M., and Brantley, S.L.,** (1992): Models of quartz overgrowth and vein formation: Deformation and episodic fluid flow in an ancient subduction zone. *Journal of Geophysical Research*, 97, 20043-20061.
- Fournier, R.O., and Potter, R.W., III,** (1982): An equation correlating the solubility of quartz in water from 25 to 900°C and pressures up to 10.000 bars: *Geochim. Cosmochim. Acta* 46, 1969-1973.
- Franke, W.,** (1989): Tectonostratigraphic units in the Variscan belt of central Europe. – *Geol. Soc. Amer., Spec. Pap.*, 230: 67-90.
- Franke, W., Dallmeyer, R.D., Weber, K.,** (1995): Geodynamic evolution. In: Dallmeyer, R.D., Franke, W., Weber, K., (Eds.), *Pre-Permian Geology of Central and Eastern Europe*. Springer-Verlag, Berlin, pp. 579-593.
- Franke, W.,** (2000): The mid-European segment of the Variscides: Tectonostratigraphic units, terrane boundaries and plate tectonic evolution. In: Franke, W., Haak, V., Oncken, O., Tanner, D., (Eds), *Orogenic Processes: Quantification and modelling in the Variscan Belt*, Geological Society, London, Special Publications no. 179, pp. 35-61.
- Fransolet, A.M., Kramm, U.,** (1983): Mineralogie und Petrologie Mn-reicher Metapelite des Venn-Stavelot Massives, Ardennen, und die varistische Metamorphose im nordwestlichen Rheinischen Schild. *Fortschr Mineral Bd* 61: 31-69.
- Fyfe, W.S., Price, N.J., Thompson, A.B.,** (1978): *Fluids in the Earth's Crust*, Elsevier, New York.
- Garven, G., Ge, S., Person, M.A., Sverjensky, D.A.,** (1993): Genesis of stratabound ore deposits in the mid-continent basins of North America, 1, role of groundwater flow. *American Journal of Science*, 293, 497-568.

- Geomare E., Catot E., Dejonghe L., Hance L., Steemans P.,** (1997): Sédimentologie Des Formations de Marteau, du Bois d'Ausse et de la partie inférieure de la Formation d'Acoz (Dévonien inférieure) dans l'est de la Belgique, au bord nord du Massif de Stavelot. *Mem Geol Surv Belg* 42: 1-168.
- Glasmacher, U.,** (1995): Variszische und postvariszische Fluidsysteme. – In: Walter, R., Glasmacher, U. & Wolf, M. (eds.): KW-relevante Eigenschaften potentieller Mutter- und Speichergesteine am Nordrand des Linksrheinischen Schiefergebirges. – RWTH Aachen, BMBF-Forschungsprojekt 032 6804 A 5, 01.04.1991 – 30.09.1994, Teil 5, 1 – 40.
- Graham, C.M., Atkinson, J., and Harmon, R.S.,** (1984): Hydrogen Isotope Fractionation in the System Chlorite-Water. *Nerc 6th Progress Report of Research 1981-1984*, NERC Publication Series D. 25: 139.
- Graham, C.M., Viglino, J.A., and Harmon, R.S.,** (1987): Experimental Study of Hydrogen-Isotope Exchange between Aluminous Chlorite and Water and of hydrogen Diffusion in Chlorite. *American Mineralogist* 72: 566-579.
- Graulich, J.M.,** (1984): Coupe géologique passant par les sondages d'Hermalle-Sous-Argenteau, Bolland, Soumagne, Sorion, Pepinster 2 et Juslenville, commentaries. *Bulletin de la Société belge de Géologie*, 93, 45-49.
- Gray, D.R., Gregory, R.T., Durney, D.W.,** (1991): Rock-buffered fluid-rock interaction in deformed quartz-rich turbidite sequences, eastern Australia. *Journal of Geophysical Research*, 96, 681-704.
- Gray, E.B., Anastasio, D.J., Holl, J.E.,** (2001): Synorogenic crustal fluid infiltration in the Idaho-Montana thrust belt. *Geophysical Research Letters*, 28, 4295-4298.
- Hanmer, S., and Passchier, C.W.,** (1991): Shear Sense Indicators: A Review. *Geological Survey Canada Papers*, 90, 1-71.
- Hardie, L.A.,** (1987): Dolomitisation: a critical view of some current views. *J. Sedim. Petrol.* 57, 166-183.
- Heinrich, C.A., Henley, R.W., Seward, T.M.,** (1989): Hydrothermal Systems. *Australian Mineral Foundation, Adelaide*, 74 pp.
- Helsen, S., Koenigshof, P.,** (1994): Conodont thermal alteration patterns in Palaeozoic rocks from eastern Belgium, northern France and western Germany. *Geol Mag* 131: 369-386.
- Hitchon, B., Friedman, I.,** (1969): Geochemistry and origin of formation waters in the western Canada sedimentary basin. I. Stable isotopes of hydrogen and oxygen. *Geochim. Cosmochim. Acta* 33, 1321-1349.
- Hodgson, C.J.,** (1989): The Structure of Shear-Related, Vein-Type Gold Deposits: A Review. *Ore Geology Reviews*, 4, 231-273.
- Hollmann, G., Walter, R.,** (1995): The Variscan deformation front between Stavelot-Venn Anticline and Brabant Massiv: a balanced geological cross section along the Liège-Theux traverse. *Neues Jahrbuch für Geologie und Paläontologie, Mh.*, 1995, 92-104.
- Hollmann, G.,** (1997): Der Variszische Vorlandüberschiebungsgürtel der Ostbelgischen Ardennen – Ein bilanziertes Modell.- *Aachener Geowissenschaftliche Beiträge*, 23, 209 S.

- Horita, J.**, (2001): Carbon isotope exchange in the system CO₂-CH₄ at elevated temperatures. *Geochim. Cosmochim. Acta* 65 (12), 1907-1919.
- Irwin, H., Curtis, C., Coleman, M.**, (1977): Isotopic evidence for source of diagenetic carbonates formed during burial of organic rich sediments. *Nature* 269, 209-213.
- Jamtveit, B., and Yardley, B.W.D.**, (1997): Fluid flow and transport in rocks: an overview. In *Fluid flow and transport in rocks* (eds. Jamtveit, B., and Yardley, B.W.D.), pp. 1-14. London: Chapman and Hall.
- Joyce, D.B., and Holloway, J.R.**, (1993): An experimental-determination of the thermodynamic properties of H₂O-CO₂-NaCl fluids at high pressures and temperatures, *Cosmochim. Acta* 57, 733-746.
- Kaszuba, J.P., Williams, L.L., Janecky, D.R., Hollis, W.K., Tsimpanogiannis, I.N.**, (2006): Immiscible CO₂-H₂O fluids in the shallow crust. *G3 – Journal of Earth Science, AGU and the Geochemical Society of America*, 7, (10), 1-11.
- Kenis, I., Sintubin, M., Mansy, J.L., Lacquement, F.**, (2000): The use of combined structural, stable isotopes and fluid inclusion study to constrain the kinematic history at the northern Variscan front zone (Bettrechies, France). *J Struc. Geol.* 22, 598-602.
- Kenis, I., Sintubin, M., Muchez, Ph., Burke, E.A.J.**, (2002): The boudinage question in the High Ardenne Slate belt: a combined structural and fluid inclusion approach. *Tectonophysics*, 348, 93-110.
- Klemd, R., Matthes, S., Schüssler, U.**, (1994): Reaction Textures and Fluid Behaviour in Very High Pressure Calc-Silicate Rocks of the Münchberg Gneiss Complex, Bavaria, Germany. *Journal of Metamorphic Geology*, 12, 735-745.
- Kishida, A., and Kerrich, R.**, (1987): Hydrothermal alteration zoning and gold concentration at the Kerr-Addison Archean lode-gold deposits. *Econ. Geol.* 82, 649-690.
- Kisters, A.F.M., Kolb, J., Meyer, F.M., Hoernes, S.**, (2000): Hydrologic Segmentation of High-Temperature Shear Zones: Geochemical and Isotopic Constraints from Auriferous Mylonites of the Renco Mine, Southern Zimbabwe. *Journal of Structural Geology*, 22, 811-829.
- Koehn, D., and Passchier, C.W.**, (2000): Shear Sense Indicators in Striped Bedding-Veins. *Journal of Structural Geology*, 22/8, 1141-1151.
- Kossmat, F.**, (1927): Gliederung des variszischen Gebirgsbaues. *Abh. Sächs. Geol. L. – Anst. Ausgabe 1 Leipzig*.
- Kramm, U.**, (1982): Die Metamorphose des Venn-Stavelot-Massives, nordwestliches Rheinisches Schiefergebirge: Grad, Alter und Ursache. *Decheniana* 135: 121-178.
- Knipe, R.J., and McCaig, A.M.**, (1994): Microstructural and Mircochemical Consequences of Fluid Flow in Deforming Rocks. *Geofluids: Origin, Migration and Evolution of Fluid in Sedimentary Basins*. J. Parnell, Geological Society Special Publication. 78, 99-112.
- Land, L.S.**, (1980): The isotopic and trace element geochemistry of dolomite: the state of the art. *Concepts and Models of Dolomitisation* (Ed. Zenger, D.H., Dunham, J.B., Ethington, R.L.) *Soc. Econ. Paleont. Mineral. Spec. Publ.* 28, 87-110.

- Legrand, R.**, (1967): Ronquières. Documents géologiques. Mem. Cartes Geol. Miner. Belg. 6, 1-60.
- Legrand, R.**, (1968): Le Massif du Brabant. Mémoires pour servir à l'Explication des Cartes Géologiques et Minières de la Belgique. 9, 1-148.
- Longstaffe, F.J., and Ayalon, A.**, (1987): Oxygen-isotope studies of clastic diagenesis in the Lower Cretaceous Viking Formation, Alberta: implications for the role of meteoric water. In: Marshall, J.D., (ed.) Diagenesis of sedimentary sequences. Geol. Soc. Spec. Publ. 36: 277-296.
- Longstaffe, F.J., and Ayalon, A.**, (1991): Mineralogical and O-isotope studies of diagenesis and porewater evolution in continental sandstones, Cretaceous Belly River Group, Alberta, Canada. Appl. Geochem. 6: 291-303.
- Losh, S.**, (1997): Stable isotopes and modeling studies of fluid-rock interaction associated with the Snake Range and Mormon Peak detachment faults, Nevada. Geological Society of America Bulletin, 109, 300-323.
- Lünenschloss B., Bayer U., Muchez Ph.**, (1997). Coalification anomalies induced by fluid flow at the Variscan thrust front: a numerical model of the palaeo-temperatures field. Geol Mijnbouw 76: 271-275.
- Lünenschloss B.**, (1998). Modellierung der Temperatur- und Fluidgeschichte an der variszischen Front (Verviers-Synklinorium und Nordeifel). PhD Katholieke Universiteit Leuven (Belgium), 132 pp.
- Machel, H.G., and Mountjoy, E.W.**, (1987): Chemistry and Environments of Dolomitisation – a reappraisal Reply to discussion by Stoessel, R.K. Earth Science, v. 24, p. 213-215.
- Manning, C.E. & Ingebritsen, S.E.**, (1999): Permeability of the continental crust: Implications of geothermal data and metamorphic systems. Reviews of Geophysics, 37, 1, pp. 127-150.
- Mansy, J.L., Everaerts, M., De Vos, W.**, (1999): Structural analysis of the adjacent Acadian and Variscan fold belts in Belgium and Northern France from geophysical and geological evidence. Tectonophysics. 309, 99-116.
- Marquer, D., Burkhard, M.**, (1992): Fluid circulation, progressive deformation and mass-transfer processes in the upper crust: the example of basement-cover relationships in the External Crystalline Massives, Switzerland. Journal of Structural Geology, 14, 1047-1057.
- McCaig, A.M., Wickham, S.M., Taylor, H.P.**, (1990): Deep fluid circulation in alpine shear zones, Pyrenees, France: field and oxygen isotope studies. Contrib. Mineral. Petrol. 106, 41-60.
- McCaig, A.M.**, (1997): The geochemistry of volatile fluid flow in shear zones. Deformation-enhanced Fluid Transport in the Earth's Crust and Mantle. Edited by M.B. Holness. Published by Chapman & Hall, London. ISBN 0 412 75290 5.
- McCuaig, T.C., Kerrich, R.**, (1998): P-T-t deformation-fluid characteristics of lode gold deposits: evidence from alteration systematics. Ore Geology Reviews, 12, 381-453.

- Micarelli, L., Benedicto, A., Invernizzi, C., Saint-Bezar, B., Michelot, J.L., Vergely, P.,** (2005): Influence of P/T conditions on the style of normal fault initiation and growth in limestones from the SE-Basin, France. *Journal of Structural Geology* 27(9), 1577-1598.
- Mikucki, E.J., and Ridley, J.R.,** (1993): The Hydrothermal Fluid of Archean Lode-Gold Deposits at Different Metamorphic Grades: Compositional Constrains from Ore and Wallrock Assemblages. *Mineralium Deposita*. 28, 469-481.
- Mikucki, E.J.,** (1998): Hydrothermal Transport and Depositional Processes in Archean Lode-Gold Systems: A Review. *Ore Geology Reviews*, 13, 307-321.
- Mroczek, Ed., and Christenson, B.,** (2000): Solubility of Quartz in Hypersaline Brine – Implications for Fracture Permeability at the Brittle-Ductile Transition.
- Muchez, Ph., Marshall, J.D., Touret, J.L.R., Viaene, W.A.,** (1994): Origin an migration of palaeofluids in the Upper Viséan of the Campine Basin, northern Belgium. *Sedimentology* 41, 133-145.
- Muchez, Ph., Zhang, Y., Dejonghe, L., Viaene, W., Keppens, E.,** (1998): Evolution of palaeofluids at the Variscan thrust front in eastern Belgium. *Geol. Rundsch.* 87, 373-380.
- Muchez, P., Sintubin, M. & Swennen, R.,** (2000): Origin and migration pattern of paleofluids during orogeny: discussion on the Variscides of Belgium and northern France. *Journal of Geochemical Exploration*, 69-70, 47-51.
- Mueller, A.G., Groves, D.I., Delor, C.P.,** (1991): The Savage Lode magnesian skarn in the Marvel Loch gold-silver mine, Southern, Cross Greenstone belt, Western Australia. 2. Pressure-temperature estimates and constrains on fluid source. *Can. J. Earth. Sci.* 28: 686-705.
- Mullis, J., Dubessy, J., Poty, B., O'Neil, J.,** (1994): Fluid regimes during late stage of a continental collision: Physical, chemical, and stable isotopes measurements of fluid inclusions in fissure quartz from a geotraverse through the Central Alps, Switzerland. *Geochim. Cosmochim. Acta* 58 (10), 2239-2267.
- Murphy, P.J., Roberts, S.,** (1997): Evolution of metamorphic fluid and its role in lode gold mineralisation in the Central Iberian Zone. *Mineralium Deposita*, 32, 459-474.
- Nesbitt, B.E.,** (1990): Fluid in Tectonically Active Regimes of the Continental Crust. *Mineralogical Association of Canada, Canada. Short Course Handbook* 18.
- Newton, R.C., and Manning, C.E.,** (2000): Quartz solubility in H₂O-NaCl and H₂O-CO₂ solutions at deep crust-upper mantle pressure and temperatures: 2-15 kbar and 500-900°C: *Geochim. Cosmochim. Acta* 64, 2993-3005.
- Ohmoto, H., and Kerrick, D.,** (1977): Devolatilisation equilibria in graphitic systems. *Am. J. Sci.* 277, pp. 1013-1044.
- Ohmoto, H., and Rye, R.O.,** (1979): Isotopes of sulphur and carbon. In: Barnes H.L. (ed.), *Geochemistry of hydrothermal ore deposits*. Wiley, New York, pp. 509-567.
- Oliver, J.,** (1986): Fluids expelled tectonically from orogenic belts: Their role in hydrocarbon migration and other geological phenomena. *Geology*, 14, 99-102.

- Oliver, N.H.S.**, (1996): Review and classification of structural controls on fluid flow during regional metamorphism. *Journal of Metamorphic Geology*, 14, 477-492.
- Oliver, N.H.S., and Bons, P.D.**, (2001): Mechanism of fluid flow and fluid-rock interaction in fossil metamorphic hydrothermal systems inferred from vein-wallrock patterns, geometry and microstructures. *Geofluids* 1, 137-162.
- Oncken, O., von Winterfeld, C., Dittmar, U.**, (1999): Accretion of a passive margin: The late Palaeozoic Rhenohertzynian fold and thrust belt (Middle European Variscides). *Tectonics*, 18: 75-91.
- Oncken, O., Plesch, A., Weber, J., Ricken, W., Schrader, S.**, (2000): Passive margin detachment during arc-continent collision. In: Franke, W., Haak, V., Oncken, O., Tanner, D., (Eds), *Orogenic Processes: Quantification and modelling in the Variscan Belt*, Geological Society, London, Special Publications no. 179, pp. 199-216.
- Oelkers, E.H., Bjorkum, P.A., Walderhaug, O., Nadeau, P.H., Murphy, W.M.**, (2000): Making diagenesis obey thermodynamics and kinetics: the case of quartz cementation in sandstones from offshore mid-Norway: *Applied Geochemistry*, 15, 295-309.
- Östereich, B., Ribbert, K.H., Wrede, V.**, (2005): Erste Ergebnisse zur biostratigraphischen und tektonischen Einordnung der Bohrung RWTH-1, unpublished report, GD-NRW 2005.
- Parry, W.T., Hedderly-Smith, D., Bruhn, R.L.**, (1991): Fluid inclusions and hydrothermal alteration on the Dixie Valley Fault, Nevada. *J. Geophys. Res.* 96, 197 33-197 478.
- Peeters, C., Swennen, R., Nielsen, P., Muchez, Ph.**, (1993): Sedimentology and diagenesis of the Viséan carbonates in the Vesder area (Verviers synclinorium, E-Belgium). *Zentralbl. Geol. Paläont. Teil 1* (5), 519-547.
- Petit, J.P., Wibberley, C.A.J., Ruiz, J.**, (2000): "Crack-Seal", Slip: A New Fault-Valve Mechanism. *Journal of Structural Geology*, 21, 1199-1207.
- Piessens, K., Muchez, Ph., Deweale, S., Boyce, A., De Vos, W., Sintubin, M., Debacker, T.N., Burke, E.A.J., Viaene, W.A.**, (2002): Fluid flow, alteration and polysulphide mineralisation associated with a low angle reverse shear zone in the Lower Palaeozoic of the Anglo-Brabant fold belt, Belgium. *Tectonophysics*. 348, 73-92.
- Pietzner, H., Vahl, J., Werner, H. & Ziegler, W.**, (1968): Zur chemischen Zusammensetzung und Mikromorphologie der Conodonten. *Palaeontographica*, Stuttgart, 128, 4-6: 115-152.
- Powell, R., Condiliffe, D. M. & Condiliffe, E.**, (1984): Calcite-dolomite geothermometry in the system $\text{CaCO}_3\text{-MgCO}_3\text{-FeCO}_3$: an experimental study. *Journal Metamorphic Geology*, 2, 33-41.
- Ramsey, J.G.**, (1980): The crack-seal mechanism of rock deformation. *Nature* 248, 135-139.
- Ramsey, J.G., and Huber, M.I.**, (1987): *The Techniques of Modern Structural Geology. Volume 2: Folds and Fractures*. New York: Academic Press.

- Redecke, P.**, (1992): Zur Geochemie und Genese variszischer und postvariszischer Buntmetallmineralisation in der Nordeifel und der Niederrheinischen Bucht. RWTH Aachen, Dissertation, 159 S.
- Ridley, J.R.**, (1993): The Relation between Mean Rock Stress and Fluid Flow in the Crust: With Reference to Vein- and Lode-Style Gold Deposits. *Ore Geology Reviews*, 8, 23-37.
- Ridley, J.R., Mikucki, E.J., and Groves, D.I.**, (1996): Archean Lode-Gold Deposits: Fluid Flow and Chemical Evolution in Vertically Extensive Hydrothermal Systems. *Ore Geology Reviews*. 10, 295-317.
- Ridley, J.R., and Diamond, L.W.**, (2000): Fluid Chemistry of Orogenic Lode Gold Deposits and Implication for Genetic Models. *Reviews in Economic Geology* 13: 141-162.
- Roedder, E.**, (1971): Fluid inclusions studies on the porphyry-type ore deposits at Bingham, Utah, Butte, Montana, and Climax, Colorado: *Economic Geology*, v. 66, pp. 98-118.
- Roedder, E.**, (1984): Fluid inclusions. In: *Reviews in Mineralogy*, vol. 12. Mineralogical Society of America, Washington, DC, pp. 494-501.
- Rumble, D., III., and Hoering, T.C.**, (1994): Analyses of Oxygen and Sulphur Isotope Ratios in Oxide and Sulphide Minerals by Spot Heating with Carbon Dioxide Laser in a Fluorine Atmosphere. *Accounts of Chemical Research* 27: 237-241.
- Savage, N.M., Lindendorfer, M.A. & McDillen, D.A.**, (1990: Amino acids from Ordovician Conodonts. *Cour. Forsch.-Inst. Senckenberg, Frankfurt a.M.*, 118: 267-275.
- Schneider, J., Haack, U., Hein, U.F. and Germann, A.**, (1999): Direct Rb/Sr dating of sandstone-hosted sphalerites from stratabound Pb-Zn deposits in the northern Eifel, NW Rhenish Massif, Germany. Pp. 1287-1290 in: *Mineral deposits: Process to processing. Proc. 5th Bienn. SGA Meeting and the 10th Quadrennial IAGOD Symposium* (Stanley, C.J. editor), London, 22-25 August, 1999.
- Schreyer, W.**, (1975): New petrologic evidence for Hercynian metamorphism in the Venn-Stavelot-Massif, Belgium. *Geol Rundsch* 64: 819-830.
- Schroyen, K., and Muchez, Ph.**, (2000): Evolution of metamorphic fluids at the Variscan fold-and-thrust belt in eastern Belgium. *Sedimentary Geology*, 131, 163-180.
- Sharp, Z.D., Masson, H., Lucchini, R.**, (2005): Stable Isotope Geochemistry and Formation Mechanisms of Quartz Veins; External Palaeoaltitudes of the Central Alps in the Neogen. *American Journal of Science*, 305, 187-219.
- Sharp, Z.D.**, (1999): Application of stable isotope geochemistry to low-grade metamorphic rocks. In Frey, M., Robinson, D.B. (Eds.), *Low-Grade Metamorphism*. Blackwell Science.
- Sharp, Z.D., Kirschner, D.L.**, (1994): Quartz-calcite oxygen isotope thermometry: a calibration based on natural isotope variations. *Geochim. Cosmochim. Acta* 58 (21), 4491-4501.

- Sharp, Z.D.**, (1999): Application of stable isotope geochemistry to low grade metamorphism rocks. In: Frey, M., Robinson, D.B., (Eds.), *Low-Grade Metamorphism*. Blackwell Science.
- Sharp, Z.D., Atudorei, V., Durakiewicz, T.**, (2001): A rapid method for determination of hydrogen and oxygen isotope ratios from water and hydrous minerals. *Chem. Geol.* 178, 197-210.
- Sheppard, S.M.F., and Taylor, H.T.**, (1974): Hydrogen and Oxygen Evidences for the Origins of Water in the Boulder Batholith and the Butte Ore Deposits, Montana. *Economic Geology* 69, 926-946.
- Sheppard, S.M.F.**, (1986): Characterizations and isotope variations in natural waters. In: Valley, J.W., Taylor, H.P., O'Neil, J.R., (Eds.), *Stable Isotopes in High Temperature Geological Processes*. Mineralogical Society of America, Chelsea, pp. 165-183.
- Shmulovich, K.I., Yardely, B.W.D., Gonchar, G.G.**, (1995): *Fluids in the Crust*, Chapman and Hall, London.
- Shock, E.L., Helgeson, H.C.**, (1988): Calculation of the thermodynamic and transport properties of aqueous species at high pressures and temperatures: standard partial molal properties of inorganic neutral species. *Geochim. Cosmochim. Acta* 53, 2157-2183.
- Sibson, R.H.**, (1990). Faulting and Fluid Flow. In: Nesbitt, B.E. (Ed.) *Short Course on Fluids in Tectonically Active Regimes of the Continental Crust*. MAC Short Course Handbook 18, 93-129.
- Sibson, R.H.**, (2000): Fluid involvement in normal faulting. *Journal of Geodynamics*. 29, 469-499.
- Sibson, R.H.**, (2001): Seismogenic framework for hydrothermal transport and ore deposition. In: Richards, J. P. & Tosdat, R. M. (Editors): *Structural Controls on Ore Genesis*. Society of Economic Geologists, *Reviews in Economic Geology*, 14, 25 – 50.
- Simpson, J.**, (1985): Stylolite-controlled layering in a homogeneous limestone: pseudo-bedding produced by burial diagenetic. *Sedimentology*, 32, 495-505.
- Smith, M.P., Yardely, W.D.**, (1999): Fluid evolution during metamorphism of the Otago Schist, New Zealand: evidence from fluid inclusions. *Journal of Metamorphic Geology*, 17, 173-186.
- Spötl, C., Vennemann, T.**, (2003): Continuous-flow IRMS analysis of carbonate minerals. *Rapid Commun. Mass Spectrom.* 17, 1004-1006.
- Stroink L.**, 1993. Zur Diagenese paläozoischer Sandsteine am Nordrand des Linksrheinisch-Ardennischen Schiefergebirges. *Aachener Geowiss. Beiträge* 1: 1-164.
- Symonds, R.B.W., Rose, W.I., Bluth, G.J.S., Gerlach, T.M.**, (1994): Volcanic gas studies: Methods, results and applications, in *Volatiles in Magmas*, edited by M.R. Carroll and J.R. Holloway, pp. 1-66, Mineral. Soc. of Am., Washington, D.C.

- Tarantola, A., Mullis, J., Vennemann, T., Dubessy, J., Capitani de, C.,** (2007): Oxidation of methane at the CH₄/H₂O-(CO₂) transition zone in the external part of the Central Alps, Switzerland: Evidence from stable isotopes investigations. *Geochemical Geology*. 237, 329-357.
- Taylor, H.P.,** (1974): The Application of Oxygen and Hydrogen Isotope Studies to Problems of Hydrothermal Alteration and Ore Deposition. *Economic Geology*. 69: 883-883.
- Taylor, H.P.,** (1977): Water/rock interactions and the origin of H₂O in granitic batholiths. *J. Geol. Soc. Lond.*, 133, 509-558.
- Taylor, H.P.,** (1977): Oxygen and Hydrogen Isotope Relationships in Hydrothermal Mineral Deposits. *Geochemistry of Hydrothermal Ore Deposits*, 2nd Edition. Barnes. New York, John Wiley: 236-277.
- Thorez, J. & Dreesen, R.,** (1986): A model of a regressive depositional system around the Old Red Continent as exemplified by a field trip in the Upper Famennian "Psammities de Condroz" in Belgium. *Ann. Soc. géol. Belg.*, 109: pp. 285-323.
- Touray, J.C.,** (1987): Transport et dépôt de l'or dans les fluides de la croûte continentale, l'apport des études d'inclusions fluides. *Chron. Rech. Min.*, 488, 43-53.
- Urey, H.C.,** (1947): The thermodynamic properties of isotopic substances. *J. Chem. Soc.*, 562-581.
- Valley, J.W., and O'Neil, J.R.,** (1981)/ 13C/12C: Exchange between calcite and graphite: a possible thermometer in Greenville marbles: *Geochim. Cosmochim. Acta* 45, pp. 411-419.
- Vrolijk, P., Myers, G., Moore, J.C.,** (1988): Warm fluid migration along tectonic melanges in the Kodiak accretionary complex, Alaska. *J. Geophys. Res.* 93 (B9), 10313-10324.
- Vry, J.K., Storkey A.C., Harries, C.,** (2001): Role of fluids in the metamorphism of the Alpine fault zone, New Zealand. *Journal of Metamorphic Geology*, 19, 21-31.
- Wall, V.J.,** (1987): The geochemistry of gold in regional metamorphism. In: *The Second Eastern Goldfields. Geological Field Conference, Abstracts and Excursion Guide*, pp. 8-23.
- Walshe, J. R.,** (1986): A six-component chlorite solid solution model and the conditions of chlorite formation in hydrothermal and geothermal systems. *Economic Geology*, 81, 681-703.
- Walter, R.,** (1995): *Geologie von Mitteleuropa*. E. Schweizerbart'sche Verlagsbuchhandlung (Nägele u. Obermiller), Stuttgart, 6. Auflage, 566 S.
- Wanless, H.R.,** (1979): Limestone response to stress: pressure solution and dolomitisation: *J. sedim. Petrol.* 49, 437-462.
- Yardley, B.W.D.,** (1986): Fluid Migration and Veining in the Connemara Schists, Ireland. *Fluid-Rock Interactions During Metamorphism*. Walther, J.V., Wood, B.J., New York, Springer-Verlag: 109-131.
- Yardley, B.W.D., and Graham, J.T.,** (2002): The Origins of Salinity in Metamorphic Fluids. *Geofluids* 2, 249-256.

-
- Zang, W. & Fyfe, W. S.**, (1995): Chloritisation of the hydrothermally altered bedrock at the Igarape ´ Bahia gold deposit, Carajas, Brasil. *Mineral. Deposita*, 30, 30-38.
- Zhang, Y., Muchez, P., Hein, U.F.**, (1997): Chlorite geothermometry and the temperature conditions at the Variscan thrust front in eastern Belgium. *Geol. Mijnbouw* 76, 267-270.
- Zheng, Y.-F.**, (1993): Calculation of oxygen isotope fractionation in anhydrous silicate minerals. *Geochim. Cosmochim. Acta* 57, pp. 1079-1091.
- Zheng, Y.-F.**, (1999): Oxygen isotope fractionation in carbonate and sulphate minerals. *Geochemical Journal*, 33, p. 109-126.

9 Appendices

9.1 Sample and Sections

In total 89 core samples at several depths from the RWTH-1 drill collected from regular depth intervals were used in this study. Whole rock, hydrothermal minerals, alteration minerals, and the relative modal proportion of minerals of these samples were studied on a total of 69 thin and polished sections, using transmitted and reflected light microscopy, cathodoluminescence microscopy, Electron Microprobe Analyses (EMPA), and X-ray diffraction (XRD). A total of 45 doubly polished thick sections were made for microthermometry, and gaschromatography, all at the RWTH-Aachen University, Germany.

Table 9.1 Sample list indicating the type and number of sections made

Core Section I					
Depth [m]	Sample	Lithologie/Vein System	Thin	Polished	Thick doubly polished
1399.63	P1	fine grained sandstone quartz-carbonate \pm chlorite quartz \pm chlorite	26567	X	993
1401.39	P2	fine grained sandstone quartz-carbonate \pm chlorite	26568	X	994
1402.42	P3	clay silty sized pelites quartz-carbonate \pm chlorite carbonate \pm chlorite quartz \pm chlorite	26569	X	995
1402.60	P4	fine grained sandstone quartz-carbonate \pm chlorite quartz \pm chlorite	26570	X	996
1403.17	P5	fine grained sandstone quartz-carbonate \pm chlorite	26571	X	997
1404.65	P101	sandstone/siltstone quartz-carbonate \pm chlorite quartz \pm chlorite	27053		

Table 9.1 Sample list indicating the type and number of sections made

Core Section I					
Depth [m]	Sample	Lithologie/Vein System	Thin	Polished	Thick doubly polished
1405.16	P102	siltstone quartz-carbonate \pm chlorite quartz \pm chlorite	27054		
1405.22	P103	siltstone quartz-carbonate \pm chlorite quartz \pm chlorite	27055		
1405.42	Px1	fine grained sandstone quartz-carbonate \pm chlorite			1059
1407.90	P6	dolomite quartz-carbonate \pm chlorite	26572	X	
1408.65	P7	dolomite quartz-carbonate \pm chlorite	26573		998
1408.77	P8	dolomite marl quartz-carbonate \pm chlorite	26574		999
1409.65	P108	dolomite marl quartz-carbonate \pm chlorite carbonate \pm chlorite	27060		
1409.70	P108a	dolomite marl quartz-carbonate \pm chlorite carbonate \pm chlorite	27061		
1411.30	P10	dolomite marl quartz-carbonate \pm chlorite	26630	X	
1412.13	P9	dolomite marl quartz-carbonate \pm chlorite carbonate \pm chlorite	26575 26975 26976	X X	1000
1417.11	PS018	dolomite marl quartz-carbonate \pm chlorite			1064
1418.40	P11	dolomite quartz-carbonate \pm chlorite carbonate \pm chlorite	26693	X	1040
1418.65	P109	dolomite marl quartz-carbonate \pm chlorite carbonate \pm chlorite	27062		

Table 9.1 Sample list indicating the type and number of sections made

Core Section I					
Depth [m]	Sample	Lithologie/Vein System	Thin	Polished	Thick doubly polished
1420.70	P13	dolomite marl quartz-carbonate ± chlorite	26631	X	981
1423.15	PS021	dolomite marl quartz-carbonate ± chlorite			1066
1427.76	P15	pelites/shale quartz-carbonate ± chlorite	26694	X	1041
1428.0	P16	nodular limestone/dolostone carbonate ± chlorite	26695	X	
1428.91	PS027	nodular limestone/dolostone carbonate ± chlorite			1067
1429.93	P17	dolomite marl carbonate ± chlorite	26696	X	1042
1430.84	P18	nodular limestone/dolostone quartz-carbonate ± chlorite	26632	X	982
1431.08	PS082	limestone/dolostone marl carbonate ± chlorite			1077
1433.34	P19	nodular limestone/dolostone quartz-carbonate ± chlorite	26633	X	983
1433.70	P20	clay silty sized pelites quartz-carbonate ± chlorite	26697	X	
1433.78	P21	nodular limestone/dolostone quartz-carbonate ± chlorite carbonate ± chlorite	26698	X	
1434.40	P22	nodular limestone quartz-carbonate ± chlorite carbonate ± chlorite	26634	X	984
1435.17	P23	nodular limestone quartz-carbonate ± chlorite carbonate ± chlorite	26635	X	985
1435.84	P2a	nodular limestone/dolostone carbonate ± chlorite	26846	X	

Table 9.1 Sample list indicating the type and number of sections made

Core Section I					
Depth [m]	Sample	Lithologie/Vein System	Thin	Polished	Thick doubly polished
1436.68	P6a	nodular limestone/dolostone quartz-carbonate ± chlorite carbonate ± chlorite	26850	X	1050
1436.90	P25	dolomite marl quartz-carbonate ± chlorite	26636	X	986
1438.25	PB1	clay/shale quartz-carbonate ± chlorite	27080		
1441.75	P27	dolomite marl carbonate ± chlorite quartz ± chlorite	26699	X	1045
1445.44	P30	silty sized pelites carbonate ± chlorite quartz ± chlorite	26700	X	
1446.38	P31	clay silty sized pelites quartz ± chlorite	26637		987
1446.74	P32	silty sized pelites quartz ± chlorite	26701	X	
1448.87	P33	silty sized pelites quartz-carbonate ± chlorite quartz ± chlorite	26702	X	1057
1450.57	P34	clay silty sized pelites quartz-carbonate ± chlorite	26703		
1455.79	P35	clay silty sized pelites quartz-carbonate ± chlorite	26704	X	
1459.24	P111	fine grained sandstone quartz-carbonate ± chlorite	27064		
1462.32	P12a	clay silty sized pelites quartz-carbonate ± chlorite quartz ± chlorite	26856	X	1053
1468.57	P37	clay silty sized pelites quartz ± chlorite	26705	X	
1469.04	P29	clay silty sized pelites quartz ± chlorite	26706	X	

Table 9.1 Sample list indicating the type and number of sections made

Core Section I					
Depth [m]	Sample	Lithologie/Vein System	Thin	Polished	Thick doubly polished
1473.58	PS049	clay silty sized pelites quartz-carbonate \pm chlorite carbonate \pm chlorite	26845	X	1069
1476.63	PS051	clay silty sized pelites quartz-carbonate \pm chlorite quartz \pm chlorite			1070
1479.20	P13a	clay silty sized pelites quartz-carbonate \pm chlorite quartz \pm chlorite	26857	X	1054
1479.83	P7a	clay silty sized pelites quartz-carbonate \pm chlorite quartz \pm chlorite	26851	X	1051
1483.30	P4a	silty sized pelites quartz-carbonate \pm chlorite quartz \pm chlorite	26848	X	1048
1483.84	P39	silty sized pelites quartz-carbonate \pm chlorite	26707		
1485.80	P40	silty sized pelites quartz-carbonate \pm chlorite	26638	X	988
1486.70	P104	siltstone/sandstone quartz-carbonate \pm chlorite	27056		
1486.85	P14a	pelites/shale quartz-carbonate \pm chlorite quartz \pm chlorite	26858	X	
1487.52	PS060	clay silty sized pelites quartz \pm chlorite	26852	X	1073
1491.48	P11a	clay silty sized pelites quartz-carbonate \pm chlorite quartz \pm chlorite	26855	X	1052
1495.42	PS063	clay silty sized pelites quartz-carbonate \pm chlorite quartz \pm chlorite		27278	1074
1498.95	P44	clay silty sized pelites quartz-carbonate \pm chlorite	26643	X	992

Table 9.1 Sample list indicating the type and number of sections made

Core Section I					
Depth [m]	Sample	Lithologie/Vein System	Thin	Polished	Thick doubly polished
1502.82	P46	silty sized pelites quartz-carbonate \pm chlorite quartz \pm chlorite	26708	X	1058
1503.02	P47	clay silty sized pelites quartz-carbonate \pm chlorite	26639/1		989
1503.25	P107	clay silty sized pelites quartz \pm chlorite	26639/2	X	27059
1507.15	P48	siltstone/sandstone quartz-carbonate \pm chlorite carbonate \pm chlorite	26709	X	
1509.15	P49	clay silty sized pelites quartz-carbonate \pm chlorite			1060
1511.10	P51	silty sized pelites quartz \pm chlorite	26644	X	
1512.48	P52	clay silty sized pelites quartz \pm chlorite	26640	X	
1512.95	P53	silty sized pelites/sandstone quartz-carbonate \pm chlorite carbonate \pm chlorite	26710	X	
1514.94	P9a	silty sized pelites/sandstone quartz-carbonate \pm chlorite quartz \pm chlorite	26853	X	

Table 9.1 Sample list indicating the type and number of sections made

Core Section II					
Depth [m]	Sample	Lithologie/Vein System	Thin	Polished	Thick doubly polished
2129,33	P56	fine grained sandstone quartz	26641	X	990
2131,64	P57	fine grained sandstone/pelite carbonate	26642	X	991
2139.75	P105	silty sized pelites/sandstone carbonate	27057		
2140.98	P106	silty sized pelites/sandstone carbonate	27058		
2142.70	P15a	fine grained sandstone carbonate quartz	26859	X	
Core Section III					
Depth [m]	Sample	Lithologie/Vein System	Thin	Polished	Thick doubly polished
2539.50	P3a	siltstone/fine grained sandstone carbonate	26847		
2539.63	P10a	clay/mudstone quartz-carbonate	26854	X	
2543.25	PS087	clay/mudstone quartz-carbonate ± chlorite			1079

9.2 Electron Micro Probe Analyser

Electron Microprobe Analysis was carried out on a JEOL JXA-8900R electron microprobe. The quantitative analyses were performed using wavelength dispersive spectrometers with an acceleration voltage of 15 kV, a beam current of 20 nA and a focused beam size. Natural and synthetic standards were used for calibration. Chlorite, occurring in different veins and alteration zones was quantitatively analyzed for Si, Al, Fe, Mg, Mn and Ti with the EMPA (Table 2). Additionally, carbonates occurring in paragenesis were quantitatively analysed for Fe, Mn, Mg, Ba, Ca, and Sr (Table 3).

Table 9.2 Representative geochemical analyses and precipitation temperatures of chlorite examples in I) alteration, II) slickensides and III) in different vein types

Chlorite analyses EMPA									
Sample Chlorite type	I	I	I	II	II	II	III	III	III
wt. %									
SiO ₂	24,25	24,33	24,63	24,49	24,40	24,37	24,23	24,92	24,11
Al ₂ O ₃	23,48	23,86	23,39	23,72	23,34	23,68	23,82	23,12	23,91
MgO	8,21	8,43	8,66	8,39	8,46	8,30	8,45	8,55	8,11
FeO	32,43	31,77	32,10	31,96	32,40	32,14	31,75	32,04	32,31
MnO	0,42	0,35	0,39	0,33	0,36	0,37	0,37	0,32	0,35
TiO ₂	0,04	0,02	0,05	0,01	0,01	0,03	0,01	0,00	0,00
Na ₂ O	0,01	0,00	0,00	0,00	0,01	0,03	0,02	0,01	0,01
Cl	0,00	0,00	0,01	0,00	0,02	0,00	0,01	0,00	0,00
K ₂ O	0,00	0,01	0,00	0,00	0,00	0,00	0,02	0,02	0,02
CaO	0,01	0,03	0,00	0,00	0,00	0,00	0,01	0,03	0,00
Cr ₂ O ₃	0,00	0,03	0,04	0,00	0,01	0,00	0,00	0,00	0,05
Total	88,84	88,82	89,28	88,89	89,01	88,93	88,69	89,00	88,86
Si	2,61	2,64	2,56	2,63	2,62	2,65	2,61	2,64	3,63
Al ^(IV)	1,38	1,36	1,42	1,37	1,39	1,35	1,39	1,36	1,37
Al ^(VI)	1,60	1,64	1,57	1,63	1,62	1,67	1,60	1,56	1,63
Fe	2,93	2,86	2,98	2,84	2,89	2,75	2,88	2,89	3,05
Mg	1,32	1,34	1,33	1,36	1,33	1,38	1,39	1,42	1,16
Mn	0,04	0,03	0,03	0,03	0,03	0,03	0,03	0,03	0,03
T°C									
Walshe (1986)	308	298	327	302	307	297	313	300	301
Cathelineau et al. (1985)	308	298	327	302	307	297	313	300	301
Zang et al. (1995)	308	298	327	302	307	297	313	300	301

Table 9.3 Representative geochemical analyses of calcite-dolomite assemblages

Sample	Mineral	Sr	Mg	Ba	Ca	Fe	Mn	Total
DS632	Cal	0,07	0,81	0,03	54,00	0,12	0,03	55,05
DS632	Cal	0,06	0,61	0,01	53,60	0,22	0,07	54,57
DS632	Dol	0,01	16,93	0,00	31,23	1,85	0,14	50,16
DS632	Dol	0,00	16,59	0,04	31,38	1,94	0,16	50,11
DS633	Cal	0,08	0,18	0,02	54,41	0,14	0,03	54,86
DS633	Cal	0,12	0,51	0,02	52,85	0,66	0,09	54,24
DS633	Dol	0,00	16,64	0,00	31,13	1,83	0,16	49,75
DS633	Dol	0,02	16,57	0,00	29,78	3,39	0,61	50,37
DS636	Cal	0,14	0,54	0,04	56,49	1,15	0,10	58,47
DS636	Cal	0,10	0,44	0,00	54,55	1,12	0,10	56,31
DS 636	Dol	0,05	17,54	0,00	32,33	2,34	0,16	52,41
DS 636	Dol	0,04	17,87	0,00	32,34	1,52	0,15	51,92

9.3 Fluid Inclusion Analyses

The investigated two phase liquid-vapour fluid inclusions always homogenise to the liquid phase. Microthermometric measurements of fluid inclusions were performed on doubly polished, 60 to 100 μm thick sections on a modified USGS cooling-heating stage with a Zeiss 50x long working-distance objective. The experimental approach is based on standard petrography and systematic, statistical evaluation of fluid inclusion types and generations in veins. On samples only containing aqueous liquid-vapor inclusions, the homogenisation temperature [Th] was first measured, followed by eutectic temperature [Te] and final melting temperature [Tm]. The stage was calibrated by measuring the Th and Tm of a synthetic H₂O fluid inclusions standard (Th = 374.1 °C), as well as Tm of a synthetic CO₂ fluid inclusion standard (Tm = -56.5 °C). The reproducibility of the measurements was in the order of 1 - 2 °C for Th and 0.1 - 0.2 °C for Tm.

Table 9.4 Microthermometric analyses of the two phase liquid-vapour fluid inclusions, from the quartz-carbonate veins (D1), recalculated using the H₂O-NaCl-[KCl] equation of Bowers & Helgeson (1994)

Thick doubly polished	M	Gr.	Ratio % Vapour	Th _{L+V}	Tm _{ice}	Te	Molal NaCl	Wt% NaCl equiv	X (NaCl)	Critical T	Critical P	Bulk Density	Bulk Molar Volume
993	Qtz	P	20	270	-3,2	-21,7	0,93	5,17	0,02	422	344	0,817	23,04
993	Qtz	P	20	307	-3,1	-21,6	0,9	5,01	0,02	420	340	0,751	25,07
993	Qtz	P	20	302	-3,2	-21,9	0,93	5,17	0,02	422	344	0,762	24,69
993	Qtz	P	10	304	-3,4	-22,4	0,99	5,47	0,02	425	352	0,763	24,66
993	Qtz	P	25	286	-3,9	-22,1	1,15	6,23	0,02	432	371	0,805	23,38
993	Qtz	P	30	272	-3,7	-21,9	1,08	5,93	0,02	429	363	0,823	22,86
993	Qtz	P	25	271	-3,4	-21,7	0,99	5,47	0,02	425	352	0,819	22,98
993	Qtz	P	50	306	-2,7	-22,1	0,79	4,39	0,01	415	324	0,744	24,76
993	Qtz	P	35	316	-2,9	-21,9	0,84	4,70	0,01	418	332	0,728	25,30
994	Qtz	P	30	380	-3,8	-21,4	1,1	6,08	0,02	430	367	0,608	30,95
994	Cc	PS	20	310	-3,1	-22,3	0,9	5,01	0,02	420	340	0,745	25,27
996	Cc	PS	30	242	-4,4	-22,1	1,28	6,96	0,02	439	390	0,876	21,50
996	Cc	PS	20	229	-3,8	-21,7	1,11	6,08	0,02	430	367	0,883	21,31
996	Cc	PS	25	234	-4,1	-22,9	1,19	6,52	0,02	434	378	0,881	21,36
996	Cc	PS	20	229	-3,8	-21,7	1,11	6,08	0,02	430	367	0,883	21,31
996	Qtz	PS	20	242	-2,7	-21,6	0,79	4,39	0,01	415	324	0,85	21,66
996	Qtz	S	25	210	-2,4	-21,1	0,7	3,92	0,01	410	312	0,887	20,77
996	Qtz	PS	25	225	-2,6	-22,4	0,76	4,23	0,01	413	320	0,871	21,14
996	Qtz	S	15	186	-1,9	-21,7	0,55	3,12	0,01	403	292	0,907	20,30

Table 9.4 Microthermometric analyses of the two phase liquid-vapour fluid inclusions, from the quartz-carbonate veins (D1), recalculated using the H₂O-NaCl-[KCl] equation of Bowers & Helgeson (1994)

Thick doubly polished	M	Gr.	Ratio %	Th _{L+V}	Tm _{ice}	Te	Molal NaCl	Wt% NaCl equiv	X (NaCl)	Critical T	Critical P	Bulk Density	Bulk Molar Volume
			Vapour										
996	Qtz	S	15	182	-1,4	-21,4	0,4	2,13	0,01	395	272	0,905	20,35
996	Qtz	S	15	184	-1,8	-21,9	0,52	2,96	0,01	401	288	0,908	20,28
996	Cal	PS	30	241	-4,1	-21,7	1,19	6,52	0,02	434	378	0,872	21,58
996	Cal	PS	20	237	-3,8	-21,2	1,11	6,08	0,02	430	367	0,874	21,55
996	Cal	PS	35	229	-24	-52							
996	Cal	PS	30	236	-24	-52							
996	Cal	PS	25	234	-24	-52							
997	Qtz	PS	25	226	-3,5	-21,9	1,02	5,62	0,02	426	355	0,89	21,15
997	Qtz	PS	20	232	-4,2	-21,7	1,22	6,67	0,02	436	382	0,907	20,75
997	Qtz	PS	30	228	-3,9	-20,8	1,14	6,23	0,02	432	371	0,897	20,98
997	Qtz	PS	20	225	-4,0	-20,2	1,16	6,37	0,02	433	375	0,902	20,88
997	Qtz	PS	25	239	-3,9	-21,4	1,14	6,23	0,02	432	371	0,907	20,75
997	Qtz	PS	15	246	-3,1		0,9	5,01	0,02	420	340	0,9	20,91
997	Qtz	S	15	209	-3,3		0,96	5,32	0,02	423	348	0,9	20,92
997	Qtz	S	25	212	-3,9	-20,9	1,14	6,23	0,02	432	371	0,904	20,82
1059	Qtz	P	25	289	-4,2	-21,4	1,22	6,67	0,02	436	382	0,805	23,37
1059	Qtz	P	20	276	-4,1	-21,7	1,19	6,52	0,02	434	378	0,824	22,85
999	Qtz	P	45	268	-4,2	-21,9	1,22	6,67	0,02	436	382	0,838	22,48
999	Qtz	P	40	274	-4,1	-21,5	1,19	6,52	0,02	434	378	0,838	22,76
999	Dol	P	50	299	5,3	-24,9	1,54	8,24	0,03	450	422	0,81	23,74
999	Dol	P	60	307	5,1	-25,1	1,48	7,96	0,03	448	415	0,793	24,25
1040	Qtz	P	25	282	-3,1	-21,2	0,9	5,01	0,02	420	340	0,796	23,66
1040	Qtz	P	20	289	-3,6	-21,9	1,05	5,78	0,02	428	360	0,8	23,71
1040	Qtz	P	20	302	-3,4	-20,8	0,99	5,47	0,02	425	352	0,767	24,54
1040	Qtz	P	25	307	-3,3	-22,1	0,96	5,32	0,02	423	348	0,755	24,92
1040	Dol	P	30	301	-4,1		1,19	6,52	0,02	434	378	0,783	24,03
1040	Dol	P	15	302	-3,9		1,14	6,23	0,02	432	371	0,778	24,20
1040	Qtz	P	40	251	-4,2	-21,3	1,22	6,67	0,02	436	382	0,861	21,86
1040	Qtz	P	25	292	-3,8	-21,7	1,11	6,08	0,02	430	367	0,793	23,73
981	Qtz	P	45	239	-2,3	-22,1	0,67	3,76	0,01	409	308	0,848	21,72
981	Qtz	P	15	279	-2,9		0,84	4,7	0,01	418	332	0,795	23,17
981	Qtz	P	30	280	-2,9		0,84	4,7	0,01	418	332	0,795	23,17
981	Qtz	P	30	350	-2,3	-21,9	0,67	3,76	0,01	409	308	0,636	28,98
981	Qtz	P	40	375	-2,3	-21,7	0,67	3,76	0,01	409	308	0,57	32,30
981	Qtz	P	20	347	-2,3		0,67	3,76	0,01	409	308	0,643	28,65
981	Qtz	P	30	315	-2,0	-21,2	0,58	3,28	0,01	404	296	0,708	26,03
981	Qtz	P	50	321	-2,9		0,84	4,7	0,01	418	332	0,718	25,66
981	Qtz	P	50	320	-2,8		0,81	4,55	0,01	416	328	0,717	25,68
981	Qtz	P	45	238	-2,3		0,67	3,76	0,01	409	308	0,848	21,72

Table 9.4 Microthermometric analyses of the two phase liquid-vapour fluid inclusions, from the quartz-carbonate veins (D1), recalculated using the H₂O-NaCl-[KCl] equation of Bowers & Helgeson (1994)

Thick doubly polished	M	Gr.	Ratio % Vapour	Th _{L+V}	Tm _{ice}	Te	Molal NaCl	Wt% NaCl equiv	X (NaCl)	Critical T	Critical P	Bulk Density	Bulk Molar Volume
1041	Dol	P	25	281	-3,4	-21,2	0,99	5,47	0,02	425	352	0,803	23,43
1041	Dol	P	20	286	-3,7	-21,9	1,08	5,93	0,02	429	363	0,801	23,50
1041	Dol	P	25	278	-3,2	-21,1	0,93	5,17	0,02	422	344	0,804	23,40
1041	Qtz	P	20	310	-3,9	-21,7	1,14	6,23	0,02	432	371	0,764	24,65
1041	Qtz	S	15	205	-1,4	-10,5	0,4	2,21	0,01	395	272	0,879	20,96
1041	Qtz	S	20	207	-1,3	-10,7	0,37	2,14	0,01	394	267	0,875	21,05
1041	Qtz	S	15	201	-1,6	-10,5	0,46	2,63	0,01	398	279	0,887	20,78
1041	Qtz	S	20	190	-1,2	-10,3	0,35	1,98	0,01	392	264	0,894	20,59
1041	Qtz	S	15	189	-1,5	-10,9	0,43	2,47	0,01	397	276	0,899	20,49
1041	Qtz	S	15	207	-1,9	-10,7	0,55	3,12	0,01	403	292	0,884	20,85
982	Cc	P	25	261	-2,6	-21,6	0,76	4,23	0,01	413	320	0,821	22,45
982	Cc	P	20	254	-2,4	-22,5	0,7	3,92	0,01	410	312	0,828	22,25
982	Cc	P	15	345	-4,9	-20,4	1,42	7,68	0,02	445	408	0,719	26,20
982	Cc	P	25	336	-4,6	-23,1	1,34	7,25	0,02	441	397	0,73	25,79
982	Qtz	P	30	320	-4,1	-21,9	1,19	6,52	0,02	434	378	0,749	25,14
982	Qtz	P	35	247	-2,4	-21,4	0,7	3,92	0,01	410	312	0,838	21,98
983	Qtz	PS	25	230	-3,8	-21,9	1,11	6,08	0,02	430	367	0,882	21,34
983	Qtz	S	30	198	-2,9	-21,7	0,84	4,7	0,01	418	332	0,907	20,32
983	Qtz	S	15	202	-3,1	-22,1	0,9	5,01	0,02	420	340	0,905	20,81
983	Qtz	S	10	201	-3,2	-21,3	0,93	5,17	0,02	422	344	0,907	20,75
983	Qtz	S	15	202	-3,1	-22,1	0,9	5,01	0,02	420	340	0,905	20,81
983	Qtz	S	10	198	-3,3	-21,6	0,96	5,32	0,02	423	348	0,911	20,65
1043	Cc	P	25	287	-3,6	23,7	1,05	5,78	0,02	428	360	0,797	23,61
1043	Cc	P	20	293	-3,2	24,2	0,93	5,17	0,02	422	344	0,779	24,17
1043	Cc	P	25	288	-3,8	22,1	1,11	6,08	0,02	430	367	0,8	23,54
984	Qtz	S	25	191	-2,3	24,1	0,67	3,76	0,01	409	308	0,907	20,31
984	Qtz	S	15	190	-3,0		0,87	4,86	0,02	419	336	0,916	20,55
984	Qtz	P	40	292	-1,1	-21,3	0,32	1,82	0,01	391	260	0,733	25,12
984	Qtz	P	30	293	-1,1		0,32	1,82	0,01	391	260	0,731	25,19
984	Qtz	S	20	180	-2,9	23,7	0,84	4,7	0,01	418	332	0,925	19,92
984	Qtz	S	15	182	-3,6		1,05	5,78	0,02	428	360	0,932	20,19
984	Qtz	S	20	179	-3,7	-22,1	1,08	5,93	0,02	429	363	0,933	20,17
984	Qtz	S	20	180	-2,9		0,84	4,7	0,01	418	332	0,925	19,92
984	Qtz	P	40	292	-1,1		0,32	1,82	0,01	391	260	0,733	25,12
1050	Qtz	P	30	317	-2,9	-23,6	0,84	4,70	0,01	418	332	0,726	25,37
1050	Qtz	P	25	328	-2,5	-24,1	0,73	4,70	0,01	412	316	0,693	26,58
1050	Cc	P	50	344	-3,1	-22,1	0,9	5,09	0,02	420	340	0,673	27,96
1050	Cc	P	45	333	-2,9	-21,3	0,84	4,70	0,01	418	332	0,692	26,61

Table 9.4 Microthermometric analyses of the two phase liquid-vapour fluid inclusions, from the quartz-carbonate veins (D1), recalculated using the H₂O-NaCl-[KCl] equation of Bowers & Helgeson (1994)

Thick doubly polished	M	Art	Ratio % Vapour	Th _{L+V}	Tm _{ice}	Te	Molal NaCl	Wt% NaCl equiv	X (NaCl)	Critical T	Critical P	Bulk Density	Bulk Molar Volume
986	Qtz	P	25	312	2,7	24,1	0,79	4,39	0,01	415	324	0,732	25,16
986	Qtz	P	30	328	2,9	23,4	0,84	4,7	0,01	418	332	0,703	26,20
986	Qtz	P	20	317	3,3	21,9	0,96	5,32	0,02	423	348	0,736	25,57
986	Qtz	P	35	334	3,1	23,1	0,9	5,01	0,02	420	340	0,696	27,06
1045	Qtz	P	40	369	-5,1	20,4	1,48	7,96	0,03	448	415	0,673	28,58
1045	Qtz	P	35	371	-4,9	-22,1	1,42	7,69	0,02	445	408	0,663	28,41
1045	Qtz	P	40	368	-5,2	-22,9	1,51	8,1	0,03	449	419	0,678	28,36
1045	Qtz	P	30	378	4,9	24,1	1,42	7,86	0,02	445	408	0,646	29,13
1045	Qtz	P	35	389	6,1	-21,7	1,76	9,32	0,03	460	449	0,484	39,72
1045	Dol	P	25	378	5,4		1,56	8,38	0,03	451	426	0,66	29,12
1045	Dol	P	30	390	5,8	-21,3	1,68	8,92	0,03	456	439	0,591	32,55
1045	Dol	P	30	385	5,6	22,8	1,62	8,65	0,03	454	432	0,597	32,23
1045	Qtz	S	15	182	-1,2	-21,7	0,35	1,98	0,01	392	264	0,903	20,39
1045	Qtz	S	20	179	-1,1	-21,5	0,32	1,82	0,01	391	260	0,905	20,35
1053	Qtz	P	45	356	-3,8	-21,6	1,11	6,08	0,02	430	367	0,666	28,25
1053	Qtz	P	35	371	-4,2	-22,5	1,22	6,67	0,02	436	382	0,642	29,31
1053	Cc	P	80	387			1,84	9,71	0,03	463	459	0,495	38,85
1053	Cc	P	30	364	-3,4	-22,1	0,99	5,47	0,02	425	352	0,635	29,64
1053	Cc	P	25	351	-4,2	-21,3	1,22	6,67	0,02	436	382	0,688	27,36
1051	Qtz	PS	30	245	-2,4	-21,6	0,7	3,92	0,01	410	312	0,841	21,09
1051	Qtz	S	25	193	-2,7	-21,7	0,79	4,39	0,01	415	324	0,91	20,25
1051	Qtz	S	20	203	-2,3	-22,1	0,67	3,76	0,01	409	308	0,894	20,61
1051	Cc	PS	25	247	-2,5	-22,2	0,73	4,07	0,01	412	316	0,903	20,40
1051	Dol	P	30	386	-3,4	21,4	0,99	5,47	0,02	425	352	0,579	32,53
1051	Dol	P	35	380	-4,2	22,8	1,22	6,67	0,02	436	382	0,62	30,34
1051	Qtz	P	25	378	-3,1	20,9	0,9	5,01	0,02	420	340	0,589	31,93
1051	Qtz	P	30	374	-3,4		0,99	5,47	0,02	425	352	0,61	30,85
1048	Qtz	P	25	352	-4,8	-21,2	1,39	7,45	0,02	444	404	0,701	26,84
1048	Qtz	P	30	366	-4,2	-21,9	1,22	6,67	0,02	436	382	0,654	28,78
1048	Qtz	P	35	328	-5,2	-21,1	1,51	8,1	0,03	449	419	0,758	25,35
1048	Qtz	P	35	333	-4,7	-21,7	1,37	7,39	0,02	442	401	0,738	25,50
1048	Qtz	P	35	343	-4,1	-22,4	1,19	6,52	0,02	434	378	0,703	26,79
1048	Qtz	S	40	207	-2,8	-10,6	0,81	4,55	0,01	416	328	0,895	20,57
1048	Qtz	S	40	209	-2,8	-10,7	0,81	4,55	0,01	416	328	0,893	20,62
1048	Qtz	S	25	207	-2,1	-10,5	0,61	3,44	0,01	406	300	0,886	20,78
1048	Qtz	S	30	199	-2,4	-10,9	0,70	3,92	0,01	410	312	0,9	20,48
1048	Qtz	S	30	202	-1,9	-10,7	0,55	3,12	0,01	403	292	0,89	20,71
1048	Qtz	S	25	189	-2,3	-10,6	0,67	3,76	0,01	409	308	0,909	20,26
1048	Qtz	S	25	207	-2,7	-10,6	0,79	4,39	0,01	415	324	0,894	20,59
1048	Qtz	S	30	208	-2,4	-10,7	0,70	3,92	0,01	410	312	0,889	20,71
1048	Qtz	P	30	332	-4,1	-22,9	1,19	6,52	0,02	434	378	0,725	25,95

Table 9.4 Microthermometric analyses of the two phase liquid-vapour fluid inclusions, from the quartz-carbonate veins (D1), recalculated using the H₂O-NaCl-[KCl] equation of Bowers & Helgeson (1994)

Thick doubly polished	M	Art	Ratio %	Th _{L+V}	Tm _{ice}	Te	Molal NaCl	Wt% NaCl equiv	X (NaCl)	Critical T	Critical P	Bulk Density	Bulk Molar Volume
			Vapour										
1048	Qtz	P	35	341	-3,9	-21,7	1,14	6,23	0,02	432	371	0,702	26,80
1048	Qtz	P	40	339	-4,3	-23,4	1,25	6,81	0,02	437	386	0,716	26,28
1048	Qtz	P	35	332	-4,2		1,22	6,67	0,02	436	382	0,728	25,86
1048	Cal	P	50	342	-3,2	-21,7	0,93	5,17	0,02	422	344	0,681	27,65
1048	Cal	P	40	339	-3,4	-21,6	0,99	5,47	0,02	425	352	0,693	27,16
1048	Qtz	P	30	332	-21	-33,6							
1048	Qtz	P	35	341	-23	-33,4							
1048	Qtz	P	40	339	-24	-33,6							
1048	Qtz	P	35	332	-24	-33,8							
988	Qtz	P	15	370	-5,4	-22,1	1,56	8,38	0,03	451	426	0,678	28,35
988	Qtz	P	35	361	-5,7	-20,7	1,65	8,78	0,03	455	436	0,706	27,25
988	Qtz	P	25	364	-5,2	-21,5	1,51	8,10	0,03	449	419	0,687	28,00
988	Qtz	P	30	359	-5,6	-20,9	1,62	8,65	0,03	454	432	0,707	27,19
988	Qtz	P	35	360	-5,3	-23,2	1,54	8,24	0,03	450	422	0,698	27,55
1055	Qtz	P	25	364	-3,4	-21,5	0,99	5,47	0,02	425	352	0,635	29,64
1055	Qtz	P	35	359	-3,2		0,93	5,17	0,02	422	344	0,641	29,36
1055	Qtz	P	30	354	-3,6	-20,7	1,05	5,78	0,02	428	360	0,665	28,30
1055	Dol	P	40	398	-4,2		1,22	6,67	0,02	436	382	0,574	32,81
1055	Dol	P	35	382	-4,1	-23,9	1,37	7,39	0,02	442	401	0,632	29,81
1055	Dol	P	40	383	-3,9		1,14	6,23	0,02	432	371	0,604	31,17
1052	Qtz	P	30	292	-3,8	-21,2	1,11	6,08	0,02	430	367	0,793	23,73
1052	Qtz	P	25	302	-3,4	-21,9	0,99	5,47	0,02	425	352	0,767	24,54
1052	Qtz	S	15	198	-1,9	-10,2	0,4	2,31	0,01	395	272	0,887	20,76
1052	Qtz	P	35	355	-4,1	-21,4	1,19	6,52	0,02	434	378	0,676	27,83
1052	Qtz	PS	20	241	-2,8	-10,7	0,81	4,55	0,01	416	328	0,853	21,60
1052	Qtz	P	45	374	-3,8	-21,7	1,11	6,08	0,02	430	367	0,623	30,20
1052	Qtz	P	35	389	-4,1	-21,2	1,19	6,52	0,02	434	378	0,594	31,68
1052	Qtz	S	25	201	-1,3	-10,9	0,37	2,14	0,01	394	267	0,882	20,87
1052	Qtz	S	25	209	-1,5	-10,7	0,43	2,47	0,01	397	276	0,875	21,04
992	Qtz	P	30	304	-3,7		1,08	5,93	0,02	429	363	0,77	24,45
992	Qtz	P	30	298	-3,2	-21,9	0,93	5,17	0,02	422	344	0,77	24,45
992	Qtz	P	30	301	-3,5		1,02	5,62	0,02	426	355	0,771	24,41
989	Qtz	P	40	351	-4,1	-23,8	1,19	6,52	0,02	434	378	0,685	27,47
989	Qtz	P	35	366	-3,9	-22,4	1,14	6,23	0,02	432	371	0,646	29,14
989	Qtz	P	35	361	-3,7	-21,4	1,08	5,93	0,02	429	363	0,652	28,88
989	Qtz	P	30	357	-4,2	-22,1	1,22	6,67	0,02	436	382	0,675	27,90
989	Qtz	P	25	362	-4,1	-22,3	1,19	6,52	0,02	434	378	0,66	28,50

Table 9.4 Microthermometric analyses of the two phase liquid-vapour fluid inclusions, from the quartz-carbonate veins (D1), recalculated using the H₂O-NaCl-[KCl] equation of Bowers & Helgeson (1994)

Thick doubly polished	M	Art	Ratio % Vapour	Th _{L+V}	Tm _{ice}	Te	Molal NaCl	Wt% NaCl equiv	X (NaCl)	Critical T	Critical P	Bulk Density	Bulk Molar Volume
1060	Qtz	P	35	361	-4,3	-23,4	1,25	6,81	0,02	437	386	0,669	28,15
1060	Qtz	P	30	369	-3,7		1,08	5,93	0,02	429	363	0,632	29,76
1060	Qtz	P	40	375	-3,9	-21,3	1,14	6,23	0,02	432	371	0,624	30,16
1060	Qtz	P	30	377	-4,1		1,19	6,52	0,02	434	378	0,625	30,14
1060	Qtz	P	20	362	-4,3	-22,5	1,25	6,81	0,02	437	386	0,666	28,25
1060	Qtz	P	35	367	-3,8	-22,3	1,11	6,08	0,02	430	367	0,64	29,39

Table 9.5 Microthermometric analyses of the primary two phase liquid-vapour fluid inclusions, from the carbonate veins (D1), recalculated using the H₂O-NaCl-[KCl] equation of Bowers & Helgeson (1994)

Thick doubly polished	M	Ratio % Vapour	Th _{L+V}	Tm _{ice}	Te	Molal NaCl	Wt% NaCl equiv	X (NaCl)	Critical T	Critical P	Bulk Density	Bulk Molar Volume
1042	Cc	35	289	-3,2	-22,9	0,93	5,17	0,02	422	344	0,786	23,96
1042	Cc	45	274	-3,7	-23,7	1,08	5,93	0,02	429	363	0,82	22,95
985	Dol	50	332	-3,2	-21,7	0,93	5,17	0,02	422	344	0,703	26,79
985	Dol	40	339	-3,1	-21,6	0,90	5,01	0,02	420	340	0,685	27,50
1044	Dol	30	330	-2,9	21,2	0,84	4,70	0,01	418	332	0,692	26,61
1044	Dol	25	297	-1,3	14,2	0,37	2,14	0,01	394	267	0,727	25,33
1044	Dol	20	298	-1,4	13,2	0,40	2,31	0,01	395	272	0,728	25,31
1044	Dol	30	297	-1,3		0,37	2,14	0,01	394	267	0,727	25,33
1044	Dol	25	297	-1,2	12,1	0,35	1,98	0,01	392	264	0,725	25,39
1044	Cc	10	263	-2,1	21,3	0,61	3,44	0,01	406	300	0,808	22,80
1044	Cc	15	274	-2,3	21,7	0,67	3,76	0,01	409	308	0,794	23,21
1044	Cc	20	273	-2,1	-21,6	0,61	3,44	0,01	406	300	0,791	23,28
1044	Cc	15	263	-2,1		0,61	3,44	0,01	406	300	0,808	22,80
1044	Cc	20	264	-2,2	22,6	0,64	3,60	0,01	407	304	0,808	22,79
1044	Cc	30	264	-2,1	21,7	0,61	3,44	0,01	406	300	0,806	22,85
1046	Dol	30	312	-3,7	-23,4	1,08	5,93	0,02	429	363	0,755	24,92
1046	Dol	35	323	-2,9		0,84	4,70	0,01	418	332	0,714	25,81
1046	Dol	35	329	-2,6	-22,8	0,76	4,23	0,01	413	320	0,694	26,56
1077	Dol	40	362	-3,5	-22,8	1,02	5,62	0,02	426	355	0,643	29,27
1077	Dol	25	355	-3,4	-23,2	0,99	5,47	0,02	425	352	0,657	28,66
1077	Dol	30	356	-3,6	-24,1	1,05	5,78	0,02	428	360	0,66	28,50
1077	Dol	20	263	-2,6	-24,1	0,76	4,23	0,01	413	320	0,817	22,53
1077	Dol	10	261	-2,5	-23,9	0,73	4,07	0,01	412	316	0,819	22,50
1077	Dol	15	261	-2,1	-21,4	0,61	3,44	0,01	406	300	0,811	22,71

Table 9.5 Microthermometric analyses of the primary two phase liquid-vapour fluid inclusions, from the carbonate veins (D1), recalculated using the H₂O-NaCl-[KCl] equation of Bowers & Helgeson (1994)

Thick doubly polished	M	Ratio % Vapour	Th _{L+V}	Tm _{ice}	Te	Molal NaCl	Wt% NaCl equiv	X (NaCl)	Critical T	Critical P	Bulk Density	Bulk Molar Volume
991	Dol	20	357	-3,2	23,1	0,76	5,23	0,01	413	320	0,694	26,56
991	Dol	25	364	-3,1	-22,8	0,90	5,01	0,02	420	340	0,626	30,09
991	Dol	50	363	-3,3	-20,2	0,96	5,32	0,02	423	348	0,634	29,67
991	Dol	30	354	-3,1	-26,1	0,90	5,01	0,02	420	340	0,745	25,27
991	Dol	40	307	-2,8	-21,7	0,81	4,55	0,01	416	328	0,744	24,77
991	Dol	40	310	-2,9	-21,4	0,84	4,70	0,01	418	332	0,74	24,89
991	Dol	25	296	-1,3	-22,3	0,37	2,14	0,01	394	267	0,729	25,26
991	Dol	25	295	-1,4	-22,1	0,40	2,31	0,01	395	272	0,734	25,10
991	Dol	25	295	-1,4	-22,4	0,40	2,31	0,01	395	272	0,734	25,10
991	Cc	25	301	-2,2	-21,2	0,64	3,60	0,01	407	304	0,815	22,61
991	Cc	25	303	-2,7	-21,4	0,79	4,39	0,01	415	324	0,853	21,59
991	Cc	30	298	-2,9	-21,9	0,84	4,70	0,01	418	332	0,854	21,56
991	Cc	10	290	-2,4	-21,9	0,70	3,92	0,01	410	312	0,848	21,72
991	Cc	20	260	-1,4	-22,1	0,40	2,31	0,01	395	272	0,724	25,46
991	Cc	15	240	-1,3	-22,3	0,37	2,14	0,01	394	267	0,721	25,55
991	Cc	25	241	-1,6	-22,4	0,46	2,63	0,01	398	279	0,729	25,28
991	Cc	30	256	-1,5	-29,0	0,43	2,47	0,01	397	276	0,707	26,05
991	Cc	15	203	-1,3	-21,9	0,37	2,14	0,01	394	267	0,88	20,93
991	Cc	20	202	-1,2	-21,3	0,35	1,98	0,01	392	264	0,88	20,93
991	Cc	10	238	-0,5	-21,1	0,14	0,83	0	382	236	0,818	22,02
991	Cc	10	201	-0,9	-24,1	0,26	1,49	0	388	252	0,877	20,54
991	Cc	20	203	-0,1	-22,4	0,03	0,17	0	376	221	0,863	20,87
991	Cc	15	200	-1,1	-23,5	0,32	1,82	0,01	391	260	0,881	20,90
991	Cc	20	205	-1,0	-22,6	0,29	1,65	0,01	389	256	0,874	21,08
991	Cc	15	202	-0,7	-21,5	0,20	1,16	0	385	244	0,873	20,64
991	Cc	15	204	-0,2	-21,7	0,06	0,33	0	377	225	0,863	20,87
991	Cc	10	203	-0,2	-21,6	0,06	0,33	0	377	225	0,865	20,83

Table 9.6 Microthermometric analyses of the two phase liquid-vapour fluid inclusions, from the quartz veins (D1), recalculated using the H₂O-NaCl-[KCl] equation of Bowers & Helgeson (1994)

Thick doubly polished	M	Gr.	Ratio % Vapour	Th _{L+V}	Tm _{ice}	Te	Molal NaCl	Wt% NaCl equiv	X (NaCl)	Critical T	Critical P	Bulk Density	Bulk Molar Volume
987	Qtz	P	30	353	-3,1	-22,1	0,9	5,01	0,02	420	340	0,652	28,86
987	Qtz	P	20	361	-2,9	-21,3	0,84	4,7	0,01	418	332	0,627	29,40
987	Qtz	P	15	357	-3,8	-22,1	1,11	6,08	0,02	430	367	0,664	28,35
987	Qtz	P	20	348	-2,7	-21,6	0,79	4,39	0,01	415	324	0,653	28,21

Table 9.6 Microthermometric analyses of the two phase liquid-vapour fluid inclusions, from the quartz veins (D1), recalculated using the H₂O-NaCl-[KCl] equation of Bowers & Helgeson (1994)

Thick doubly polished	M	Gr.	Ratio % Vapour	Th _{L+V}	Tm _{ice}	Te	Molal NaCl	Wt% NaCl equiv	X (NaCl)	Critical T	Critical P	Bulk Density	Bulk Molar Volume
1057	Qtz	P	25	341	-3,6	-21,9	1,05	5,78	0,02	428	360	0,694	27,12
1057	Qtz	P	30	354	-3,5	-20,1	1,02	5,62	0,02	426	355	0,662	28,43
1057	Qtz	P	25	342	-3,3	-22,5	0,96	5,32	0,02	423	348	0,684	27,54
1057	Qtz	S	15	204	-3,7		1,08	5,93	0,02	429	363	0,91	20,69
1057	Qtz	S	20	207	-4,3	-22,1	1,25	6,81	0,02	437	386	0,914	20,60
1057	Qtz	S	15	211	-4,9	-21,7	1,42	7,68	0,02	445	408	0,916	20,54
1054	Qtz	S	15	198	-1,9	-10,7	0,55	3,12	0,01	403	292	0,894	20,60
1054	Qtz	S	20	201	-2,1	-10,6	0,61	3,44	0,01	406	300	0,893	20,62
1054	Qtz	S	15	205	-1,7	-10,2	0,49	2,79	0,01	400	283	0,883	20,86
1054	Qtz	S	25	189	-1,4	-11,1	0,4	2,31	0,01	395	272	0,898	20,52
1054	Qtz	S	20	197	-1,9	-10,4	0,55	3,12	0,01	403	292	0,895	20,57
1054	Qtz	P	25	344	-3,8	-21,6	1,11	6,08	0,02	430	367	0,693	27,16
1054	Qtz	P	30	352	-3,4	-20,9	0,99	5,47	0,02	425	352	0,664	28,36
1054	Qtz	P	25	347	-3,7	-22,2	1,08	5,93	0,02	429	363	0,684	27,53
1058	Qtz	P	30	382	-3,1	-21,4	0,9	5,01	0,02	420	340	0,579	32,52
1058	Qtz	P	35	391	-3,8	-21,7	1,11	6,08	0,02	430	367	0,579	32,48
1058	Qtz	P	30	385	-3,4	-21,6	0,99	5,47	0,02	425	352	0,581	32,38
1058	Qtz	P	25	350	-2,8	-20,9	0,81	4,55	0,01	416	328	0,65	28,33
1058	Qtz	P	20	357	-2,9	-22,4	0,84	4,70	0,01	418	332	0,636	28,94
1058	Qtz	PS	30	256	-2,8		0,81	4,55	0,01	416	328	0,831	22,16
1058	Qtz	PS	30	266	-2,4		0,7	3,92	0,01	410	312	0,809	22,77
990	Qtz	S	15	207	-3,8		1,11	6,08	0,02	430	367	0,908	20,73
990	Qtz	S	10	208	-4,1	-22,1	1,19	6,52	0,02	434	378	0,91	20,68
990	Qtz	S	20	210	-4,2	-21,7	1,22	6,67	0,02	436	382	0,909	20,70
990	Qtz	S	30	178	-2,5	-21,1	0,73	4,07	0,01	412	316	0,922	19,97
990	Qtz	S	10	177	-2,8	-22,1	0,81	4,55	0,01	416	328	0,926	19,89
990	Qtz	S	10	178	-2,5	-21,6	0,73	4,07	0,01	412	316	0,922	19,97
990	Qtz	S	15	180	-2,6	-21,9	0,76	4,23	0,01	413	320	0,922	19,99
990	Qtz	S	15	192	-2,7		0,79	4,39	0,01	415	324	0,911	20,22
990	Qtz	S	30	207	-3,1		0,9	5,01	0,02	420	340	0,899	20,93
990	Qtz	S	30	207	-3,0		0,87	4,86	0,02	419	336	0,898	20,96
990	Qtz	S	10	179	-2,3	-21,8	0,67	3,76	0,01	409	308	0,919	20,04
990	Qtz	S	25	180	-2,3	-21,4	0,67	3,76	0,01	409	308	0,918	20,06
990	Qtz	S	20	180	-2,5	-22,4	0,73	4,07	0,01	412	316	0,92	20,01
990	Qtz	S	20	178	-2,7	-24,2	0,79	4,39	0,01	415	324	0,925	19,92
990	Qtz	S	25	181	-3,1	-21,2	0,9	5,01	0,02	420	340	0,926	20,33
1056	Qtz	P	20	273	-2,3	-21,6	0,67	3,76	0,01	409	308	0,795	23,16
1056	Qtz	P	25	301	-2,9	-22,4	0,84	4,70	0,01	418	332	0,757	24,32
1056	Qtz	P	15	298	-2,4	21,1	0,7	3,92	0,01	410	312	0,752	24,49
1056	Qtz	P	25	302	-2,9	-22,4	0,84	4,70	0,01	418	332	0,757	24,32
1056	Qtz	P	20	283	-2,3	-21,6	0,67	3,76	0,01	409	308	0,795	23,16

9.4 Stable Isotopes Analyses

Oxygen, hydrogen, and carbon isotopes were analysed at the University of Lausanne, Switzerland in collaboration with Prof. Torsten Vennemann.

Table 9.7 Sample list indicating the isotope analyses completed on the different host rocks and vein systems

Core Section I						
Depth [m]	Core Sample	Isotope Sample	Lithologie/Vein System	Oxygen	Hydrogen	Carbon
1399.63	P1	73 52/52b 52a/53	fine grained sandstone quartz-carbonate ± chlorite quartz ± chlorite	Qtz/Cc Chl	WR Chl	Cc
1402.60	P4	54/54a	fine grained sandstone quartz-carbonate ± chlorite quartz ± chlorite	Qtz/Cc/Dol		Cc/Dol
1403.17	P5	24a/24b	fine grained sandstone quartz-carbonate ± chlorite	Chl/Qtz/Cc	Chl	Cc
1405.16	P102	21	siltstone quartz-carbonate ± chlorite quartz ± chlorite	Qtz		
1408.65	P7	PE3	dolomite quartz-carbonate ± chlorite	WR		WR
1408.77	P8	26	dolomite marl quartz-carbonate ± chlorite	Cc/Dol		Cc/Dol
1411.30	P10	PE2	dolomite marl quartz-carbonate ± chlorite	WR		WR
1417.11	PS018	60b 60/60a	dolomite marl quartz-carbonate ± chlorite	Qtz/Cc/Dol	WR	Cc/Dol
1430.84	P18	58/58a	nodular limestone/dolostone quartz-carbonate ± chlorite	Qtz/Cc/Dol		Cc/Dol
1434.40	P22	PE1	nodular limestone quartz-carbonate ± chlorite carbonate ± chlorite	WR		WR
1435.17	P23	22	nodular limestone quartz-carbonate ± chlorite carbonate ± chlorite	Cc		Cc

Table 9.7 Sample list indicating the isotope analyses completed on the different host rocks and vein systems

Core Section I						
Depth [m]	Core Sample	Isotope Sample	Lithologie/Vein System	Oxygen	Hydrogen	Carbon
1435.50	P1a	23a/23b/25	nodular limestone/dolostone quartz ± chlorite	Chl	Chl	
1436.68	P6a	40	nodular limestone/dolostone quartz-carbonate ± chlorite carbonate ± chlorite	Cc		Cc
1436.90	P25	37c 37/37a/37b/	dolomite marl quartz-carbonate ± chlorite	Chl/Qtz/Cc	WR Chl	Cc
1438.25	PB1		clay/shale quartz-carbonate ± chlorite			
1441.75	P27	39	dolomite marl carbonate ± chlorite quartz ± chlorite	Dol		Dol
1446.74	P32	PB2	silty sized pelites quartz ± chlorite		WR	
1448.87	P33	44	silty sized pelites quartz-carbonate ± chlorite quartz ± chlorite	Qtz		
1459.24	P111	24 50/51a	fine grained sandstone quartz-carbonate ± chlorite	Chl/Dol	WR Chl	Dol
1479.20	P13a	57b 56/57a	clay silty sized pelites quartz-carbonate ± chlorite quartz ± chlorite	Chl	WR Chl	
1485.80	P40	29	silty sized pelites quartz-carbonate ± chlorite	Chl	Chl	
1486.70	P104	32/30c 30/30a/30b	siltstone/sandstone quartz-carbonate ± chlorite	Qtz Chl/Qtz/Dol	WR Chl	Dol
1486.85	P14a	PB3	pelites/shale quartz-carbonate ± chlorite quartz ± chlorite		WR	
1487.52	PS060	62a/62b	clay silty sized pelites quartz ± chlorite	Chl/Qtz	Chl	

Table 9.7 Sample list indicating the isotope analyses completed on the different host rocks and vein systems

Core Section I						
Depth [m]	Core Sample	Isotope Sample	Lithologie/Vein System	Oxygen	Hydrogen	Carbon
1491.48	P11a	62	clay silty sized pelites quartz-carbonate ± chlorite quartz ± chlorite	Dol		Dol
1502.82	P46	PB2	silty sized pelites quartz-carbonate ± chlorite quartz ± chlorite		WR	
1503.25	P107	36 35/35a/35b	clay silty sized pelites quartz ± chlorite	Chl/Qtz/Dol	Chl	Dol
1507.15	P48	PB4	siltstone/sandstone quartz-carbonate ± chlorite carbonate ± chlorite		WR	
1512.48	P52	11	clay silty sized pelites quartz ± chlorite		WR	
Core Section II						
2129,33	P56	38 33	fine grained sandstone quartz	Qtz Qtz		
2131,64	P57		fine grained sandstone/pelite carbonate			
2142.70	P15a	70 34	fine grained sandstone carbonate quartz	Qtz Qtz		

9.4.1 Oxygen isotope analysis

Oxygen isotopes were analysed using a Conventional collector and a Laser Line (Table 1). The conventional method following Asprey (1976) and Clayton & Mayeda (1963), was applied to the whole rock due to its ability to analyse larger sample sizes thus reducing the effect of homogeneity, with an accuracy of $\pm 0,2$ ‰, whereas the Laser Line described after Rumble and Hoering (1994) was used for the analysis of mineral fractions as the sample size smaller with a higher accuracy of $\pm 0,1$ ‰. The analyses are measured using a Finnigan MAT 252 mass spectrometer, referred to using the notation $\delta^{18}\text{O}$ after referencing to the Vienna Standard Mean Ocean Water (VSMOW) standard. The Mineral-water oxygen fractionation factors are listed in Table 2; these are used for the isotopic composition of the fluid to be calculated.

Conventional Method

The quantity of the sample necessary is dependent on the estimated proportion of oxygen, generally between 5 and 30 mg are required. The sample is sealed in a nickel bomb with bromine pentafluoride (BrF_5) in a vacuum environment for 12 to 15 hours at 650°C ; all but the most refractory minerals are amenable during this technique. The liberated O_2 is converted to CO_2 by reacting it with a heated (1000°C) graphite rod.

Laser Line

The sample size is smaller approximately $<2,5$ mg and is heated in a fluorine-rich atmosphere to 2000°C with a CO_2 laser, the mineral reacts with the fluorine and releases O_2 . The O_2 is removed by cryogenic absorption onto a molecular sieve.

Table 9.8 Oxygen isotopes from the selected samples

Depth [m]	Sample	Veining/Alteration/Whole Rock Samples	$\delta^{17}\text{O}$	$\delta^{18}\text{O}$
1399,63	52a	Chlorite (Quartz)	14,73	18,50
1435,50	23a	Chlorite (Quartz)	14,84	18,45
1436,90	37a	Chlorite (Quartz)	15,23	18,45
1479,20	56	Chlorite (Quartz)	16,22	17,67
1488,25	62a	Chlorite (Quartz)	18,71	17,98
1503,25	35a	Chlorite (Quartz)	21,88	17,82
1403,17	24a	Chlorite (Dolomite)	28,32	18,33
1486,70	30a	Chlorite (Dolomite)	26,23	17,86
1399,63	52b	Quartz -Carbonate (Calcite)	14,73	18,50
1402,60	54	Quartz -Carbonate (Calcite/Dolomite)	34,56	19,02
1403,17	24b	Quartz -Carbonate (Calcite)	28,32	18,33
1417,16	60	Quartz -Carbonate (Calcite/Dolomite)	18,07	19,24
1430,69	58	Quartz -Carbonate (Calcite/Dolomite)	15,16	18,02
1436,90	37b	Quartz -Carbonate (Calcite)	14,37	18,45
1486,70	30b	Quartz -Carbonate (Dolomite)	26,19	17,86
1488,25	62b	Quartz -Carbonate (Dolomite)	18,71	17,98
1405,16	21	Quartz	27,56	16,76
1448,87	44	Quartz	24,37	16,46
1503,25	35b	Quartz	23,13	17,76
2129,50	33	Quartz	32,27	16,26
2142,70	34	Quartz	24,52	16,28
1399,63	53	Chlorite Alteration	17,75	15,91
1435,50	23b	Chlorite Alteration	24,73	14,90
1459,24	51	Chlorite Alteration	17,01	15,04
1479,20	57	Chlorite Alteration	21,07	15,27
1485,80	29	Chlorite Alteration	24,62	15,16
1486,70	32	Whole Rock		14,96
1503,25	36	Whole Rock		14,85
1436,90	71	Whole Rock		14,87
2142,70	38	Whole Rock	24,65	14,54
2142,70	70	Whole Rock	15,16	14,37
		Qtz / Standart LS	32,32	18,04
		Qtz / Standart LS	14	18,55
		Qtz / Standart NBS28	20,40	9,62
		Qtz / Standart NBS29	9,51	9,75

9.4.2 Hydrogen isotope analysis

Measurements of the hydrogen isotope compositions of minerals were made using high-temperature (1450°C) reduction methods with He-carrier gas and a TC-EA linked to a Delta Plus XL mass spectrometer from Thermo-Finnigan on 2 to 4 mg sized samples according to a method adapted after Sharp et al. (2001). The results are given in the standard δ -notation, expressed relative to the Vienna Standard Mean Ocean Water (VSMOW) standard in permil (‰). The precision of the in-house kaolinite standard and NBS-30 biotite for hydrogen isotope analyses was better than $\pm 2\text{‰}$ for the method used; all values were normalised using a value of -125‰ for the kaolinite standard and -65‰ for NBS-30 analysed during the same period as the samples. The Mineral-water oxygen fractionation factors are listed in Table 2; these are used for the isotopic composition of the fluid to be calculated.

Hydrogen collector

The sample size varies between 40 and 120 mg, dependent on the estimated H content. The sample is heated with a fuel-gas-oxygen torch to 1400°C, the released H_2O is collected in liquid nitrogen, and additional hydrogen is reacted with CuO held at 700°C and converted to H_2O . The total H_2O is then transferred into a Pyrex tube containing zinc and heated for 12 minutes at 500°C producing ZnO and H_2 .

Thermo-Chemical Elemental Analyser

The sample size is small 0.1 μl of water (or equivalent from hydrous phases) for hydrogen isotope ratio determinations. The technique involves the reduction of H_2O or solid hydrous samples by reacting them with glassy carbon at high temperatures (1450°C). The product gases are then separated by gas chromatography.

Table 9.9 Hydrogen isotopes from the selected samples

Depth [m]	Sample	Veining/Alteration/Whole Rock Samples	δD VSMOW	wt% water
1399,63	52a	Chlorite/Quartz	-53	3,52
1435,50	23	Chlorite/Quartz	-59	4,06
1436,90	37a	Chlorite/Quartz	-59	3,69
1479,20	56	Chlorite/Quartz	-52	4,21
1488,25	62a	Chlorite/Quartz	-58	1,41
1503,25	35	Chlorite/Quartz	-56	4,05
1403,17	24a	Chlorite/Dolomite	-65	1,53
1486,70	30a	Chlorite/Dolomite	-66	2,28
1399,63	53	Chlorite alteration	-62	1,81
1435,50	25	Chlorite alteration	-66	2,28
1459,24	51a	Chlorite alteration	-61	0,74
1479,20	57a	Chlorite alteration	-64	0,98
1485,80	29	Chlorite alteration	-60	3,17
1399,63	73	Whole Rock	-51	2,14
1417,16	60b	Whole Rock	-49	2,17
1436,90	37c	Whole Rock	-51	4,50
1459,24	51b	Whole Rock	-50	3,47
1479,20	57b	Whole Rock	-51	2,10
1486,70	30c	Whole Rock	-50	2,13
1512,43	11	Whole Rock	-53	0,60
1486,85	PB3	Whole Rock / Red Pellites	-51	4,50
1507,18	PB4	Whole Rock / Red Pellites	-53	3,00
1446,36	PB2	Whole Rock / Grey Pellites	-56	4,18
1502,78	PB2	Whole Rock / Grey Pellites	-57	4,04

9.4.3 Carbon isotope analysis

Carbonate samples of 100 - 200 µg were analysed in the Gas Bench II (Thermo-Finnigan) with 100% orthophosphoric acid (H₃PO₄) digestion technique at 70°C (Spötl and Vennemann, 2003). The CO₂ produced was transported in a He carrier flow across two Nafion[®] water taps and gas-chromatograph for CO₂ - N₂ separation, before measurement of the isotopic composition with a Thermo-Finnigan Delta plus XL mass-spectrometer. The measured $\delta^{18}\text{O}$ values for carbonates were corrected for acid fractionation (at 25°C, $\alpha = 1,01025$, Friedman and O'Neil, 1977; at 50°C, $\alpha = 1,00931$, Swart et al., 1991). All $\delta^{18}\text{O}$ values are reported relative to the Vienna Standard Mean Ocean Water (VSMOW) standard in permil (‰); $\delta^{13}\text{C}$ values are relative to PDB, where for NBS-19, $\delta^{13}\text{C}$ (PDB) is 1,95 ‰ and $\delta^{18}\text{O}$ (PDB) is -2,20 ‰ (Hut, 1987) and $\delta^{18}\text{O}_{\text{SMOW}} = 1,03091 \delta^{18}\text{O}_{\text{PDB}} + 30,91$ (Coplen et al., 1983). A $\delta_{(\text{CO}_2\text{-H}_2\text{O})}$ value of 1,0412 was used (e.g., Friedman and O'Neil, 1977).

Table 9.10 Carbon isotopes from the selected samples

Depth [m]	Sample	Veining/Whole Rock Samples	$\delta^{13}\text{C}$ VPDB	$\delta^{18}\text{O}$ VPDB	$\delta^{18}\text{O}$ VSMOW
1399,63	52	Quartz-Carbonate (Calcite)	-4,74	-14,10	16,38
1402,60	54	Quartz-Carbonate (Calcite/Dolomite)	-0,88	-13,40	17,10
1403,17	24	Quartz-Carbonate (Calcite)	-4,63	-14,43	16,03
1408,65	PE3	Dolostone	-0,05	-8,57	22,08
1408,77	26	Quartz-Carbonate (Dolomite/Calcite)	-0,44	-12,31	18,22
1411,30	PE2	Dolostone	-0,06	-8,57	22,07
1417,16	60	Quartz-Carbonate (Calcite/Dolomite)	-1,52	-13,93	16,55
1430,69	58	Quartz-Carbonate (Calcite/Dolomite)	-1,06	-14,27	16,20
1434,40	PE1	Limestone	-1,04	-13,83	16,65
1435,17	22	Quartz-Carbonate (Calcite)	-5,62	-14,43	16,03
1436,68	40	Carbonate (Calcite)	-7,93	-14,46	16,00
1436,90	37	Quartz-Carbonate (Calcite)	-9,18	-14,51	15,95
1441,75	39	Carbonate (Dolomite)	-10,58	-12,26	18,27
1459,24	50	Quartz-Carbonate (Dolomite)	-17,31	-14,04	16,44
1486,70	30	Quartz-Carbonate (Dolomite)	-19,86	-14,46	16,00
1491,48	62	Quartz-Carbonate (Dolomite)	-19,98	-14,49	15,97
1503,25	35	Quartz-Carbonate (Dolomite)	-17,36	-13,09	17,41
	CMSTD1	Standards only	2,06	-1,62	29,24
	CMSTD2	Standards only	2,05	-1,67	29,19

Table 9.11 Mineral-water hydrogen/oxygen fractionation calculations of chlorites in paragenesis with quartz and/or dolomite as well as chlorite alteration

Depth [m]	Sample	Veining/Alteration	δD VSMOW	δD to Fluid	$\delta^{18}O$ VSMOW	$\delta^{18}O$ to Fluid
1399,63	52a	Chlorite/Quartz	-53	-19.5	18,50	18,83
1435,50	23	Chlorite/Quartz	-59	-25.5	18,45	18,78
1436,90	37a	Chlorite/Quartz	-59	-25.5	18,45	18,78
1479,20	56	Chlorite/Quartz	-52	-18.5	17,67	18,00
1488,25	62a	Chlorite/Quartz	-58	-24.5	17,98	18,31
1503,25	35	Chlorite/Quartz	-56	-22.5	17,82	18,15
1403,17	24a	Chlorite/Dolomite	-65	-31.5	18,33	15,37
1486,70	30a	Chlorite/Dolomite	-66	-32.5	17,86	18,19
1399,63	53	Chlorite Alteration	-62	-28.5	15,91	16,25
1435,50	25	Chlorite Alteration	-66	-32.5	14,90	15,23
1459,24	51	Chlorite Alteration	-61	-27.5	15,04	15,37
1479,20	57	Chlorite Alteration	-64	-30.5	15,27	15,61
1485,80	29	Chlorite Iteration	-60	-26.5	15,16	15,49

Table 9.12 Mineral-water oxygen fractionation calculations of quartz/carbonate pears

Depth [m]	Sample	Veining	$\delta^{18}O$ Qtz	$\delta^{18}O$ Cc/Dol	$\delta^{18}O$ Qtz to Fluid	$\delta^{18}O$ Cc/Dol to Fluid	Isotope T [°C]
1399,63	52b	Quartz-Carbonate (Calcite)	18,50	16,38	12,91	11,82	399 °C
1402,60	54	Quartz-Carbonate (Calcite/Dolomite)	19,02	17,10	13,43	12,47	433 °C
1403,17	24b	Quartz-Carbonate (Calcite)	18,33	16,03	12,74	11,47	373 °C
1417,16	60a	Quartz-Carbonate (Calcite/Dolomite)	19,24	16,55	13,65	11,92	324 °C
1430,69	58	Quartz-Carbonate (Calcite/Dolomite)	18,02	16,20	12,43	11,57	455 °C
1436,90	37b	Quartz-Carbonate (Calcite)	18,45	15,95	12,86	11,25	347 °C
1486,70	30b	Quartz-Carbonate (Dolomite)	17,86	16,00	12,27	11,30	445 °C
1488,25	62b	Quartz-Carbonate (Dolomite)	17,98	15,97	12,39	11,24	417 °C

9.5 δD and $\delta^{13}C$ Values of Fluids

Fluids contained in fluid inclusions of quartz, calcite and dolomite grains of the different vein types were extracted to mechanical/crushing decrepitation in a vacuum extraction line. Released H_2O and CO_2 were trapped under vacuum in a liquid nitrogen-cooled U-tube. CH_4 was separated from H_2O and CO_2 by careful expansion into an isolated part of the vacuum line, then oxidized to H_2O and CO_2 by passing it over copper oxide cycled at temperatures between 700 to 760°C in a system close to the U-trap containing original H_2O and CO_2 from the fluid inclusions. Methane-derived H_2O and CO_2 were trapped in a second liquid nitrogen-cooled U-tube and then separated cryogenically using an ethanol- liquid nitrogen slush trap at about -90°C, where CO_2 is released as a vapor once more. H_2O and CO_2 , first the products of methane oxidation and thereafter in a similar way those for fluid inclusion H_2O and CO_2 , were then cryogenically transferred into small Pyrex[®] glass tube for the transfer to the mass spectrometers. The isotopic composition of CO_2 was analysed by dual inlet mass spectrometry on a Finnigan MAT 253, or for samples less than 3 μ mol in size using a Gas Bench II and carrier gas system linked to a Thermo-Finnigan Delta plus XL mass spectrometer with all gas being passed through gas chromatograph to isolate the CO_2 for analyses.

The H_2O was transferred cryogenically into a small 1/4 in. (outer diameter) stainless steel U-tube of a specially constructed vacuum line linked to the TC-EA via a 1/16th in outer diameter stainless steel line. After thawing of the water at 100°C, it was flushed with He into the He-stream of the TE-CA, allowing it to react with graphite at 1350°C and passing the product H_2 (and CO) over a gas chromatograph into the mass spectrometer as for the measurements of D/H from the solid samples. The δD values for H_2O , obtained from the oxidation of methane and from the fluid inclusions, were calibrated against those of three laboratory standards with δD values +3, -58, and -160‰. The standards, introduced into the same vacuum line via injection with a vacuum-tight micro-syringe, reproduced to within ± 5 ‰.

Table 9.13 Hydrogen/(oxygen) isotopy of fluid inclusion water

Depth [m]	Sample	Vein Type and Mineral	H ₂ O mV M 2	δD H ₂ O raw	δD (VSMOW)	δ ¹⁸ O (VSMOW)
1403.68	P5	quartz- calcite ± chlorite	395	-83	-104	16,03
1417.03	P8	quartz -carbonate ± chlorite	190	-62	-89	19,24
1430.69	P9	quartz -carbonate ± chlorite	2837	-73	-99	18;02
1436.90	P7	quartz -carbonate ± chlorite	92	-42	-94	18,45
1486.7	P6	quartz -carbonate ± chlorite	2472	-84	-98	17,86
1503.25	P3	quartz- dolomite ± chlorite	371	-109	-113	17,41

Table 9.14 Carbon isotopy (VSMOW) of quartz-carbonate pairs

Depth [m]	Sample	Vein Type and Mineral	CH ₄ mbar	CO ₂ mbar	d ¹³ C CH ₄	d ¹³ C CO ₂
1403.68	P5	quartz- calcite ± chlorite	4	8	too small	-22,3
1408.75	P11	quartz- dolomite ± chlorite	6	28	too small	-12,8
1417.03	P8	quartz -carbonate ± chlorite	20	39	-28,9	-13,3
1430.69	P9	quartz -carbonate ± chlorite	6	7	too small	-13,0
1436.68	P4	quartz- calcite ± chlorite	17	6	-28,5	-19,9
1436.90	P7	quartz -carbonate ± chlorite	13	33	-26,9	-17,4
1459.24	P12	quartz- dolomite ± chlorite	15	74	-28,3	-17,8
1479.20	P2	quartz -carbonate ± chlorite	2	33	too small	-21,0
1486.7	P6	quartz -carbonate ± chlorite	2	33	too small	-23,3
1503.25	P3	quartz- dolomite ± chlorite	3	8	too small	-18,0

Lebenslauf

Name: Markus Josef Lögering

geboren: 31.03.1972 in Emsbüren (Niedersachsen)

Anschrift: Duinweg 31
2202 RC Noordwijk
The Netherlands

Telefon: +310611525098

E-mail: m.leogering@panterra.nl

Beruf/Studium/Ausbildung:

2007 "Junior Reservoir Geologist" bei der Firma PanTerra Geoconsultants BV, Leiderdorp, Netherlands

2004-2007 Doktorandenstelle am Institut für Mineralogie und Lagerstättenlehre an der Rhein Westfälischen Technischen Hochschule

2003 Hochschulabschluss: "Diplom-Geologe" an der Universität Leipzig, Sachsen

2002-2003 Diplomarbeit an der Universität Alberta, Edmonton, Kanada

2000-2003 Hauptstudium in Geologie an der Universität Leipzig

1998-2000 Vordiplom in Geologie an der Universität Leipzig

1996-1998 Grundstudium in Bodenwissenschaften an der Fachhochschule Osnabrück

1994-1995 Zivildienst bei der Caritas Freiburg im Breisgau

1991-1994 Ausbildung zum staatlich anerkannten technischen und praktischen Landwirt

1991 Hochschulreife in Lingen/Ems

Noordwijk, 04.07.2008